ERDA/SE/EC(11-1)-2721/FR/76/1

COO/2721-76/1
Distribution Category UC-63

Prepared with the Support of the

ENERGY RESEARCH AND DEVELOPMENT ADMINISTRATION
Washington, D.C. 20050

Under

ERDA Grant EC(11-1)-2721, initiated in April, 1975

RESEARCH AND DEVELOPMENT OF LOW COST PROCESSES FOR INTEGRATED SOLAR ARRAYS

by

C.D. Graham, S. Kulkarni, E. Louis, A.G. MacDiarmid, G.T. Noel
D.P. Pope, K. Thallum, J.H. Wohlgemuth, M. Wolf, and J.N. Zemel

University of Pennsylvania
Philadelphia, Penna. 19174

and

L.D. Crossman, V.D. Dosaj, L.P. Hunt, and J.R. McCormick

Dow Corning Corp.
Hemlock, Mich. 48626

January 1976

FINAL REPORT
COVERING THE PERIOD April 15, 1974 TO January 14, 1976

(Any opinions, finding, conclusions or recommendations expressed in this publication are those of the authors and do not necessarily reflect the views of the Energy Research and Development Administration.)

DISCLAIMER

ABSTRACT

Results of a program to study process routes leading to a low cost large area integrated silicon solar array manufacture for terrestrial applications are reported. Potential processes for the production of solar-grade silicon are evaluated from thermodynamic, economic, and technical feasibility points of view. Upgrading of the present arc-furnace process is found most favorable. Experimental studies of the Si/SiF_4 transport and purification process show considerable impurity removal and reasonable transport rates. Silicon deformation experiments indicate production of silicon sheet by rolling at 1350° C is feasible. Significant recrystallization by strain-anneal technique has been observed. Experimental recrystallization studies using an electron beam line source are discussed. A maximum recrystallization velocity of ~9 m/hr is calculated for silicon sheet. A comparative process rating technique based on detailed cost analysis is presented.

TABLE OF CONTENTS

TABLE OF CONTENTS (continued)

LIST OF ILLUSTRATIONS

LIST OF ILLUSTRATIONS (continued)

LIST OF TABLES

LIST OF TABLES (continued)

SUMMARY

Progress during the past eighteen months in selecting the most probable process for producing solar-grade silicon at less than $10/kg and as a production level in excess of the goal of approximately 2000 metric tons per year by 1985 is discussed. The selection process involved examination of processes for preparing silicon that were used in the past as well as those that are commercially employed today. In addition, over 200 chemical reactions were considered by which the preparation of silicon might have been possible by the reduction of readily available silicon compounds. The theoretical feasibility of each of these reactions for preparing silicon was tested thermodynamically through free energy calculations. All reactions that favorably passed the thermodynamic screening were then examined in terms of their raw materials costs less than $2.50/kg Si were further considered in terms of the degree of existing technology that might allow them to be made into an actual process. Upgrading of the metallurgical-grade silicon process was deemed the most probable means of meeting ERDA goals for solar-grade silicon since only standard chemical techniques need be applied to an already commercial process which is able to produce large-tonnage silicon for a price of only about $1/kg.

Purification techniques are discussed by which Dow Corning has upgraded metallurgical silicon-grade quality with respect to all impurity elements, except boron and phosphorus. An upgrading technique is postulated by which these two elements might be reduced to a level low enough for fabricating greater than 10% efficient solar cells. Preliminary analyses indicate that experimental proof of this concept has a high probability of success.

It is recommended that further work be continued on upgrading the metallurgical-grade silicon process with emphasis directed toward boron and phosphorus reduction through use of purer raw materials used in the arc furnace.

The results of an experimental study of a silicon vapor transport process wiht potential for low cost silicon purification and silicon sheet growth are discussed. The processes makes use the cyclic reaction sequence

$$Si(Solid + SiF_4(gas) \xrightarrow{T_1} 2SiF_2(gas) \qquad (a)$$

$$2\ SiF_2(gas) \xrightarrow{T_2} Si\ (solid) + SiF_4(gas) \qquad (b)$$

The forward reaction (a) takes place at $T_1 > 1150^{\circ}C$ while the reverse reaction occurs at temperatures in the range 500-900°C depending on thermal gradient conditions. The process has been studies at both low pressure and at atmospheric pressure, and it has been shown that higher transport rates will occur at the higher pressures. The rate limiting step in the transport process is the formation of SiF_2. Deposition rates up to 12 micrometers per minute have been observed and film thicknesses up to 0.75 mm have been obtained.

Spectrographic analysis of silicon deposits from the silicon fluoride transport process show a reduction in the concentration of metallic impurities below the levels present in the metallurgical-grade starting material. Almost all metals were lowered significantly. The major impurities after transport are still aluminum and iron, but at reduced levels. X-ray analysis indicates that aluminum is transported along with the silicon and is deposited at the lower temperatures as AlF_3.

An experimental determination of the equilibrium constant for the SiF_2 yielded a value of 0.035. Based on this value a standard heat of formation of -155 Kcal/mole was calculated.

The silicon transport species in the SiF_4 gas stream at one atmosphere have been found to be very stable at elevated temperatures and can, in the absence of a temperature gradient, be transported over significant distances without decomposition. Experiments involving cooling the gas stream emerging from the high temperature zone to room temperature and below indicate that higher order silicon fluoride compounds of the Type $Si_xF_{2x}+_2$ with $x>1$ play a primary role in the transport process at a pressure of one atmosphere.

Processes which will lead to the formation of large area (∿1 meter wide) thin (∿100 micrometers) silicon sheet are discussed and compared. Processes considered include rolling, extrusion, ribbon alloying, casting, binary and elemental melt growth techniques, CVD, V-L-S, and vacuum evaporation. Experimental work on silicon deformation is reported. Successful deformation of polycrystalline samples at 1350°C is demonstrated. It is concluded that rolling of silicon in this temperature range will be a cold working process rather than a hot working process. Recrystallization of polycrystalline silicon samples after deformation and annealing has been observed and the texture of the samples at various stages of the process have been characterized by the Schultz method. Grain growth from an initial size of 20-30 μm to a final size of the order of 1 mm has been found.

A study of the known characteristics of various silicon binary alloy systems indicates that the binary solution growth technique is not as suitable as a sheet growth process as some of the other processes considered.

Theoretical and experimental investigations of the traveling molten zone recrystallization process as applied to the sheet geometry are presented. The theoretical calculations indicate a maximum velocity of about 9 m/hr for recrystallizing sheet 1 meter wide and 0.01 thick. The power required would be 2040 W. The effect of several heat removal techniques on the maximum velocity is considered.

A line source electron beam gun based on the Pierce concept was designed and constructed. Molten zones were produced and moved in several silicon bar samples; however, a stable molten zone without edge pull in (i.e., maintaining the rectangular shape) has not been observed to date.

Recrystallization by thermal cycle annealing was found not to be feasible for the goals of this program. The degree of recrystallization produced is inadequate.

A formalism for the comparative techno-economic evaluation of alternative process candidates is outlined. The formalism is based on cost analysis techniques. A major difficulty is in estimating the success potential of a process on the basis of available knowledge, since processes about which little is known tend to be assessed more optimistically than those for which a larger volume of data is available. An analysis of the economics of the Czochralski process is developed. The results indicate that crucible costs will probably dominate future crystal pulling costs.

I. INTRODUCTION

This report covers work on a program which has been funded for 1-3/4 years, first by NSF-RANN, and then continued by ERDA. The program is the result of a proposal entitled "Research and Development of Low Cost Processes of Integrated Solar Arrays", which was submitted to NSF-RANN in March, 1973. That proposal outlined a 3 stage, 10 year program for the development of a new process sequence from the raw materials to finished array, based on the silicon single crystal approach, with the goal for the finished array cost being in or below the $\$15.00-\$40.00/m^2$ ($0.10-$0.30/watt) range (exclusive of encapsulation costs), in order to open the largest possible terrestrial market. The proposal was based on the philosophy that the evolving process has to be a high yield, high speed, fully automated process consisting of a minimum number of steps which are optimally matched to each other. The product of the process should be large area sheets of silicon containing a multitude of internally series connected cells (Fig. 1), in order to avoid the significant cost of assembly of individual cells into arrays. A key point in the proposed development work was to continually keep the total process flow in mind in order to arrive at an optimal match of the individual process steps.

The objective of the first program stage, projected as a 3 year effort, was to carefully evaluate the attributes of all candidate processes or phenomena for their potential suitability for incorporation into such a sequence, and to determine the 2 or 3 process sequences with the highest probability for reaching the program goals. These processes would then, in the second stage, be developed and tested in full scale bench set-ups (3 years), and developed into an automated pilot line in the 3rd stage.

By the end of the current contract period (Jan. 15, 1976), approximately 60% of the 3 years time for the first stage will have been used, but only ca. 45% of the originally proposed program cost will have been spent. This is in part due to a reduction i

the scope of the program, at the direction of the grantor to concentrate work on the process steps leading to the production of silicon sheets, since it was felt that the process for the generation of integrated arrays within such sheets was more readily achievable on the basis of current technology.

It was recognized in the proposal that considerable differences exist in the amount of available knowledge about the attributes of various potential processes. This would make evaluation difficult. Consequently, additional research was to be carried out to gain adequate information on some of these processes to permit proper comparision. Such research was to be directed primarily to processes with especially large payoff potential. On processes which are under development or active research at other organizations, additional work would not be performed in this first stage, but rather the progress of this work would be observed, the results would be used in the evaluation of competing process approaches, and, if so indicated, the processes would be incorporated into the evolving process sequence.

The program was split into two work areas: the reduction of the raw material to silicon and its purification; and its transformation into single crystal or large crystalline sheets. The term "large crystalline sheets" is used here to mean that the crystallite size has to be sufficiently large such that the polycrystallinity does not result in significant degradation of device performance from that obtained from single crystal devices. The Dow-Corning Corp. was subcontracted by the University of Pennsylvania to perform the primary activities in the reduction and purification area. The results of their activity indicate that the arc furnace process using the starting material quartzite with carbon added as a reducing agent, appears to be the most economical process by a significant margin. It is expected that this process can be improved to yield silicon of considerably higher purity than the current metallurgical grade. As further

purification steps, gas blowing and controlled freezing have been tentatively identified. A methodology for the evaluation of competing processes in this area has been evolved, which is based on the evaluation of raw and indirect material costs and energy consumption.

The University of Pennsylvania effort has concentrated on pinpointing process approaches which appear to have great positive attributes in comparison to processes which are currently used or are being explored elsewhere. In this endeavor, five process approaches had originally been identified, two of which have since been eliminated.

One of the approaches which are being further evaluated is a transport process based on the SiF_4/SiF_2 reaction, which has attributes suitable for combined chemical purification and CVD, leading directly to polycrystalline sheets. Its raw material could be the molten silicon emerging from the upgraded arc furnace process. It thus combines into one step 7 major steps of the current process, which steps cause a 250-fold cost increase over the starting material, metallurgical grade silicon (MGSi). Indirect materials are not consumed in this process, except possibly for binding the small amounts of impurities removed, and by-products are thus not generated in large amounts. Since extremely little was known about the properties of this chemical reaction, considerable research work had to be done, and additional work is still required to complete the characterization of this process.

The second process is based on plastic deformation, such as rolling. Rolling is a very widely used and well developed process in the metal industry, with the attribute of providing large form changes at extremely high speeds, up to 60 mph. The primary question to be answered is; are the high temperature mechanical properties of polycrystalline silicon, which have not been previously characterized, conducive to such plastic deformation at adequate speeds? From the research carried out under this program, these properties are now beginning to emerge so that

analytical evaluation can be performed. It has been established that plastic deformation of polycrystalline silicon at temperatures below its melting point is possible. Parameters relevant to the speed of the process are currently being investigated. An interesting byproduct of this effort is the observation that considerable grain growth results from annealing the silicon after the deformation.

The third process is based on the assumption that polycrystalline sheets of high purity silicon can be obtained from a number of different process, including CVD or rolling. A transformation of these sheets, at low cost, to a high purity sheet of adequate crystal structure seems to be required to fabricate high performance devices. The process being investigated for this purpose is a floating molten zone recrystallization process to be carried out on sheets of silicon. The process speed would essentially equal that of the EFG process, being limited by the same heat transfer conditions. However, the impurity introduction and boundary origination problems resulting from the use of the die in the EFG process, would be entirely avoided. Like the Czochralski or the EFG process, the float zone process is essentially a crystal growth from a molten meniscus. While in the Czochralski process, the meniscus size is determined only by the already grown ingot, in the EFG and the float zone processes, the meniscus shape is determined by both the die or the unmolten polycrystal sheet, respectively, and the already grown ribbon or sheet. The primary requirement for functioning of the float zone process is the maintenance of a molten zone of adequately small height which is estimated to be a maximum of about 3 times the thickness of the sheet. An electron beam heating system has been developed for this purpose.

The processes which have been eliminated from further consideration, as a result of early work in this program are sheet growth from a solution of silicon, and grain growth by temperature cycle annealing. All potential solvents for silicon and

the characteristics of the solutions have been tabulated, and it has been found that the attributes of all low temperature solutions are such as to limit the process speed to greatly inadequate values. These low temperature processes would provide considerable advantages from the viewpoints of process control, maintenance of purity, and energy consumption.

During this program, considerable progress has been made in process identification and evaluation and the determination of potential process sequences. Figure 2 illustrates a number of possible routes from the basic silica (SiO_2) to single crystal or large grain polycrystalline sheets of solar grade silicon (SoG-Si) based on the evaluative work of this program. The processes and sequences shown in this figure are discussed in detail in the body of this report.

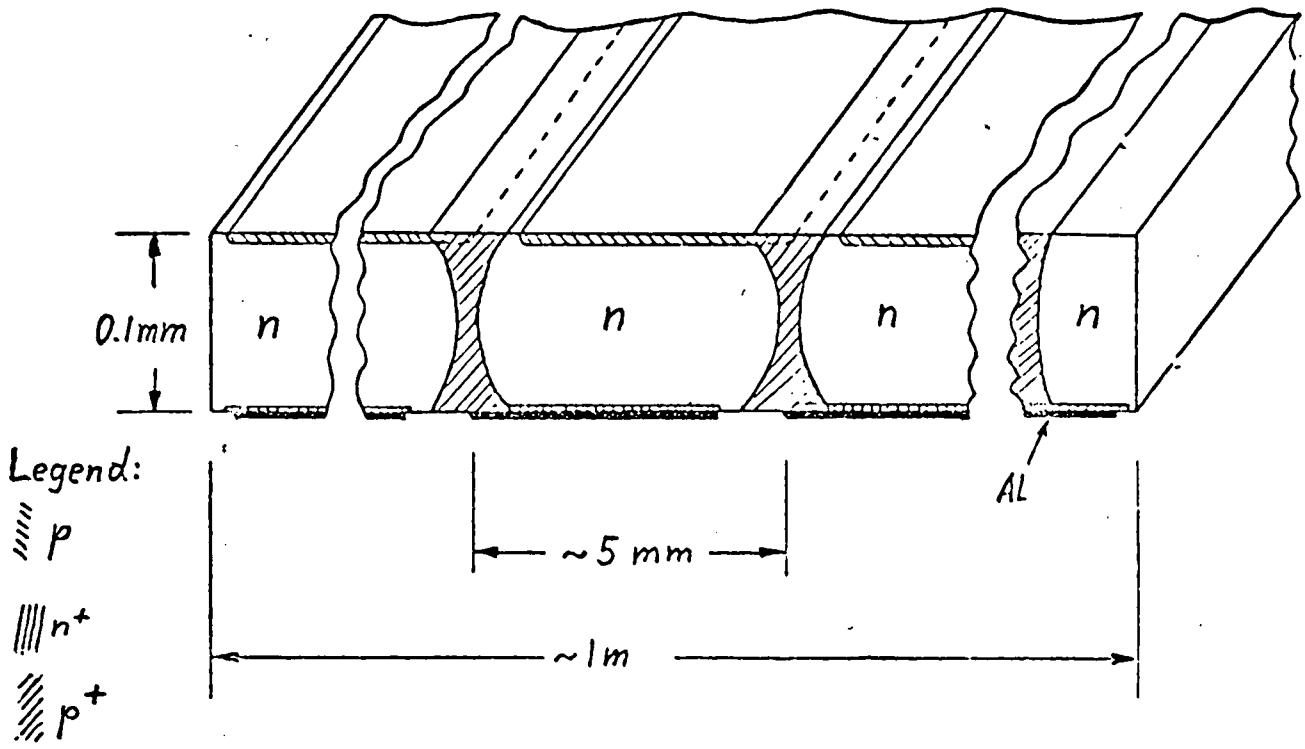

Fig. 1

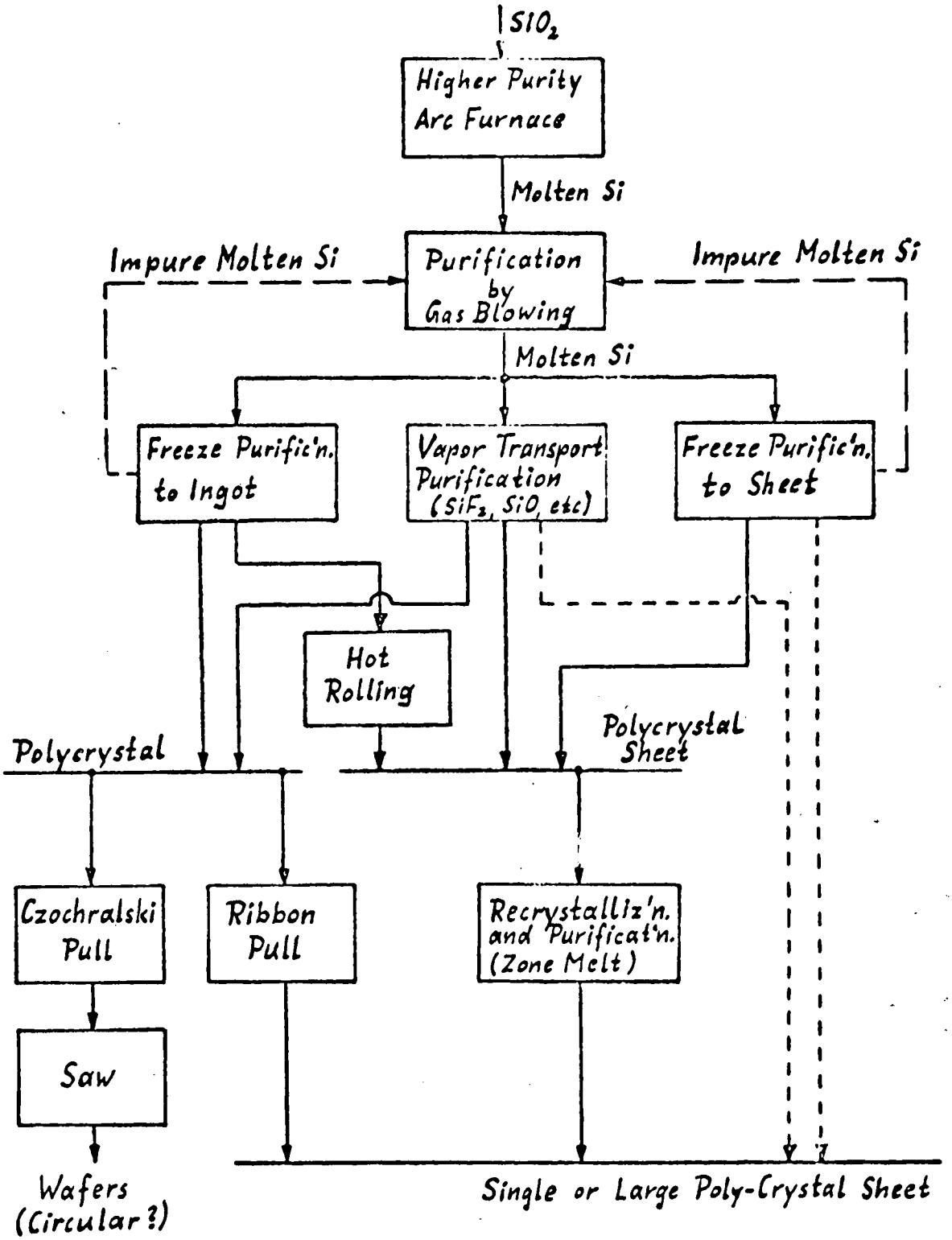

Figure 2. Potential Process Sequences Including Upgrading MG-Si

II. PREPARATION OF SOLAR GRADE SILICON

A. Introduction

This section summarizes progress during the eighteen month contract period in selecting a process or series of processes for producing solar-grade silicon at less than $10/kg and at a production level in excess of the goal of approximately 2000 metric tons per year by 1985. In this effort, the Dow Corning Corporation, under subcontract to the University of Pennsylvania, examined over 200 chemical reactions by which the preparation of silicon might have been possible by the reduction of readily available silicon compounds. These reactions were subjected to thermodynamic, economic, and technological screening to determine the most probable process for meeting the above goals (Fig. 3). As a result of this work, Dow Corning concluded that upgrading the existing metallurgical grade silicon production process has the highest potential for meeting the goals at present. Several possible upgrading techniques were suggested, and preliminary experimental studies to establish the feasibility of some of the techniques were conducted.

Other experimental studies relevant to this area were conducted by the University group. These involved investigations of the Si/SiF_4 transport process which holds considerable promise as a means of purifying metallurgical grade silicon and could be coupled directly to the arc-furnace process. The Si/SiF_4 process could also lead directly to the growth of large area silicon through CVD.

Details of this work is presented in the following subsections.

B. Thermodynamic Screening

For the purposes of this analysis, the variously concevied reaction routes to silicon were divided into classes or types. The thermodynamic feasibility of each reaction was then calculated upon the very well established laws of thermodynamics.

If one considers a reversible reaction between ideal gases of the type

$$A(g) + B(g) \underset{k^1}{\overset{k}{\rightleftharpoons}} C(g) + D(g),$$

the rate of formation of C and D equals $k\, p_A p_B$ and the rate of formation of A and B equals $k^1\, p_C p_D$, where p_i is the partial pressure of species i in atmospheres. At equilibrium the forward and reverse rates are equal and

$$\frac{p_C p_D}{p_A p_B} = \frac{k}{k^1} = K = \text{equilibrium constant.}$$

The equilibrium constant is also related to the Gibbs free energy of reaction, $\Delta G^{\circ}_{R,T}$, through the following relationship

$$\Delta G^{\circ}_{R,T} = -RT\ln K$$

where R is the ideal gas constant and T is the absolute temerature. This free energy of reaction is conveniently calculated from readily available tabulated standard free energies of formation, ΔGf°_{T}, of the reacting species. The sources of these data are indicated on the appropriate Figures and Tables. The free energy of reaction is simply the sum of free energies of the products minus the sum of the free energies of the reactants, or,

$$\Delta G^{\circ}_{R,T} = \sum_i \nu_i \Delta Gf^{\circ}_{T,i}$$

where ν_i is the stoichiometric coefficient.

The relationship between the free energy change and the degree of completion of the reaction which results in the conversion of A and B to C and D is shown in Fig. 4 at temperatures of 298°, 1000°, and 2000°K for the particular reaction considered.* For $\Delta G^{\circ}_{R,T}$ = 10 kcal/mol, conversions reach no higher than about 21% over the temperature range considered. The significance of the relationship between $\Delta G^{\circ}_{R,T}$ and both the extent of a reaction and the equilibrium constant is further accentuated in Table 1. It is clear that if the free energy contained in the products from a reaction is much more than that contained in the reactants, the reaction cannot proceed to any appreciable extent. As a general guide line for the screening procedure, then, it is considered safe to say that any reaction for which $\Delta G^{\circ}_{R,T}$ is greater than 10 kcal/mol is infeasible from a commercial point-of-view.

Chemical reactions for which $\Delta G^{\circ}_{R,T}$ values are small or negative must be regarded as <u>potentially</u> able to take place. Negative ΔG°_{R} values for any process are no assurance that the chemical process will take place. It will take place only if a mechanism is available. This is the field of chemical kinetics.

All of the results discussed in this section deal with the chemical potential of a given reaction as written. The free energy change of each reaction is given as a function of

---

* Different relationships arise depending upon the nature of each individual reaction.

temperature. The general coordinate system for reporting many of the results is shown in Fig. 5. Note that the shaded area is the region for infeasible chemical reactions. The negative of the free energy change has been plotted so that favorable curves have a positive slope with increasing temperature.

The sources of the free energy data used are indicated on the individual Figures and Tables. Where condensed phases are involved, such as $SiO_2(c)$ and $Si(c)$, the "c" designation refers to condensed. Calculations were made using solid phase data since free energies of condensed phase transitions are normally small. This minor approximation does not affect the feasible-nonfeasible decision.

Results Of Thermodynamic Screening

a. Pyrolysis

The free energy changes in Fig. 6 for the pyrolysis of SiO_2 and many of the halosilanes SiH_nX_{4-n}, where X =F, Cl, Br, and I and where n=0→4. These reactions are of the type

$$SiO_2(c) = Si(c) + O_2(g)$$

$$SiX_4(g) = Si(c) + 2X_2(g)$$

$$SiHX_3(g) = Si(c) + X_2(g) + HX(g)$$

$$SiH_2X_2(g) = Si(c) + 2HX(g)$$

$$SiH_3X(g) = Si(c) + H_2(g) + HX(g).$$

As would be expected, SiF_4 and SiO_2 pyrolysis to silicon is completely impossible. The pyrolysis of the remaining compounds becomes more favorable as X goes from F → I and n goes from 0 → 4, as has been proven by experimental data in the literature.

Those compounds that can be feasibly pyrolyzed below a temperature of 2000K are SiI_4, $SiHI_3$, SiH_2X_2, SiH_3X, and SiH_4.

b. Reduction By Nonmetals

The free energy changes for the reduction of silica by the nonmetals H_2, C, S, and P are shown in Fig. 7 for the following reactions

$$SiO_2(c) + 2H_2(g) = Si(c) + 2H_2O(g)$$
$$SiO_2(c) + 2C(s) = Si(c) + 2CO(g)$$
$$SiO_2(c) + C(s) = Si(c) + CO_2(g)$$
$$SiO_2(c) + 2S(s) = Si(c) + 2SO(g)$$
$$SiO_2(c) + S(s) = Si(c) + SO_2(g)$$
$$SiO_2(c) + P(c) = Si(c) + PO_2(g)$$
$$SiO_2(c) + \frac{4}{5}P(c) = Si(c) + \frac{1}{5}P_4O_{10}(g)$$

The only possible reactions for producing silicon are those involving carbon as reductant. Of these, the much more favorable one is the overall reaction generally considered as representing the process occuring in the present-day arc-furnace process.

Free energy changes for the reduction of the tetra - and trihalosilanes by hydrogen are presented in Fig. 8 for the reactions

$$SiX_4(g) + 2H_2(g) = Si(c) + 4HX(g)$$
$$SiHX_3(g) + H_2(g) = Si(c) + 3HX(g).$$

Similar reactions involving the more hydrogenated halosilanes are in fact pyrolysis reactions rather than hydrogen reductions.

As is confirmed by experimental data in the literature, the chloro-, bromo- and iodosilanes are feasibly reduced by hydrogen at temperatures about 1000 degrees lower than the fluorosilanes.

Silicon production by nonmetal (except H_2) reduction of SiF_4 and $SiCl_4$ were found to be infeasible for the reactions below.

$$SiF_4(g) + C(s) = Si(c) + CF_4(g)$$

$$SiF_4(g) + \frac{2}{3} S(c) = Si(c) + \frac{2}{3}SF_6(g)$$

$$SiF_4(g) + S(c) = Si(c) + SF_4(g)$$

$$SiF_4(g) + \frac{4}{3} P(c) = Si(c) + \frac{4}{3}PF_3(g)$$

$$SiCl_4(g) + C(s) = Si(c) + CCl_4(g)$$

$$SiCl_4(g) + \frac{4}{3}P(c) = Si(c) + \frac{4}{3} PCl_3(g)$$

The free energy changes appear in Table 2 for temperatures of 298, 1000, and 2000 K. Additional reactions involving $SiCl_4$, or $SiBr_4$ and SiI_4, were not included since thermochemical data for the high temperature, gaseous, nonmetal halides are not available. The trends in Table 2 indicate that any such reactions would also be infeasible.

c. Reduction By Metals

Free energies of reaction are shown in Table 3 for the reduction of silica by forty different metals to give both elemental silicon and the corresponding metal oxide in their solid state according to the general reaction:

$$4/n\ M(s) + SiO_2(s) = Si(s) + \begin{cases} 2/n\ M_2O_n(s), & n = \text{odd} \\ 4/n\ MO_{n/2}(s), & n = \text{even} \end{cases}$$

Transition points for the metal oxides are indicated, should they be needed for other considerations later. The metals are listed here, and in later tables and figures, according to group number as one progresses from left to right across the long form of the periodic chart. The free energy data for the metal reduction of silica also appears in bar-graph form in Fig. 9 for a temperature of 298 K. This temperature was chosen since more data is tabulated in the literature at 298 K and because the free energies are not very temperature-dependent over the 298 to 1000 K range presented here. In addition, the free energies tend to become less favorable at higher temperature.

Figure 8 shows that several groups of metals from the periodic chart are capable of reducing silica to silicon: groups IIA, IIIB, IVB, and the rare earths. Aluminum and gallium are also feasible reductants. Somewhat surprising, however, is that only lithium is a feasible reducing agent from the group IA elements. This indicates that the strong electropositive nature of the alkali metals is not a sufficient criterion by itself for judging reaction potential.

Free energies of reaction are presented in Table 4 for the proposed reduction of gaseous silicon tetrafluoride by various metals to yield solid silicon and the corresponding metal fluoride, in the indicated physical state, according to the general reaction,

$$4/n\ M(s) + SiF_4(g) = Si(s) + 4/n\ MF_n.$$

The bar-graph presentation of this data appears in Fig. 10 The feasible metal reductants are very similar to the oxide case: groups IA, IIA, IIIB, IVB, the rare earths, and aluminum.

Free energy of reaction data for the reduction of $SiCl_4$ to silicon are given in Table 5 and Figure 11 in exactly the same way as for SiF_4. Data are for the general reaction:

$$4/n\ M(s) + SICl_4(g) = Si(s) + 4/n\ MCl_n$$

In addition to the feasible metal reductants listed above for SiF_4, it is possible to also include Cr, Mn, Zn, and Cd. Other metals that are somewhat marginal as indicated by their free energies, especially at high temperatures, are Fe, Ga, Sn, and Pb.

Silicon tetrabromide has been included in this report for completeness sake even though its availability is much lower as compared to SiF_4 and $SiCl_4$. The free energies of reaction for the reduction of $SiBr_4$ to silicon are listed in Table 6 and Figure 12 according to the reaction:

$$4/n\ M(s) + SiBr_4(g) = Si(s) + \$/n\ MBr_n$$

The feasible reductants for $SiBr_4$ are the metals from groups IA, IIA, IIIB, IVB, and the rare earths, in addition to Al, Cr, Mn, Zn, Cd. Marginal metal reductants, especially at higher temperatures, are Fe, Co, Ni, Cu, Sn, and Pb.

d. Reduction By Compounds

The potential of using the somewhat common compounds CH_4 and NH_3 to reduce SiO_2, SiF_4, and $SiCl_4$ according to the following reactions are demonstrated in Fig. 13.

$$SiO_2(c) + \frac{4}{5}NH_3(g) = Si(c) + \frac{4}{5}NO(g) + \frac{6}{5}H_2O(g)$$

$$SiO_2(c) + \frac{2}{3}CH_4(g) = Si(c) + \frac{2}{3}CO(g) + \frac{4}{3}H_2O(g)$$

$$SiF_4(g) + \frac{1}{2}CH_4(g) = Si(c) + 2HF(g) + \frac{1}{2}CF_4(\ )$$

$$SiCl_4(g) + \frac{1}{2}CH_4(g) = Si(c) + 2HCl(g) + \frac{1}{2}CCl_4(g)$$

As might be expected, SiF_4 is too stable to be reduced while the other reactions begin to show promise only in the 2300 - 3000 K temperature range. Therefore, these reactions are of little interest.

Early thoughts concerning new routes to silicon suggested that recycle-type reactions of the kind below might be low cost processes if the metal oxide or halide could be recycled.

$$SiO_2 + MO \longrightarrow Si + MO_3$$

$$\uparrow -O_2 \quad \text{(recycle)}$$

$$SiX_4 + 2MX \longrightarrow Si + 2MX_3$$

$$\uparrow -2X_2 \quad \text{(recycle)}$$

Investigation into reactions of the type above made it clear that the lower-valent (i.e. semireduced) metal compounds of interest only existed in the gas phase at high temperatures and, hence, must be generated by an additional high temperature reaction. The need for a partially reduced compound is clear in that it must be readily oxidizable in order to reduce the silicon compound.

It becomes apparent that reactions of the type above do not represent low cost routes to silicon when the additional reaction is considered by which the semireduced intermediate is prepared. The overall reaction is demonstrated below by summing the reduction reaction and the semireduced, intermediate preparation reaciton.

$$SiO_2(s) + 4\,AlO(g) \longrightarrow Si(s) + 2Al_2O_3(s)$$

$$2Al_2O_3(s) \longrightarrow 4AlO(g) +)O_2(g)$$

$$SiO_2(s) \longrightarrow Si(s) + O_2(g)$$

In essence, an attempt was made to carry out the overall infeasible reaction by using two reactions. Therefore, recycle type reactions are more difficult processes for attempting to carry out a one-step simpler process. A similar case is shown below for the reduction of $SiCl_4$.

$$SiCl_4(g) + 2AlCl(g) \longrightarrow Si(s) + 2AlCl_3(g)$$

$$2AlCl_3(g) \rightarrow 2AlCl(g) + 2Cl_2$$

$$SiCl_4(g) \longrightarrow Si(s) + WCl_2\,(g)$$

Since compounds of electropositive elements such as aluminum are known not to readily disproportinate to products in which free O_2 or Cl_2 are present, one is tempted to consider a more obious preparation of the semireduced intermediate by reacting the fully oxidized compound with excess metal. Again, however, this turns out to be a more complex way to carry out a simpler reaction as shown below.

$$SiO_2(s) + 4AlO(g) \longrightarrow Si(s) + 2Al_2O_3(s)$$

$$\frac{4}{3}\,Al_2O_3(s) + \frac{4}{3}\,Al(s) \longrightarrow 4AlO(g)$$

$$SiO_2(s) + \frac{4}{3}Al(s) \longrightarrow Si(s) + \frac{2}{3}Al_2O_3(s)$$

$$SiCl_4(g) + 2AlCl(g) \longrightarrow Si(s) + 2AlCl_3(g)$$

or $$\frac{2}{3}AlCl_3(g) + \frac{4}{3}Al(s) \longrightarrow 2AlCl(g)$$

$$SiCl_4(g) + \frac{4}{3}Al(s) \longrightarrow Si(s) + \frac{4}{3}AlCl_3(g)$$

In both cases, the overall reaction is simply the straight forward metal reduction of the silicon starting material.

Summary of Thermodynamically Feasible Reactions for Reduction

Listed below are those reactions just considered which have favorably filtered thorugh the thermodynamic screening process. It is only these feasible reactions that are further considered in the economic screening process. The remaining reactions are infeasible and will not be pursued any farther.

Pyrolysis Reactions

SiI_4 →

$SiHI_3$ →

SiH_2X_2 →

SiH_3X →

SiH_4 →

Reduction by Nonmetals

$SiO_2 + C$ →

$SiX_4 + H_2$ → (except X = F)

$SiHX_3 + H_2$ → (except X = F)

Reduction by Metals

$SiO_2 + M$ → (see Table 7 for M)

$SiX_4 + M$ → (see Table 7 for M)

Transport

SiF_2 →

$SiCl_2$ →

SiO →

C. Economic Screening

Economic analysis requires a more refined definition of the product silicon at this point. Two distinct approaches exist for preparing SoG-Si for array fabrication. In one case bulk silicon is transformed into sheet form, where-as in the other, silicon is epitaxially deposited onto a substrate. In the latter case, epi-layers with thicknesses in the range of microns represent only a small fraction of the overall cost as compared to the substrate. Therefore, any of the processes being considered are economically feasible for preparing epi-silicon. The following economic analysis is, then, oriented toward bulk silicon where raw materials are a major contributor to the overall cost.

Economic analysis at this early stage is only based upon raw materials, since well-defined chemical processes do not exist for most of the proposed reactions. Since raw materials make up only a relatively small percentage of the total cost or selling price of the product silicon (e.g. see Table 8 , it is not possible to precisely compare all proposed reactions. Some economic screeing can be done, however, because an upper limit of $10/kg has been set for the cost of SoG-Si.

Material prices appear in Table 9 for many of the reactants involved in the reactions being considered. The listed material prices are also compared upon either their dollar value per kilogram of contained silicon or upon their dollar value to stoichiometrically produce one kilogram of silicon from one of the silicon-containing raw materials discussed in the Section on reduction by nonmetals. Since prices change drastically in times of high inflation, it must be assumed that the prices listed in Table 9

will increase in about the same ratio relative to one another. When this assumption is no longer valid, an updated price comparison must be made. It is also stressed that todays prices are determined by the current supply and demand situation. The creation of a 100,000 ton/year SoG-Si business could conceivably change the price of what is now a plentifully abundant and low cost raw material.

The materials listed below SoG-Si in Table 9 can be eliminated immediately since their prices, per kilogram of silicon, are higher than the $10/kg price goal of bulk SoG-Si itself. Since economic analyses of the MG-Si and SoG-Si businesses indicate that raw materials make up a relatively small portion of the selling prices of elemental silicon, it is considered very conservative to say that raw materials must compose less than 25% of the MG-Si price, i.e. < $2.50/kg Si. This, then, eliminates all materials except those shown in Table 10 as possible reactants for the preparation of SoG-Si.

Definite decisions concerning the fluorosilanes SiH_2F_2 and SiH_3F are difficult due to the lack of published economic information. They are expected to be considerably more expensive than SiF_4, however, when one considers the high price ratio of $SiH_2Cl_2/SiCl_4$ which is 88. Applying this ratio to SiF_4 puts SiH_2F_2 at a relative price of 1500. Even higher prices would be expected for the fluorine compounds due to the higher corrosive problems experienced compared to the chlorine compounds. The pyrolysis of SiH_2F_2 and SiH_3F are, therefore, eliminated from further consideration.

The material prices in Table 9 also allow the rejection of many of the other halosilanes as silicon sources. If one assumes the $SiBr_4/SiCl_4$ price ratio is the same as the $SiCl_4/SiF_4$ ratio, the calculated relative price of $SiBr_4$ at 440 closely approaches that of SoG-Si at 530. Since bromine is 350 times less

abundant than chlorine in the lithosphere, the actual price of $SiBr_4$ would even be higher. Therefore, $SiBr_4$ and SiI_4 are economically ruled out as starting materials for the preparation of SoG-Si. If one further compares the price of technical-grade $SiCl_4$ and $SiHCl_3$, it is also possible to eliminate the other bromo- and iodosilanes as economically interesting raw materials.

The only remaining silicon-containing materials for the production of SoG-Si at this point are SiO_2, SiF_4, $SiCl_4$, and MG-Si. The remaining metals to be considered for reducing SiO_2 are Al and Mg while Na is an additional alternative for reducing SiF_4.

D. Technological Screening

The amount of technical information available concerning possible processes for conducting the twelve reactions surviving the economic screening step varies from near zero for some processes to sufficiently complete for others. The reaction in Table 10 involving the silicon intermediate $SiCl_4$ can be eliminated from further consideration when one compares it to $SiHCl_3$ which is used to produce semiconductor silicon at a price of about \$70/kg. Since the theoretical as well as experimental conversion efficiency of $SiCl_4$ to silicon is considerable lower than that for $SiHCl_3$ under conditions used to commercially produce polycrystalline silicon (1,2), the greater thermal stability of $SiCl_4$ causes silicon to be deposited more slowly and, of course, at a higher cost. Use of increased temperature to offset the greater $SiCl_4$ stability also results in higher costs due to increased energy usage per kilogram of silicon. Therefore, $SiCl_4$ is considered infeasible for the production of SoG-Si since the resulting silicon would be more expensive than the \$70/kg Si process using $SiHCl_3$.

The plurality of reactions in Table 10 involve the conversion of silica to the intermediate, high-temperature species silicon monoxide using reductant, R, according to the reaction

$$SiO_2(s) \xrightarrow{R} SiO(g).$$

The SiO might then be transported to another reaction zone where reduction would be compleged to silicon according to the reaction

$$SiO(g) \longrightarrow Si(s).$$

Although a large amount of literature exists on various aspects of gaseous SiO, very little is concerned with its reduction to silicon. In addition, nothing has been reported concerning the transport efficiency of impurity oxides from SiO_2 to Si along with the SiO

intermediate. In fact, no known data have been reported concerning the actual transport of SiO; e.g., as to what the half-life is of this gaseous species as a function of system temperature and pressure. A further complication is the formation of a metastable solid upon condensation of Sio vapors. This material is thought to be an amorphous mixture of SiO_2(s) + Si(s) rather than SiO(s). When this material is heated it disproportionates to silicon and silica with the reaction rarely having been observed to go to completion. We do not believe that a silicón monoxide process could meet the ERDA time goals for producing low-cost SoG-Si due to the considerable research and development effort that would have to be applied to obtain necessary data and to circumvent some of the problems indicated above. In short, neither sufficient time nor money is available to properly analyze the technical feasibility of a silicon monoxide process which is required to be at pilot scale in 1980 and at a large plant scale in 1985.

A major problem associated with carrying out the aluminum reduction of SiO_2, see Table 10, is that the produced silicon will be contaminated by the p-type aluminum reductant. This contamination problem is particularly accentuated by the low melting point of aluminum (660°C) since most silicon production processes are carried out at temperatures near or above that of the melting point of silicon (1410°C). The molten aluminum drains to the bottom of the chemical reactor and alloys with silicon rather than remaining intimately mixed in the reaction bed with SiO_2. Smith (3) has described process details for separating silicon from silicon-aluminum alloys. After nucleation and growth of silicon crystals from the melt over a 6-48 hour period, the crystals are separated by either high-temperature filtration, high-temperature centrifugation, by pulling single crystals from the molten alloy, or by dissolving the excess aluminum in acid. The pure silicon crystals must then be separated from adhering aluminum impurities by acid washing. The crystals are then subjected to desliming, filtering, washing, and

flotation. Finally they are acid washed again before a second flotation. The final unspecfied silicon purity is attained through either further chemical treatment or float-zone refining. The large number of purification processes outlined above point out the difficulty of upgrading alloy-grade silicon to a purity level necessary for the solar cell or semiconductor industry. One further comment concerning the use of aluminum as a reductant involves its energy content. It requires 175 kWh (4) of equilvalent coal energy to produce the aluminum that is required to yield one kilogram of silicon metal according to the following reaction assuming it proceeds to completion:

$$SiO_2 + 4/3\ Al \rightarrow Si + 2/3\ Al_2O_3.$$

This energy is considerably higher than the 65 kWh (5) of equivalent coal energy necessary to produce one kilogram of MG-Si via the arc furnace process. The degree to which the higher energy intensive aluminum increases the energy pay-back time for silicon cells is not known due to the general lack of information pertaining to total energy usage from SiO_2 to finished solar cell. In conclusion, then, it is not planned to further pursue the aluminum reduction of SiO_2 due to the anticipated process, purification, and energy difficulties described above.

The transport reaction in Table 10 involving the high-temperature species SiF_2 will not be considered independently at this point. It is being considered by the University of Pennsylvania and Motorola as a possible alternative for the upgrading of MG-Si which is actually the product of the more basic process of reducing SiO_2 with carbonaceous materials.

The preceeding method for technologically screening the reactions listed in Table 10 has eliminated all the reactions with the exception of the present-day, commercial process for producing MG-Si

which sells on the market place at approximately $1.00/kg; this is one order-of-magnitude lower than the ERDA goal for SoG-Si. The next section details Dow Corning's approach for upgrading MG-Si to solar-grade quality within the ERDA goal of $10/kg. It is this process which Dow Corning recommends for the production of solar cell silicon.

E. Metallurgical Grade Silicon Purification

The previous section, for the most part, discussed the technical feasibility of reactions by which some unknown grade of silicon might be able to be prepared on an experimental basis. The probability of these processes surviving through the research and development phase to pilot plant scale and eventual large plant commercialization becomes less and less favorable as the level of scale-up increases. It is partially for this reason that Dow Corning recommends upgrading of the MG-Si process as the means of achieving SoG-Si because the submerged-electrode, arc furnace process is capable today of producing MG-Si at rates in excess of 10,000 metric tons/year per furnace for a selling price of $1.00/kg. A process already exists by which only one furnace is capable of producing five times the estimated requirement for SoG-Si in 1985. This implies that no research and development time need be spent on proving whether or not silicon can be produced by this concept. The R&D efforts can be concentrated on methods by which the silicon produced in the primary reduction process can be upgraded to solar-grade quality. Essentially, then, what is required in MG-Si purification is the upgrading of an existing process rather than development of a new process all the way from the concept stage. The simpler the upgrading process can be made, the more certain will be the attainment of cost and time goals. Meeting the cost goal appears particularly favorable in view of the MG-Si selling price being a factor of ten lower than the $10/kg ERDA goal.

The concept, experimental plan, and results to date for the approach by which Dow Corning is pursuing MG-Si purification is con-

cisely given in Appendix A; this is a preprint of a paper to be presented at the International Symposium on Solar Energy at the May, 1976 Meeting of The Electrochemical Society. In summary, a collection of proven processes is being assembled such that the sum of the individual purification steps provides silicon of solar-grade quality. This collection involves (a) use of purified raw materials in the arc furnace, (b) use of purer materials-of-construction associated with the arc furnace production of MG-Si, (c) gas refining and slagging of the molten silicon after it is tapped, (d) acid leaching of the solidified material, and (e) unidirectional solidification.

The success of using gas refining, acid leaching, and unidirectional freezing for MG-Si purification is demonstrated in Appendix A. Results obtained, after termination of program funding, from the sequential treatment of MG-Si by slagging and acid leaching are indicated in Table 4. These impurity analyses are compared to data from typical MG-SI (6) and to proposed maximum impurity levels allowable in SoG-Si (7). Except for boron and phosphorus, all impurity levels in the upgraded material are either near or below the maximum limits suggested for SoG-Si Either optimization of the slagging-acid leaching technique or implementation of one of the other upgrading processes will cause the remaining impurities to be reduced significantly below the suggested limits. The success of this overall approach is further exemplified by the data in Table 12 for MG-Si that was upgraded by acid leaching followed by one Czochralski pull. The aluminum level could have been easily reduced beforehand by refining the molten silicon with chlorine. Boron and phosphorus levels may be reduced through use of purer arc furnace raw materials as indicated by the paper in Appendix A. The indicated paper also suggests that a boron level of 0.3 ppma may be an acceptable upper limit in solar-grade material.

F. The SiF_4 Silicon Transport and Purification Process

1. Introduction

Silicon tetrafluoride, a toxic and colorless gas under ordinary conditions, is produced in large quantities as an unwanted by-product of the processing of phosphate rock to produce superphosphate and other fertilizer materials. The superphosphate process consists basically of treating the phosphate rock with sulphuric acid. The reaction of one of the constitutents (CaF_2) of the rock with the acid results in:

$$CaF_2 + H_2SO_4 \longrightarrow 2HF + CaSO_4$$

The hydrogen fluoride then reacts with the silica present in the rock to yield SiF_4:

$$4HF + SiO_2 \longrightarrow SiF_4 + 2H_2O$$

Because of its toxicity, the silicon tetrafluoride is removed from the effulent gases by reacting with water to form fluosilicic acid.

Silicon tetrafluoride is the basic compound used in a new process for the purification and transport of silicon which is presently under investigation at the University. The availability of the compound in large quantities from the phosphate treatment process is one of the factors which contributes to the attractiveness of the fluoride transport process as a low cost technique. A second contribution to the potential cost effectiveness of the technique is the cyclic nature of the process which, in principle, will allow the continued recycling of the silicon tetrafluoride with very little loss (i.e., the silicon tetrafluoride is not consumed).

The basic chemistry of the transport process is summarized by

$$\text{heat} + \text{Si}_{(\text{solid})} + \text{SiF}_4\ (\text{gas}) \rightleftharpoons 2\text{SiF}_2\ (\text{gas})$$

Either an increase in temperatures or a decrease in pressure or both will shift the equilibrium further to the right. This equilibrium may be broken down into the two separate steps below which are utilized in silicon fluoride transport process.

$$\text{Si(solid)} + \text{SiF}_4\text{(gas)} \xrightarrow{1150^\circ\text{C}} 2\text{SiF}_2\text{(gas)} \qquad \text{(d)}$$

$$2\text{SiF}_2\text{(gas)} \xrightarrow{500^\circ\text{C}} \text{Si(solid)} + \text{Sif}_4\text{(gas)} \qquad \text{(e)}$$

The SiF_4 reacts with metallurgical grade silicon at 1150°C or higher to yield SiF_2 which in turn decomposes at 500°C resulting in a deposit of solid silicon and SiF_4 gas. A complete cycle of the process is then

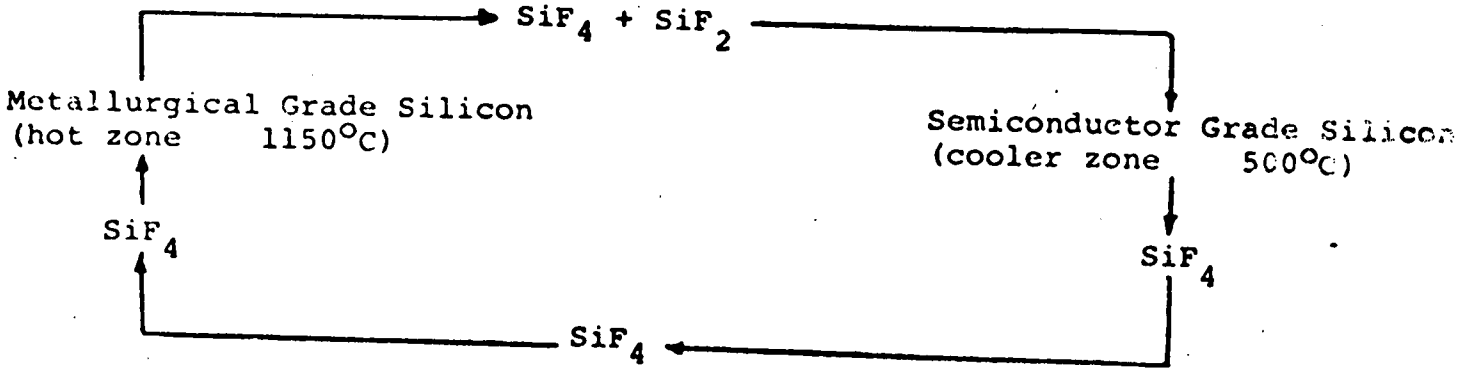

At higher pressures (~1 atmosphere) and lower temperatures ($\leq 25^\circ$C) other reactions are possible which result in the formation of compounds with the general formula $Si_x F_{2x+2}$. These compounds may dominate the transport process under those conditions.

The product formed from the reaction of SiF_4 with impurities in the Si will be principally metal fluorides. These have much higher boiling points than, for example, metal chlorides (which would be formed if $SiCl_4$ were used instead of SiF_4) and hence can be condensed from the silicon dihalide gas stream very much more easily. For this reason, the fluoride transport process is felt to offer high potential as a purification technique for metallurgical grade silicon.

The University's research on the transport process during the past two years has been aimed at characterizing the important rate controlling parameters of the reaction, demonstrating the potential for purification by the process, and identifying the chemical species which participate in the transport process under realistic operational conditions. The following material briefly summarizes the key results of this work.

2. Summary of Results of Initial Investigations

a.) Low Pressure Investigations

i. Experimental Apparatus

The experimental apparatus used in this work is depicted in Figure 14. A quartz tube (Q_1) of dimensions 20 mm I.D. and 100 cms length was placed inside of a tube furnace (F_1). The quartz tube was filled with a column (22 cms long) of crushed metallurgical grade silicon obtained fom Fischer Scientific Co. The silicon lumps were of dimension 3 mm x 8 mm and filled the column up to the hottest zone in the furnace. One end of the quartz tube was connected to a vacuum system and the other end was connected to a vacuum system and the other end was connected to pretreatment furnace F_{pt} which in turn was connected to SiF_4 gas bulb B. The system was evacuated completely and SiF_4 was heated to attain a constant temperature of 1150°C. SiF_4 was passed over hot pure iron in another quartz tube (Q_2) maintained at 800°C in the furnace F_{pt} (in some experiments silicon was used instead of the iron wire). This treatment removed traces of oxygen and sulphur dioxide from the SiF_4. Then SiF_4 was

passed through the hot column of crushed silicon. Gases coming out of the quartz tube Q_1 travelled thorugh approximately 5 feet of glass tubing at room temperature before they were led into a quartz trap T_1 maintained at a temperature in the range of 500°-600°C in the furnace F_2. In trap T_1, disproportionation of SiF_2 took place and pure silicon was deposited on the walls of the trap. Residual gases which contained mostly SiF_4 and traces of SiF_2 were collected in the trap T_2 which was maintained at liquid nitrogen temperature (-196°C). Both traps T_1 and T_2 could be detached from the vacuum system and were weighed to determine the amount of SiF_4/SiF_2 condensed and the amount of pure silicon deposited.

The amount of SiF_4 passed through the system was measured by recording the pressure drop in the manometer M, attached to the gas bulb B. Throughout the experiment the system was continuously pumped by the vacuum pump.

ii. Results and Discussion

In these experiments the absolute pressure of the SiF_4 was approximately 0.2 mm Hg and the flow rate was maintained at about 33 mg of SiF_4 per minute. The experiments were designed to explore the temperature range over which reaction (e) could be expected to occur to a significant degree (i.e., to yield significant amounts of silicon), to determine also the constituents of the gas evolving from the reaction tube and their relative proportions, and, thirdly, to investigate the character of the silicon films deposited from the transport stream.

In the experimental investigation of the disproportionation reaction the system was operated as outlined above, with the heated trap T_1 (Figure 14) maintained at temperatures ranging from slightly below 450°C to slightly above 750°C. It was found that no detectable silicon deposits occurred in the trap when it was maintained at temperatures below 450°C and above 750°C. Only negligible deposits were observed when the trap temperature was held exactly at one or the other of these temperatures (although signifi-

cant deposits occurred in cooler parts of the trap when its peak temperature was 750°C). The maximum deposition, as determined by the optical density of the deposited film, was obtained when the temperature was in the vicinity of 500°C. It is clear from this that reaction (e) is significant only in a relatively narrow temperature range and that the most favorable temperature for the reaction is in the vicinity of 500°C. The constitution of the gas mixture exiting from the reaction tube was investigated by first condensing the gas in a cold trap maintained at liquid nitrogen temperature (-196°C). The relative proportions of the two constituents (SiF_4 and SiF_2) was then determined by measuring the amount of SiF_4 evolved on warming and the weight of the remaining, non-volatile, polymer $(SiF_2)_x$. Based on these data a conversion factor of 50% for the transformation of SiF_4 to SiF_2 (i.e., 66% of the exiting gas was SiF_4) was calculated for the specified conditions (i.e., a pressure of 0.2 mm Hg and a reaction temperature of 1150°C). This figure is in close agreement with the results quoted by Margrave and co-workers, however, it should be noted that significant deposits of silicon (resulting from SiF_2 disproportionation) occur in the exit end of the reaction tube at the location corresponding to a temperature of about 500°C.

Inspection of the silicon deposited in the cooler portion of the reaction tube and in the heated trap indicates that the morphology ranges fron dendritic crystallites through polycrystalline films to "amorphous" silicon under the condition used in these tests. There is some evidence that the formation of "amorphous" deposits is favored at the higher end of the deposition temperature range.

The low pressure regime of operation was used initially because the work of Margrave, et.al., indicated that the efficiency of conversion of SiF_4 to SiF_2 is more faborable at these pressures. This supposition is born out by the theoretically determined curves of Figure 15. Concurrent with the low pressure experiments, calculations of the maximum absolute silicon transport rate were made for this mode of operation. These calculations revealed that for the gas pressures used, and the conversion efficiencies of Figure V-2, an

SiF_4 flow velocity approaching the supersonic would be require to effect transport rates which would allow the growth of silicon sheet at a rate compatible with the rate set as a goal for this program. These results prompted a closer examination of the pressure variation of both the percent conversion of SiF_4 to SiF_2 and the absolute amount of SiF_2 per unit volume of gas along the following lines.

If α is the fraction of moles of SiF_4 converted to SiF_2 then at equilibrium there will be $(1-\alpha)$ moles of SiF_4 and (2α) moles of SiF_2. That is:

$$\underset{(1-\alpha)}{Si(s)} + \underset{(1-\alpha)}{SiF_4(g)} \rightleftharpoons \underset{2\alpha}{2SiF_2(g)}$$

Then the total number of moles of gas is: $1-\alpha+2\alpha = 1+\alpha$

The fraction of SiF_4 at equilibrium is then: $\frac{1-\alpha}{1+\alpha}$

and the fraction of SiF_2 at equilibrium is: $\frac{2\alpha}{1+\alpha}$

If the total pressure of the system is P atmospheres then the equilibrium constant in terms of the partial pressures of the gases can be expressed as

$$K_P = \frac{P^2_{SiF_2}}{P_{SiF_4}} = \frac{\left(\frac{2\alpha}{1+\alpha} \cdot P\right)^2}{\left(\frac{1-\alpha}{1+\alpha} \cdot P\right)}$$

which reduces to: $K_p = \frac{4\alpha^2}{1-\alpha^2} \cdot P$

Transposing, one obtains:

$$\alpha = \left[\frac{K_p}{K_p + 4P_{total}}\right]^{\frac{1}{2}}$$

also:

$$P_{SiF_2} = \left[K_p \, P_{SiF_4}\right]^{\frac{1}{2}}$$

These latter two expressions show first that the fractional conversion of SiF_4 to SiF_2 decreases with the increase of total pressure and secondly that the partial pressure of SiF_2 will increase as the square root of the partial pressure of SiF_4. These results clearly indicate that the absolute amount of SiF_2 in the system could increase if the pressure of SiF_4 in the system is increased. It was further speculated that at higher pressures other reactions favorable to the deposition of elemental silicon might occur.

These findings prompted a switch of the experimental studies to higher pressure regimes.

b.) High Pressure (~ Atmospheric) Investigations

i. Experimental Apparatus

A more advanced apparatus for investigating the silicon fluoride transport process was constructed. The apparatus allows the measurement of both the amount of silicon deposited and the weight loss of the MG-Si charge. The system provides a full range of pressure (including above atmospheric) and flow rate control, with a maximum flow rate capability of approximately 3000 ℓ/h and is designed for fast turn-around. Provision has also been made for sampling of the circulating gas during the operation of the

system. The new system is shown schematically in Figure 16. The region in which the SiF_4 reacts with the MG-Si (high temperature region) consists of a 3 zone furnace with a relatively flat high temperature zone with a length of approximately 20 inches. The MG-Si is contained in a removeable quartz boat incorporating an integral gas seal which forces the SiF_4 to flow through the MG-Si. The present boat can hold a charge of approximately 1000 grams of MG-Si and larger boats can be accommodated. The silicon deposition region (low temeprature region) also consists of a furnace with three independently controllable zones and has a flat (thermally) zone length of approximately 17 inches. The removeable deposition tube is inserted into this region and slides onto a nozzle in the high temperature region which provides support and acts as a gas seal to prevent the flow of gas outside of the deposition tube. The two furnaces can be run with a separation between them. This "expands" the transition temperature region and allows a more accurate evaluation of the phenomena occurring at temperatures between the reaction and deposition temperatures. A diaphram type pump is used to recirculate the SiF_4 after it exits from the deposition region, and a mechanical type vacuum pump is used to evacuate the system prior to insertion of the SiF_4.

ii. Results

Using the new transport system, a series of experiments designed to characterize various aspects of the SiF_4/SiF_2 transport process was initiated. Most of this experimental work was conducted at a pressure slightly above atmospheric (780 mm Hg). The concentration of the work on higher pressure operation (in contrast to the earlier low pressure studies) is desirable since it was shown that the total silicon transport rate will increase with increasing SiF_4 pressure even though the efficiency of conversion of SiF_4 to SiF_2

decreases as the pressure increases.

The initial runs with the apparatus revealed some interesting facts. First, it was found that after the creation of the SiF_2 in the 1150°C zone no reverse reaction occurred until the gas moved through the remainder of the high temperature region to a region where the temperature drops below 1100°C. the first silicon deposition (at this pressure) occurs at a temperature slightly less than 1000°C and at a distance of separation from the MG-Si in the high temperature zone of approximately 10 inches. For the flow rates used in these experiments (40-80 ℓ/h at 300°K and 1 atmosphere) this implied a minimum lifetime of the SiF_2 at temperatures $\geq$ 1000°C of 1 second. In the temperature range between 1000°C and approximately 700°C (a distance of about 6 inches in the present set up) a relatively thick silicon deposit having a porous, brownish, amorphous appearance generally occurs. At temperatures between 700° and approximately 400°C a thinner silicon layer having a grayish color and a more crystalline appearance is deposited. This layer also extends under the amorphous appearing layer in the higher temperature region and hence is present throughout the entire region of deposition. Figure 17 is a cross sectional picture of a typical deposition tube showing the deposition regions outlined above. The deposition silicon layers are strongly adherent to the quartz deposition tube. This quite often leads to shattering of the tube in the case of thick deposits, due to the thermal expansion mismatch.

The maximum rate of transport (in terms of moles of Si deposited per mole of SiF_4 flow) observed during these high pressure experiments was approximately 8%, while the average was about 5%. These experiments also indicate that the percentage of the reacted silicon recovered in the reverse reaction ($2SiF_2 \rightleftharpoons Si + SiF_4$) can exceed 90% under the present configuration and operating conditions.

The maximum observed efficiency of converison of SiF_4 to SiF_2 was approximately 10%, with an average of about 7%. It is clear (as anticipated on the basis of the theoretical calculations) that the rate of the reaction between the SiF_4 and the MG-Si is the limiting factor here.

An experiment to test the hypothesis that the deposition of silicon in this process requires the catalytic assistance of certain impurities present in the quartz, and hence, will be limited by their depletion, was conducted. The test consisted of depositing for a fixed period of time (105 minutes) onto a deposition tube, stopping the reaction to measure the deposition on the tube, and replacing the tube to allow deposition to continue for a similar interval, etc. This was done for three successive 105 minute deposition intervals during one experiment. No significant change in the growth rate was observed during these experiments, indicating that the presence of impurities in the quartz substrate is probably not an essential factor to the growth process.

In another set of experiments, silicon was deposited on quartz plates and single crystal silicon wafers placed at strategic locations within the deposition tube. It was found that the deposit on these substrates duplicated that on the walls of the deposition tube in the immediate vicinity, both in terms of the amount of material deposited and its apparent structure (i.e. "amorphous" or crystalline). Deposits on the quartz and the silicon wafers appeared similar. In general, the amount of material deposited on a wafer located in the region of amorphous deposition was equivalent to a single crystal silicon layer of the order of 100-300 micrometers thick for a typical one hour run. For wafers positioned in the region in which a more crystalline appearing layer is deposited, the amount of material deposited is considerably less, ranging from about 1-4 micrometers. The deposits on the silicon wafers did not appear to be epitaxial and it is suspected that more careful surface preparation would be required to allow proper nucleation for epitaxial growth.

c.) Thermodynamic evaluation of the SiF_2 reaction

To relate the current work on the SiF_2 transport process to the thermodynamic studies on all Si Reactions and to previously published work on SiF_2, it was found necessary to analyze the approaches used by various workers in the field, particularly those of Margrave et al who published experimental data on SiF_2 formation and the derivation of the currently used value for the heat of formation of SiF_2 from these experimental values. Further, these studies permit certain predictions for the future applicability of this reaction as a large scale transport process. Details for such predictions have to be obtained, however, from experimental studies of reaction kinetics. The conclusions of the thermodynamic analyses can be summarized as follows:

1. The equilibrium constant values obtained in ref. 8 show a remarkable temperature independence in the 1400 to 1600 degree K range. This would indicate that the current experiments, carried out at 1423 degrees K, are likely to be representative of the anticipated future operations at 1700 degrees K for the SiF_2 formation region.
2. The pressure dependence of the equilibrium constant in ref. 8 may be an experimental artifact or an indication of the pressure of other species, such as SiF_3 or polymers for which several references are found in the literature.
3. The standard heat of formation values (T = 298 degrees K) for SiF_2 in ref. 8 may show a definite dependence on reaction temperature, about which the authors remark in their paper. The authors have not indicated how they arrived at their - very small - temperature dependence of the enthalpy and entropy data used in the computations. Using the current correction data for the enthalpies and and entropies of the species involved results in a reaction-temperature independent value of $\Delta Hf_{SiF_2,\ 298}$,

   which provides considerable confidence in the - unusual - temperature independence of the experimentally determined equilibrium constant.

4. The nature of the interrelation of the data is such that a less than 2% variation in the standard heat of formation of SiF_2 results in a factor of 4 change in the equilibrium constant for the formation of SiF_2 from SiF_4 and Si.
5. The amount of SiF_2 generated in a given volume in equilibrium increases with the square root of the total pressure in the system. For systems not deviating too far from equilibrium, their relationship may tentatively be assumed to hold also for the generation rate in a transport situation. More information can be obtained only after kinetic studies.
6. The observed high reaction rates at atmospheric pressure do not permit any new thermodynamic conclusions since they have not been obtained in equilibrium conditions.

3. Summary of Results of Current (Last Six Months) Investigations

a.) Materials Characterization and Purification

i. Background

The initial reason for investigating the SiF_4/SiF_2 transport process was to explore its potential as an economical means for purifying metallurgical grade silicon. During the earlier work, experi--ents and measurements designed to characterize the effectiveness of the process in separating key impurities were initiated. The measurements were of two types: emission spec. measurements were made at National Spectrographic Laboratories of Cleveland, Ohio and were aimed at characterizing the behavior of a wide range of metallic impurities. Because of the desire to cover a wide range of materials in the initial runs, the results of the preliminary measurements are semi-quantitative in nature (i.e. concentration levels are bracketed within specified limits rather than uniquely specified). Subsequent analyses will be restricted to a more limited range of elements and will allow accurate quantitative evaluation.

X-ray diffraction studies were performed at the university, using equipment available in the Laboratory for Research aon the Structure of Matter. The initial purpose of these studies was to characterize the morphology of the transported and deposited silicon, since there was some suspicion that both amorphous and crystalline

deposits could occur, depending on specific deposition parameters (primarily temperature and temperature gradient.). High concentrations of impurity elements and compounds can also be detected by this technique.

The analyses performed were designed to evaluate the separation occurring as a result of the basic transport process. The temperature profile used in preparing the samples for these tests was a straight-forward transition from a flat zone of 1150°C in the forward reaction region to a flat zone of 550°C in the deposition region. No attempt was made to provide additional purification by intermediate processes (making a room temperature transition for example). This, of course, will be the subject of future studies. Samples for the emission spec. studies were taken from the higher temperature portion of the deposition region (region of heaviest deposit) because of difficulties in separating the thinner deposits from the substrate without contamination. X-ray studies were performed on samples covering the entire length of the deposition region.

ii. Emission Spectrographic Analyses

For these studies, a sample of a specific lot of metallurgical grade silicon (the MG-Si was nominally 98.4% Si as supplied by Ventron) was submitted for analysis. Silicon from this lot was then used in several transport runs, and samples of the transported silicon from these runs were subsequently submitted for analysis.

Table 13 shows the results of the tests for the metallurgical grade silicon and for samples of transported silicon taken from two different transport runs. The concentration ranges are as designated by National Spectrographic. The two major impurities present in the metallurgical grade material are, as expected, iron and aluminum at a level of 0.1-1.0% atomic. Titanium and calcium are detected at a level approximately an order of magnitude below the primary impurities and below them are manganese, chromium, and vanadium.

Finally, detected at the trace level, are magnesium, nickel, copper, boron, and zirconium. This is followed by a large number of elements which were undetected. The limits of detection for the various elements are shown in Table 14. A few elements of interest (P for example) were omitted from these analyses. These will be included in future tests.

The two right hand columns show the concentration level of these elements in transported silicon from two runs. The results were essenstially identical for both runs. The aluminum, although reduced by about a factor of 10 from its concentration in the MG-Si, is the major metallic impurity present in this material. More will be said about this in the discussion of the X-ray diffraction results. Iron is reduced to a level somewhat below that of aluminum while titanium and calcium are both reduced to the trace level. Boron, chromium, nickel, and vandium are reduced below their limits of detection. Elements showing no significant separation include magnesium, copper, and zirconium. Sodium and barium, which were not detected in the metallurgical grade sample, appear at significant concentrations in the transported silicon. It is suspected that these impurities were introduced by the quartz tubing and other parts of the transport system rather than being increased in concentration by the transport process. This point will require further confirmation.

These results, while semi-quantitative in nature, clearly show that the concentration of a number of the important metallic elements are significantly reduced by the transport process without any attempt to induce impurity fall out through the use of special temperature profiles or distillation steps as discussed in this and earlier reports. This is an important result. More precise quantitative measurements and comparison with solar grade silicon specification will indicate to what degree special techniques will be required to effect the separation of some of the more tenacious elements. The results the x-ray diffraction tests, discussed below, have already shed some additional light in this area.

iii. X-ray Diffraction Measurements

In preparation for these measurements, a thin (2-4 mils) quartz fiber is supported in the center of the deposition tibe during a transport run, thus allowing deposition of the silicon on the fiber as well as the tibe. The fiber is then broken up into pieces suitable in size for use in the diffraction camera, and each piece is catalogued according to its location in the deposition region. Each piece is subjected to x-ray diffraction and the resulting patterns analyzed. Two significant facts were revealed by these analyses. First, it appears that the silicon deposited is polycrystalline no matter which temperature region it occurs in. There was some suspicion, based primarily on physical appearances and color, that the silicon deposits in some temperature regions were amorphous. Secondly, aluminum trifluoride (AlF_3) was found to be present in some areas in significant enough quantities to be detected in the x-ray analysis. Aluminum was shown to be the major impurity present after transport by the emission spec. Analysis. The x-ray results indicate that it is present primarily as AlF_3 and has been transported in this form from the MG-Si. The AlF_3 is not present in detectable amounts (by x-ray diffraction) in the higher temperature deposits (greater than $700^{\circ}C$), but the concentration increases as the temperature is reduced and its highest at the exit end of the $550^{\circ}C$ furnace ($T \sim 500^{\circ}C$). The preferential deposit of the AlF_3 at low temperatures is promising in that the possibility of its removal by a rapid transition to room temperature is indicated. It is also conceivable that the aluminum may be removed from the metallurgical grade silicon by one of the earlier stage treatmenst which have been suggested (reactive gas blowing of the MG-Si melt for example). Chemical and Spectrographic analyses also indicate that the following elements are preferentially deposited at the lower temperatures; Mg, Ca, Tk, Cu, Ni.

As part of the effort to evaluate the purification capabilities of the SiF_4 transport process analytical studies of the formation and transport of fluorides of the key impurities found in metallurgical grade silicon were performed using a thermodynamic screening technique. Thermodynamic feasibility can be assessed from the Gibbs free energy change of a reaction as discussed in Section II·B above.

The free energy for the reaction of the key impurities with SiF_4 to form various fluorides was determined from standard compilations such as the JANAF tables. This information along with knowledge of the melting and boiling points of the fluoride compounds was used to assess the probability of vapor transport of the impurity as a fluoride. A knowledge of the vapor pressure of the compounds at the various temperatures would allow a more accurate assessment, however, this data has not yet been compiled. It should be noted that in cases where vapor transport is not probable fluoride compounds could still be transported as "smokes" (i.e. particles suspended in the gas stream).

Tables 15 and 16 summarize the initial results of the assessment for key impurities. Table 15 is for a $1500^{o}K$ reaction zone temperature, which is close to the temperature at which we have been operating, and Table 16 is for a temperature of $1700^{o}K$, which is near the projected operating temperature at the silicon melting point. The results are reasonably consistent with the spectrographic findings on impurity transport shown in Table 13 with a few exceptions, notably copper and possibly iron. The melting poing and boiling point data show that some of the fluorides likely to transport at the higher temperatures such as MG and Zr may be separable by room temperature trapping. Others may be removable by low temperature trapping or by successive transport passes. Suspended particles can presumably be removed by special filtering techniques.

6). Reaction Kinetics

A series of experiments to determine the equilibrium coefficient and characterize the kinetics of the forward reaction was conducted. These experiments were conducted in the cyclic system, with a forward reaction zone temperature of 1150°C with the flat zone of the deposition area at 550°C. The technique consisted of measuring the moles of metallurgical grade silicon transported per mole of SiF_4 gas flowing for flow rates varying from 0.1 liters/minute to 3 liters per minute. Analysis of this data also allows a determination of thermodynamic quantities such as the enthalpy of formation..

Figure 18 summarizes the results of these experiments. It had been previously determined that the rate limiting step in the transport process is the formation of SiF_2 at temperatures of 1100 to 1200 degrees Celsius rather than the reverse reaction which results in the depositon of silicon at 500-900 degrees Celsius. It should be noted that the formation of SiF_2 in the high temperature region has not been directly proven, although the formation of such a simple molecule should be favored at these temperatures. The formation of SiF_2 polymer after quenching of the gas from the high temperature to -196 degrees Celsius at low pressure, followed by warming to temperatures above approximately -78 degrees Celsius, is described in the literature (9). After quenching the gas to temperatures from -196 degrees Celsius to +25 degree Celsius, at atmospheric pressure, however, SiF_2 could not be detected, but the presence of various silicon fluorides of the form Si (x)F(2x+2) compounds in their atmospheric pressure experiments at temperatures of 605 to 730 degrees Celsius. It is thus probable that the SiF_2 is formed at temperatures above 1100 degrees Celsius, and that it reacts at lower temperatures with the plentifully available SiF_4 to form the various fluorides of lesser silicon content.

The fraction of SiF_4 converted to SiF_2 at 1150°C begins to saturate for flow rates less than 0.5 mol/hr and approaches an equilibrium value of approximately 0.1. The flow rate at which saturation occurs is not of significance, since saturation could occur

at higher or lower flow rates depending on the geometry of the MG-Si container, the MG-Si particle size, etc. Using the low flow rate data, an equilibrium constant of 0.035 was calculated. From this, a value for the standard heat of formation of silicon difluoride was determined which is somewhat larger (-155 kcal/mole) than the one found by Margrave and coworkers in their experiments at low pressure (-139 to -148 kcal/mole), which includes the value given in the JANAF tables (3). However, our value is lower than the one found by Kanaan and Margrave in their lower temperature, atmospheric pressure experiments (-163 kcal/mole). It should be noted that, as mentioned earlier in this section, the equilibrium constant for reaction depends very sensitively on the values of heats of formation and entropies of the various participants in the reaction. The results of the reaction kinetics studies also confirmed our earlier theoretical determination that the transport rate of silicon will increase approximately in proportion to the square root of the SiF_4 flow rate. This effect takes place although the fraction F of the SiF_4 which reacts with Si at the high temperature and forms SiF_2, decreases as the flow rate of the SiF_4 is increased above the level at which the reaction ceases to take place in the equilibrium condition. Extrapolation to quadruple the highest flow rate used in the 1150 degrees Celsius experiments yields a probable transport rate for a practical process. It should again be noted that different arrangements can readily be visualized which would give higher F-values, and consequently higher transport rates at the intermediate and higher flow rates.

From thermodynamic computations, it was determined that the reaction rate should increase approximately five-fold by increasing the reaction temperature from 1150 degrees to 1420 degrees Celsius, that is to the molten state of silicon, as originally planned.

This expected increase of the reaction rate is based on the assumption that the primary reaction product is SiF_2.

C). Identification of Transport Species

At low pressures, the silicon transport specie has been identified as SiF_2. At atmospheric pressure and above, there is reason to believe that other species may predominate. Current experimental work is aimed at adentifying and isolating these species. The work involves the use of low temperature (room temp. to $-198^{o}C$) traps to separate various compounds and identify their roles in the process and the use of spectrographic analysis for identification.

In a recent set of experiments it was found that the gas stream can be rapidly cooled at atmospheric pressure form the temperature silicon/silicon tetrafluoride reaction to room temperature (or lower temperatures), with some silicon deposition taking place only in the temperature gradient zone. The gas is stable at room temperature, and it can be heated to the temperature range around 500 degrees Celsius, where decomposition and silicon deposition take place, similar to that observed in the preceding experiments where the gas did not attain temperatures below deposition temperature before reaching the deposition zone held at various temperatures above 500 degrees Celsius. Through careful and repeated mass-spectrographic analyses, as well as through selective freezing of the components of the gas stream, it has been determined that silicon difluoride is not present after cooling of the gas to room temperature or to dry ice temperature (-78 degrees Celsius) at atmosphere pressure. The silicon carrier gas has been transformed during cooling to the lower temperatures from silicon difluoride (possibly mixed with Si2F6, Si3F8, Si4F10, and other higher order silicon fluoride compounds primarily of the type Si(x) F (2x+2). While transport rates and yields have not yet been quantively investigated for the process with intermediate gas cooling, the basic characteristics of the transport process do

not seem to differ considerably from those investigated without intermediate cooling of the gas.

G) Electrolytic Process

1. Introduction

The electrochemical processes for silicon production were investigated as possible alternative ways of producing high-volume, low-cost silicon for solar cells. Silicon, the second most abundant element in the earths crust, occurs as an oxide or silicate. This is due to the strong electropositive nature of silicon which prevents it from being present in the free state. Since silicates form the largest group of minerals, it would be attractive to use them as raw materials for large-scale production of silicon. The present most widely used method to produce silicon and its alloys is the carothermic reduction of quartzite in an electric arc furnace.

Electrochemical processes to obtain silicon from a silicate or silica-containing electrolyte were investigated as early as the eighteenth century. Attempts to obtain silicon from aqueous solutions by electrolysis have not been very successful although negatively charged iron wire has been known to deposit very small quantities of silicon from aqueous silica solutions. This is due to the insoluble nature of silica and silicates in water. In the case of silica, its insolubility in water is a result of the partially covalent nature of the silicon-oxygen bond. Since

silica does not dissolve in water and pure water does not conduct electricity, it will not be possible to electrolyze a mixture of SiO_2 in water. For an electrolytic cell to conduct electricity, electrical charges must be able to flow not only within the electrolytic solution in the cell but also across the electrolyte-electrode interface. For silica or silicates to carry current they should exist in the molten ionic state.

Electrochemical processes to produce silicon have been broadly classified under the following headings:

---- High temperature reductions for silicon production utilizing electrical current to supply the energy.

- Electrolysis of silica dissolved in molten solvent electrolytes.
- Electrolytes containing silicon other than in the oxide form.
- Electrochemical transport or electrolytic refining.
- Recovery of silicon by electrolysis of slags.

---- Low temperature electrolysis.

---- Silane - Sundermeyer process.

These processes are discussed in turn below.

2. High Temperature Reductions for Silicon Production Utilizing Electrical Current to Supply the Energy.

Consider two electrodes immersed in a molten electrolyte. If a potential is applied across the electrodes by means of an external battery, there will be a positive electrode called the anode and a negative electrode called the cathode. In an ionic conducting electrolyte an electrochemical reaction proceeds because of loss of electrons at the anode and gain of electrons at the cathode. Considering an electrolytic solution containing Si^{4+} and O^{2-} ions, application of a potential across the electrodes will cause O^{2-} ions to be attracted toward the anode and Si^{4+} ions will be attracted toward the cathode. At the anode O^{2-} ions will be oxidized according to

$$2O^{2-} = O_2 + 4e^-$$

and at the cathode silicon ions will be reduced according to

$$Si^{4+} + 4e^- = Si$$

As a result oxygen will be liberated at the anode, supplying electrons, and the silicon will be reduced at the cathode by the electrons. This is a somewhat simplified picture of the reactions.

Silicon which has a strong tendency to exhibit tetrahedral co-ordination in molten solutions, tends to form complex anions such as $(SiO_4)^{4-}$ or $(Si_2O_5)_n^{2n-}$. The partially covalent nature of the silicon-oxygen bond accounts for the stability of this anion, and this stability is the reason for the resistance to breakdown of these complex anions into simpler species such as Si^{4+} and O^{2-} ions.

To understand the deposition mechanism in a typical electrolytic system, consider an electrolyte made up of sodium fluoride-silicate solution. On passing current, the Na^+ ions will move toward the cathode and O^{2-} and F^- ions will move toward the anode resulting in liberation of oxygen. Fluoride ions due to their high oxidation potentials will remain in solution. At the cathode, Na^+ ions after being reduced will react with silica resulting in liberation of silicon. The anodic process is then postulated to be

$$(Si_2O_5)_2^{4-} \rightarrow 4SiO_2 + O_2 + 4e^-$$

and the cathodic process may be considered as the electrolytic reduction of the cation followed by silica reduction according to

$$SiO_2 + 4Na = 2Na_2O + Si$$

The final result being deposition of silicon at the cathode.

a. Electrolysis of Silica Dissolved in Molten Solvent Electrolyte.

This category of electrolytes has been most extensively investigated from the point of view of the electrolytic deposition of silicon. Table 17 summarizes the various studies of this nature. Of all the electrolytes considered, cryolite as the solvent for electrodepositing silicon has yielded most promising results. A number of authors (28, 29, 30, 31) have investigated this system. Most of the experiments were carried out with an electrolyte ranging from 3010% SiO_2 in Na_3AlF_6 at a temperature of approximately 1000°C. Current efficiencies

obtained were close to 90%. The silicon deposited was stripped from the cathode periodically. The deposit so obtained was saturated with cryolite and had to be treated with acid before the silicon could be recovered. However, it was mentioned that electrodeposited silicon had to be further refined (not indicated how) for electronic and industrial use (28). During electrodeposition of silicon any impurities present in the electrolyte and small quantities of aluminum from the cryolite will also be codeposited.

The following assumptions were made in estimating the deposition rate using the data from (28):

i. Silica depleted by electrolytic deposition was continucusly replaced in the bath.

ii. Silicon deposition was via four electron reduction of the Si^{4+} ion at the cathode.

Passing one Faraday of electrical current through the electrolytic cell will yield one gram-equivalent of the element (7.02g Si). For a current passed across the electrodes of 400 amps, the number of coulombs passed through the cell equals 14.9 Faraday/hour. The silicon deposition rate, then, equals 104 g/hour. If the current efficiency is assumed to be 90%, the silicon deposition rate becomes 94 g/hour.

The rate of deposition in the above process may be explained in terms of the rate limiting step in electrodeposition. The slowest step during electrolysis will govern the rate of deposition. It could be either the transport of ions from

the electrolyte to the electrode or the reduction of the ion at the electrode. In an attempt to obtain higher yields, higher current densities may be used. Exceeding the current densities above a certain limit, however, will result in decomposition of the cryolite and deposition of an aluminum-silicon alloy.

A calculation of the energy consumption during the process was made using data were taken from references (28) and (30).

Voltage across the electrodes	= 7 volts.
Current through the electrolytic cell	= 400 amps.
Decomposition potential of SiO_2	= 1.1 volts.
Total voltage for the electrolytic operation	= 8.1 volts.
Energy consumption per hour	= 3240 watt
Silicon deposition rate	= 94 gms/hour
	= 34 watt-hour/gm
	= 34 KWH/kgm Si

The energy also partially heats the electrolyte to maintain the required temperature.

Table 18 compares the electrolysis and arc furnace production of silicon. Although the silicon purity obtained by electrolysis of the above system is claimed to be greater than 99%, this does not give the true analytical results.

The deposit after stripping from the cathode has to be treated with a dilute acid to dissolve the adhering electrolyte. This would also remove small quantities of aluminum and other impurities present along with silicon in the deposit.

The energy consumption in the electrolysis process is more than twice that associated with the arc furnace. Also, the silicon deposition rate in the electrolysis process is many times slower than the 1000 kg/h rate experienced in the arc furnace production of silicon at roughly the same equivalent purity level. Therefore, an electrolytic process of this type cannot be competitive for the high-volume, low-cost production of solar-grade silicon.

b. Electrolytes Containing Silicon Other Than in the Oxide Form

Potassium hexafluorosilicate is one of the most commonly used compounds to form part of the electrolyte for recovering silicon. 3 Studies based on such electrolytes are summarized in Table 19 along with references. K_2SiF_6 when heated above 700 °C (electrolysis temperature) dissociates with the formation of SiF_4. Commonly used solvents to stabilize the melt are NaCl and KCl.

Wartenberg (32) electrolyzed a solution of K_2SiF_6 - NaCl in the mole ratio of 1:3 at a temperature of 700 °C. The silicon which was obtained in the form of a pear shape, consisted of silicon up to 10% by weight of the deposit. The deposit was then crushed and washed with dilute acid to dissolve the electrolyte. The purity of silicon so obtained was 98% and major impurities analyzed were Fe, Ni, Na, K, and C.

A further analysis of the system is made based on the numerical values generated from this process. Electrolysis of

K_2SiF_6 - NaCl solution for six hours at 3-5 amps resulted in a cathodic deposit of approximately 100 grams. Of this deposit only 10 g of silicon was obtained after dissolving the adhering electrolyte. Because of the low yield, poor purity, and difficulty in separating silicon from the deposit, this group of electrolytes will not be considered any further as future processes for preparing solar silicon.

c. Electrochemical Transport or Electrolytic Refining.

In this process impure silicon or silicon alloy which is present as one of the electrodes is generally dissolved in a silicon combining electrolyte by passing current through the cell in the appropriate direction. The silicon is electrochemically transported via the flux and subsequently deposited on the other electrode. The growth rate of silicon in this process is controlled by the various operating conditions of the cell such as voltage applied to the electrodes, anodic and cathodic current density, electrical conductivity and the nature of the electrolyte used.

Stern, et al. (35) described the preparation of elemental silicon by anodic dissolution of silicon carbide in an electrolyte of K_2SiF_6-NaCl-KCl. The electrolysis was carried out at 760-790 °C. On passing current through the cell, silicon from silicon carbide dissolved in the electrolyte and was deposited on the cathode. The probable mechanism for electrolytic refining of silicon, thus, consisted of its conversion into a cation at the anode which went into solution

followed by the reverse reaction at the cathode. This process can be explained in terms of SiF_6^{-2} ion present in the electrolyte which allows silicon to go into solution at the anode; the ion is then reduced at the cathode to give silicon.

It should be noted that the above process is not generally used for generating silicon but only for purifying it. The process does have some disadvantages: (1) the starting electrolyte has to be of high purity; otherwise the impurity in the electrolyte will be electrodeposited at the cathode along with silicon. (2) Impure silicon during anodic dissolution will pass on its impurities into the electrolyte. Therefore, it is desirable to devise a method to remove the impurities from the electrolyte continuously during electrolysis.

In light of the above factors, and also considering the slow deposition rates due to the electrochemical nature of the reaction, this process is felt not to be suitable for low-cost, high-volume production of solar-grade silicon.

d. Recovery of Silicon by Electrolysis of Slags

Silicate slags have been a subject of investigation by various authors. A number of high-temperature electrochemical studies have been carried out on these systems. Slags which are by-products of the steel industry can be classified as basic and acidic slags.

A typical weight percent analysis of these slags is shown in the following table.

Component	Basic Slag (%)	Acidic Slag (%)
SiO_2	40	50
CaO	45	35
Al_2O_3	15	15

Most electrochemical measurements in slags have been made from the point-of-view of reaction kinetics in iron and steel making.

Slags contain large amounts of undesirable heavy metal impurities making them unsuitable for their use as electrolytes for electrowinning silicon.

For further details of electrochemical studies in slags one is referred to references (41) through (53).

3. Low Temperature Electrolysis for Depositing Silicon

Zyazev (54) studied the separation of silicon electrolytically from salt solutions in organic solvents at temperatures of 20-40 °C. The salts included quarternary amine salts and pyridine salts. The silicon was deposited as an amorphous material of 92% purity on a platinum electrode. The starting material and the silicon purity obtained limits this process to academic interest only.

4. Silane - Sundermeyer Process

The silane process uses the thermal decomposition of SiH_4, which melts at -184 °C, boils at -112 °C, and decomposes around 500 °C forming silicon and hydrogen. Economically the thermal decomposition of silane is attractive since 28 grams

of silicon are obtained from only 32 grams of silane, i.e.,

$$SiH_4(g) \rightarrow Si(s) + 2H_2(g)$$

The Sundermeyer process (55) consists of the electrochemical preparation of silane by electrolysis of a melt consisting of lithium hydride dissolved in a LiCl/KCl eutectic through which silicon tetrachloride is passed resulting in a reaction of the type

$$4LiH + SiCl_4 \rightarrow SiH_4 + 4LiCl.$$

At the same time LiCl is electrolysed to give

$$4LiCl \rightarrow 4Li + 2Cl_2.$$

Hydrogen when passed at the cathode where lithium is generated would result in formation of lithium hydride according to

$$4Li + 2H_2 \rightarrow 4LiH$$

and the lithium hydride so formed is dissolved in the electrolyte. Silane, thus, can be produced on a continuous basis with the recycle of lithium, hydrogen, and also chlorine when the following reaction is considered:

$$SiO_2 + 2C + 2Cl_2 \rightarrow SiCl_4 + 2CO.$$

The present cost of producing silane apparently excludes its possibility for low-cost production of solar silicon. For detailed economical analysis of raw materials for making silicon, one is referred to the data in section II·C above, which shows SiH_4 to cost about \$850/kg Si, almost two orders-of-magnitude above the <\$10/kg goal for solar silicon.

Conclusions

Of all the processes considered, the most attractive method for producing low-cost, high-volume silicon by electrolysis is that using a silica-cryolite electrolyte. The drawbacks of the above process, however, have been brought forward in the relevant section. The main disadvantage in the electrochemical production of silicon is the slow rate of silicon deposition and, at the same time, higher cost per kilogram of silicon compared to the arc furnace process. Furthermore, the batch type nature of the electrolytic processes and the difficulty in separating the silicon from the electrodeposit, along with the above considerations, make the electrolytic processes very unattractive as a potential way of producing low-cost silicon on a large scale.

G. References - Section II

1. L.P. Hunt, J. Electrochem. Soc., 119, 1741 (1972).

2. V.S. Ban, ibid., 122, 1389 (1975).

3. W.E. Smith, U.S. Patent 2,955,024 (1960).

4. J.C. Bravard, H.B. Flora, II and C. Portal, Oak Ridge National Laboratory Report ORNL-NSF-EP-24 [NTIS] (1972).

5. L.P. Hunt, data prepared for future publication.

6. C.D. Graham, et al., "Research and Development of Low-Cost Processes for Integrated Solar Arrays", Second Semi-Annual Progress Report (1 July 1974 - 31 December 1976), NSF/RANN/SE/GI-29729X/PR/74/4.

7. G.F. Wakefield, et al., "Solar Silicon Definition", Final Report (15 October 1974 - 15 September 1975), NSF/RANN/SE/AER75-03972/FR/75/1.

8. Margrave, J.L., et al; J. Phys. Chem. 66, 1200 (1962)

9. Margrave, J.L., Kanaan, A.S., and Pease, D.C.; J. Phys. Chem. 66, 1200 (1961)

10. Kanaan, A.S. and Margrave, J.L.; Inorg: Chem ___, 1037 (1964)

11. JANAF Thermochemical Tables, U.S. Dept. Comm., NBS

12. H. Davy, Gilb. Ann. 32, 365-96, 391 (1809).

13. H. Sainte Claire Deville, Ann. Chim. Phys. 43 (3), 5-33, 31 (1854).

14. H. Sainte Claire Deville, Ann. Chim. Phys. 49 (3), 62-78, 69 (1857).

15. G. Gore, Chem. 50, 113 (1884).

16. A. Gratzel and V. Gratz, Ger. Pat. 58, 600 (1890).

17. A. Minet, C.R. 112, 1215-8 (1891).

18. L. Andrieux and M. Dodero, C.R. 198, 753-5 (1934).

19. M. Dodero, Compt. Rend. 198, 1593 (1934).

20. N. S. Fortunatov, Mem. Inst. Chem. Ukrain. Acad. Sci. 2, 257-9 (1935).

21. M. Dodero, Bull Soc. Chim. 6, 209-18 (1939).

22. M. Dodero, Colloq. intern. Centre Natl. recherche Sci. Paris 39, electrolyse C 11-14 (1952).

23. M. Dodero, Silicium, Schwetel, phosphate, Colloq. Sek. Anorg. Chem. Intern. Union Reine U. Angew. Chem. Munster 1954, 15-20 (1955).

24. R. Monnier and D. Barakat, Ind. Chim. belge, Suppl. 1, 828-33 (1959).

25. M. J. Barbier - Andrieux, Compt. Rend. 242, 235 (1956).

26. Monnier & Giacometti, Helv. Chim. Acta 47, 345-53 (1964).

27. E. N. Schetnikov, Zh. Priklkhim. 38 (1), 197-201, (1965).

28. General Trustee Co. Inc., British Patent 1,080,589 (1967).

29. K. Grjotheim and K. Matiasovsky, 25(4), 249-52, (1971).

30. G. Boe, et al., Can. Met. Quart. 10 (4), 281-5 (1971).

31. G. Boe, et al., Can. Met. Quart. 11 (3), 463-7, (1972).

32. H. V. Wartenberg, Z. Fur. Anorganische und Allgemeine Chemie 265, 186-200 (1951).

33. M. Dodero, Comp. Rend. 799 (1939).

34. S. Alconard, Bull. Soc. Chim. 1, 34 (1961).

35. D. R. Stern, et al., U.S. Patent 2,892,763 (1959).

36. Yu. K. Delimarskii, Ukr. Khim. 2h. 34, 1227-34 (1968).

37. Yu. K. Delimarskii, et al., Nauk. Ukr., R SR, Ser B. 30 (10), 933-5 (1968).

38. R. V. Chernov, et al., Ukr. Khim. Zh., 37 (5), 422-6 (1971).

39. Yu. K. Delimarskii, et al., U.S.S.R. 264,696, 1970, from Otkrytiya, Izobret, Prom. Obraztsy. Tovarnye Znaki 47 (a), 105 (1970).

40. M. J. Dshems-Levy, Russ. Patent 39,088 (1934).

41. Akira Adachi and Kazumi Ogino, Denk. Kagaku 32 (2), 145-9 (1964).

42. W. R. Dickson, Trans. AIME 224, 505-11 (1962).

43. V. A. Chechulin, Liteinoe Proizv 28-31 (1962).

44. A. Sotnikov, et al., Vyssh. Ucheb. Zaved. Cheri. Met. 10, 5-10 (1967).

45. O. M. Ivanova, Tr. Gor'k. Politekn. Inst. 1967, 23 (4), 28-32 (1967).

46. Ashizuka Masahiro, et al., Tetsu To Mogane 54 (14), 1447-56 (1968).

47. A. K. Strel'tsov and E. A. Osin, Elektrokhimiya 5 (2), 159-65 (1969).

48. Akira Adachi, et al., Trans. Iron Steel Inst. Jap. 1969, 9 (2), 153-61.

49. G. A. Toporishchev, et al., Fiz. Khim. Elektrokhim. Rasplav. Solei Shlakov., Tr. Vses. Soveshch., 2 79-86 (1969).

50. ibid, 2 85-93 (1969).

51. S. Sugiura, et al., Tohoku. Daigaku Senko Seiren Kenkyusho Iho 27 (1-2), 101-7 (1971).

52. L. N. Barmin, et al., Fiz. Khim. Osn. Proizvod. Stali. Mater. Simp. Met. Metalloved 279-82 (1968).

53. L. N. Barmin, et al., Termodin. Kinet. Protsessov Vosstanov Metal., Mater. Knob. 157-60 (1972).

54. Yu. A. Zyazev, et al., Sb. Tr. Agron. Fiz. 13, 32-8 (1966).

55. W. Sundermeyer, Chem. Unserer. Zeit 1, 150-7 (1967).

Table 1. Relationship between free energy change, equilibrium constant, and degree completion of the reaction A(g) + B(g) = C(g) + D(g).

Degree Completion (%)	K	$\Delta G^{\circ}_{R,298}$ (kcal/mol)
85	32.	-2
70	5.	-1
50	1.	0
30	0.2	+1
15	0.03	+2
7	0.006	+3
0.02	4×10^{-8}	+10

Table 2. Free energies of reaction for silicon synthesis by the reduction of silicon tetrafluoride and chloride by nonmetals (except H_2).

	$\Delta G^{\circ}_{R,T}$ (kcal/mol)*		
	298	1000	2000
$SiF_4(g) + C(s) = Si(c) + CF_4(g)$	164	165	164
$SiF_4(g) + 2/3S(c) = Si(c) + 2/3SF_6(g)$	198	215	244
$SiF_4(g) + S(c) = Si(c) + SF_4(g)$	199	202	214
$SiF_4(g) + 4/3P(c) = Si(c) + 4/3PF_3(g)$	81	68	75
$SiCl_4(g) + C(s) = Si(c) + CCl_4(g)$	135	136	134
$SiCl_4(g) + 4/3P(c) = Si(c) + 4/3PCl_3(g)$	65	53	58

* JANAF (3)

Table 3. **The Standard Free Energy Change for the Metal Reduction of SiO_2 to Silicon According to the Following Reaction:**

$$4/n\ M(s) + SiO_2(s) \rightarrow Si(s) + \begin{cases} 2/n\ M_2O_n & \text{if n is odd} \\ 4/n\ MO_{n/2} & \text{if n is even} \end{cases}$$

Metal Oxide	$\Delta G^\circ_{R_{298}}$ kcal/mole	$\Delta G^\circ_{R_{800}}$ kcal/mole	$\Delta G^\circ_{R_{1000}}$ kcal/mole	Transitions	References
$Li_2O(s)$	-64	-58	-48		JANAF
$Na_2O(s)$	23	31	41	T_m = 948 K	JANAF
$K_2O(s)$	51	59	67		JANAF
$BeO(s)$	-68	-66	-65		BM605
$MgO(s)$	-67	-65	-61	T_m = 923 K	JANAF
$CaO(s)$	-83	-82	-79		SCHINK
$SrO(s)$	-63	-62	-60		BM605
$BaO(s)$	-47	-47	-48		BM605
$Sc_2O_3(s)$	-55	-53	-51		BM605
$Y_2O_3(s)$	-84	-83	-80		BM605
$TiO_2(s)$	-8	-8	-8		JANAF
$ZrO_2(s)$	-43	-42	-41		BM605
$HfO_2(s)$	-47	-46	-45		BM605
$V_2O_5(s)$	68		66	T_m = 948 K	BM605
$Nb_2O_5(s)$	35		34		BM605
$Ta_2O_5(s)$	22	22	21		BM605
$CrO_2(s)$	75	74			BM605
$MoO_2(s)$	86	84	81		BM605
$WO_2(s)$	80		79		BM605
$MnO(s)$	31	28	26		BM605
$ReO_3(s)$	119		111	T_m = 433 K	BM605
$FeO(s)$	88	85*	81		KUB.
$CoO(s)$	101	99	95		BM605
$NiO(s)$	104	104	103		BM605

*650 K

›le 3. Continued:

Metal Oxide	$\Delta G^\circ_{R_{298}}$ kcal/mole	$\Delta G^\circ_{R_{600}}$ kcal/mole	$\Delta G^\circ_{R_{1000}}$ kcal/mole	Transitions	References
$Cu_2O(s)$	136	133*	130		KUB.
$Ag_2O(s)$	200		182		BM605
$ZnO(s)$	53	54	57		KUB.
$CdO(s)$	97	103	109		BM605
$HgO(s)$	177	179	186		BM605
$B_2O_3(s)$	15	15	14	T_m = 723 K	KUB.
$Al_2O_3(s)$	-47	-45	-42		JANAF
$Ga_2O_3(s)$	-34				270-3
$In_2O_3(s)$	6				270-3
$SnO_2(s)$	81	83*	86		KUB.
$PbO(s)$	115	116	118		BM605
$As_2O_3(s)$	11	16	15	T_b = 730 K	BM605
$Sb_2O_3(s)$	105	105	105	T_m = 929 K	BM605
$Bi_2O_3(s)$	126	125	127		BM605
$Ce_2O_3(s)$	-70	-67	-63		BM605
$Lu_2O_3(s)$	-40				Est.
$\Delta Gf^\circ[SiO_2(s)]$ = -205		-192	-175	T_t = 847 K	JANAF

REFERENCES

BM605: C. E. Wicks and F. E. Block, Thermodynamic Properties of 65 Elements--Their Oxides, Halides, Carbides, and Nitrides, Bur. Mines Bull. 605 (1963)

JANAF: D. R. Stull and H. Prophet, Eds. JANAF Thermochemical Tables, 2nd ed., Nat. Bur. Stand. NSRDS-NBS, 37 (1971).

KUB.: O. Kubaschewski, E. L. Evans, and C. B. Alcock, Metallurgical Thermochemistry, Pergamon Press, New York (1967).

SCHINK: H. L. Schink, "Thermodynamics of Certain Refractory Compounds," Academic Press, New York (1966).

270-3: D. D. Wagman, W. H. Evans, V. B. Parker, I. Halow, S. M. Bailey, and R. H. Schumm, NBS Tech. Note 270-3 (1968).

Table 4. The Standard Free Energy Change for the Metal Reduction of SiF_4 to Silicon According to the Following Reaction:

$$4/n\ M(s) + SiF_4(g) \rightarrow Si(s) + 4/n\ MF_n$$

Metal Fluoride	$\Delta G^\circ_{R_{298}}$ kcal/mole	$\Delta G^\circ_{R_{600}}$ kcal/mole	$\Delta G^\circ_{R_{1000}}$ kcal/mole	Transitions	References
LiF(s)	-187	-169	-146		JANAF
NaF(s)	-145	-125	-99		JANAF
KF(s)	-139	-120	-95		JANAF
BeF_2(s)	-92	-88	-66	T_m = 825°K	JANAF
MgF_2(s)	-136	-121	-103		JANAF
CaF_2(s)	-185	-171	-154		JANAF
SrF_2(s)	-179				BM605
BaF_2(s)	-173	-159	-144		BM605
ScF_3(s)	-90		-62		BM605
YF_3(s)	-96		-66		BM605
TiF_3(s)	-58	-46	-30		JANAF
ZrF_2(s)	-62		-40		BM605
HfF_4(s)	-37		-11		BM605
VF_2(s)	+38		+64		BM605
NbF_3(s)	+51				270-5
TaF_3(s)	+11				270-5
CrF_2(s)	+32				KUB.
MoF_6(ℓ)	+120			T_b = 309°K	KUB.
WF_6(ℓ)	+116				270-4
MnF_2(s)	+16				KUB.
ReF_3(s)	+171	+197			BM605
FeF_2(s)	+59	+68	+80		JANAF
CoF_2(s)	+76	+87	+99		JANAF
NiF_2(s)	+83				KUB.
CuF_2(s)	+137	+150	+165		JANAF
AgF(s)	+198		+197		BM605

Table 4. **The Standard Free Energy Change for the Metal Reduction of SiF_4 to Silicon According to the Following Reaction:**

$$4/n\ M(s) + SiF_4(g) \rightarrow Si(s) + 4/n\ MF_n$$

Metal Fluoride	$\Delta G^\circ_{R_{298}}$ kcal/mole	$\Delta G^\circ_{R_{600}}$ kcal/mole	$\Delta G^\circ_{R_{1000}}$ kcal/mole	Transitions	References
LiF(s)	-187	-169	-146		JANAF
NaF(s)	-145	-125	-99		JANAF
KF(s)	-139	-120	-95		JANAF
BeF_2(s)	-92	-88	-66	T_m = 825°K	JANAF
MgF_2(s)	-136	-121	-103		JANAF
CaF_2(s)	-185	-171	-154		JANAF
SrF_2(s)	-179				BM605
BaF_2(s)	-173	-159	-144		BM605
ScF_3(s)	-90		-62		BM605
YF_3(s)	-96		-66		BM605
TiF_3(s)	-58	-46	-30		JANAF
ZrF_2(s)	-62		-40		BM605
HfF_4(s)	-37		-11		BM605
VF_2(s)	+38		+64		BM605
NbF_3(s)	+51				270-5
TaF_3(s)	+11				270-5
CrF_2(s)	+32				KUB.
MoF_6(ℓ)	+120			T_b = 309°K	KUB.
WF_6(ℓ)	+116				270-4
MnF_2(s)	+16				KUB.
ReF_3(s)	+171	+197			BM605
FeF_2(s)	+59	+68	+80		JANAF
CoF_2(s)	+76	+87	+99		JANAF
NiF_2(s)	+83				KUB.
CuF_2(s)	+137	+150	+165		JANAF
AgF(s)	+198		+197		BM605

le 4. Continued:

Metal Fluoride	$\Delta G^\circ_{R_{298}}$ kcal/mole	$\Delta G^\circ_{R_{600}}$ kcal/mole	$\Delta G^\circ_{R_{1000}}$ kcal/mole	Transitions	References
$ZnF_2(s)$	+35				KUB.
$CdF_2(s)$	+66				270-3
$HgF_2(s)$	+172	+188	+240	T_d = 949°K	JANAF
$BF_3(g)$	+19	+15	+9		JANAF
$AlF_3(s)$	-80	-65	-47	T_m = 728°K	JANAF
$GaF_3(s)$	+30				BM605
$InF_3(s)$					
$SnF_2(s)$	+79				BM605
$PbF_2(s)$	+74	+85	+96		JANAF
$AsF_3(\ell)$	+86				BM605
$SbF_3(s)$	+106				BM605
$BiF_3(s)$	+109				BM605
$CeF_3(s)$	-120		-87		BM605
$LuF_3(s)$	-90		-59		BM605
$\Delta G^\circ_f[SiF_4(g)]$ =	-375.86	-365.44	-351.55		JANAF

REFERENCES

BM605: C. E. Wicks and F. E. Block, Thermodynamic Properties of 65 Elements--Their Oxides, Halides, Carbides, and Nitrides, Bur. Mines Bull. 605 (1963).

JANAF: D. R. Stull and H. Prophet, Eds. JANAF Thermochemical Tables, 2nd ed., Nat. Bur. Stand. NSRDS-NBS, 37 (1971).

KUB.: O. Kubaschewski, E. L. Evans, and C. B. Alcock, Metallurgical Thermochemistry, Pergamon Press, New York (1967).

270-3: D. D. Wagman, W. H. Evans, V. B. Parker, I. Halow, S. M. Bailey, and R. H. Schumm, NBS Tech. Note 270-3 (1968).

270-4: Ibid., May, 1969.

270-5: Ibid., Mar., 1971.

Table 5. The Standard Free Energy Change for the Metal Reduction of $SiCl_4$ to Silicon According to the Following Reaction:

$$4/n\ M(s) + SiCl_4(g) \rightarrow Si(s) + 4/n\ MCl_n$$

Chloride	$\Delta G^\circ_{R_{298}}$	$\Delta G^\circ_{R_{900}}$	$\Delta G^\circ_{R_{1000}}$	Transitions	References
LiCl(s)	-220	-205	-187	T_m = 883°K	JANAF
NaCl(s)	-220	-202	-179		JANAF
KCl(s)	-243	-224	-201		JANAF
$BeCl_2$(c,α)	-66	-55	-42	T_m = 688°K	JANAF
$MgCl_2$(s)	-135	-122	-105	T_m = 987	JANAF
$CaCl_2$(s)	-210	-197	-181		JANAF
$SrCl_2$(s)	-226	-258	-198		BM605
$BaCl_2$(s)	-239	-225	-208		BM605
$ScCl_3$(s)	-124		-95		BM605
YCl_3(s)	-139		-119		BM605
$TiCl_3$(s)	-75	-61	-44		JANAF
$ZrCl_2$(s)	-120		-98		BM605
$HfCl_4$(s)	-85		-95		BM605
VCl_2(s)	-64	-52	-37		BM605
$NbCl_x$					
$TaCl_x$	+1.6				
CrF_2(s)	-28				KUB.
$MoCl_2$(s)	+78		+94		BM605
WCl_2(s)	+93				BM605
$MnCl_2$(s)	-63				KUB.
$ReCl_3$(s)	+95		+118		BM605
$FeCl_2$(s)	+3	+12	+22	T_m = 950°K	JANAF
$CoCl_2$(s)	+12				KUB.
$NiCl_2$(s)	+24				KUB.
CuCl(s)	+32	+38	+42	T_m = 703°K	JANAF
AgCl(s)	+43	+49	+49		BM605

Table 5. Continued:

Chloride	$\Delta G^\circ_{R_{298}}$	$\Delta G^\circ_{R_{600}}$	$\Delta G^\circ_{R_{1000}}$	Transitions	References
ZnCl(s)	-29				270-3
$CdCl_2$(s)	-17				270-3
$HgCl_2$(s)	+74	+72	+101		JANAF
BCl_3(g)	+24	+19	+13		JANAF
$AlCl_3$(s)	-53	-39	-23	T_m = 465.7°K	JANAF
$GaCl_3$(s)	+3				BM605
$InCl_x$					
$SnCl_2$(s)	+4				JANAF
$PbCl_2$(s)	-3				270-3
$AsCl_3$(ℓ)	+66				270-3
$SbCl_3$(s)	+44				270-3
BiCl(s)	+44				270-3
$CeCl_3$(s)	-166		-139		BM605
$LuCl_3$(s)	-134		-106		BM605
$\Delta G^\circ_f[SiCl_4(g)]$	-147.56	-138	-125.61	T_b = 330.7°K	JANAF

REFERENCES

BM605: C. E. Wicks and F. E. Block, Thermodynamic Properties of 65 Elements--Their Oxides, Halides, Carbides, and Nitrides, Bur. Mines Bull. 605 (1963).

JANAF: D. R. Stull and H. Prophet, Eds. JANAF Thermochemical Tables, 2nd ed., Nat. Bur. Stand. NSRDS-NBS, 37 (1971).

KUB.: O. Kubaschewski, E. L. Evans, and C. B. Alcock, Metallurgical Thermochemistry, Pergamon Press, New York (1967).

270-3: D. D. Wagman, W. H. Evans, V. B. Parker, I. Halow, S. M. Bailey, and R. H. Schumm, NBS Tech. Note 270-3 (1968).

Table 6. The Standard Free Energy Change for the Metal Reduction of $SiBr_4$ to Silicon According to the Following Reaction

$$4/n\ M(s) + SiBr_4(s) \rightarrow Si(s) + 4/n\ MBr_n$$

Metal Bromide	$\Delta G^\circ_{R_{298}}$ kcal/mole	$\Delta G^\circ_{F_{600}}$ kcal/mole	$\Delta G^\circ_{R_{1000}}$ kcal/mole	Transitions	References
LiBr(s)	-223	-210	-193	T_m = 823°K	JANAF
NaBr(s)	-231	-214	-192		JANAF
KBr(s)	-261	-242	-219		JANAF
$BeBr_2$(s)	-50		-35	T_m = 761°K	BM605
$MgBr_2$(s)	-135	-123	-107	T_m = 987°K	JANAF
$CaBr_2$(s)	-215	-202	-187		KUB.
$SrBr_2$(s)	-230	-217	-201	T_m = 917°K	BM605
$BaBr_2$(s)	-247		-213		BM605
$ScBr_3$(s)	-116		-98		BM605
YBr_3(s)	-118		-88		BM605
$TiBr_4$(s)	-38	-34	-34	T_b = 505°K	JANAF
$ZrBr_4$(s)	-80			T_b = 630°K	BM605
$HfBr_4$(s)	-99			T_b = 595°K	BM605
VBr_3(s)	-34		-10		BM605
$NbBr_3$(s)	2			T_b = 634°K	BM605
$TaBr_3$(s)	-5			T_b = 620°K	BM605
$CrBr_3$(s)	-12				BM605
$MoBr_4$(s)	64		66	T_s = 893°K	BM605
WBr_4(s)	75		78		BM605
$MnBr_2$(s)	-70	-59*	-48		BM605
$ReBr_3$(s)	80		94		BM605
$FeBr_2$(s)	-10	-2*	8	T_m = 957°K	KUB.
$CoBr_2$(s)	8		25	T_m = 951°K	BM605
$NiBr_2$(s)	7		35		BM605
$PtBr_4$(s)	78				BM605
CuBr(s)	7	15		T_m = 761°K	JANAF
AgBr(s)	26	33		T_m = 703°K	BM605
$ZnBr_2$(s)	-46	-33	-29	T_b = 923°K	KUB.

*650K

Table 6. Continued:

Metal Bromide	$\Delta G^\circ_{R_{298}}$ kcal/mole	$\Delta G^\circ_{R_{600}}$ kcal/mole	$\Delta G^\circ_{R_{1000}}$ kcal/mole	Transitions	References
$CdBr_2$	-40		-11	T_m = 840°K	BM605
$HgBr_2$(s)	31			T_b = 592°K	BM605
BBr_3(g)	30	25	19		KUB.
$AlBr_3$(s)	-61			T_b = 528°K	BM605
$GaBr_3$(s)	18			T_b = 565°K	270-3
$SnBr_2$(s)	-14			T_b = 913°K	BM605
$PbBr_2$(s)	-21	-9	4	T_m = 643°K	BM605
$AsBr_3$(s)	41			T_b = 494°K	BM605
$SbBr_3$(s)	29			T_b = 553°K	BM605
$BiBr_3$(s)	29			T_b = 734°K	BM605
$CeBr_3$(s)	-143				BM605
$LuBr_3$(s)	-106				BM605
$\Delta G^\circ_f[SiBr_4(g)]$ =	-103	-95	-83	T_b = 426°K	Hunt

REFERENCES

BM605: C. E. Wicks and F. E. Block, Thermodynamic Properties of 65 Elements--Their Oxides, Halides, Carbides, and Nitrides, Bur. Mines Bull. 605 (1963).

Hunt: L. P. Hunt, Dow Corning Research Report No. 3864 (1971).

JANAF: D. R. Stull and H. Prophet, Eds. JANAF Thermochemical Tables, 2nd ed., Nat. Bur. Stand. NSRDS-NBS, 37 (1971).

KUB.: O. Kubaschewski, E. L. Evans, and C. B. Alcock, Metallurgical Thermochemistry, Pergamon Press, New York (1967).

270-3: D. D. Wagman, W. H. Evans, V. B. Parker, I. Halow, S. M. Bailey, and R. H. Schumm, NBS Tech. Note 270-3 (1968).

Table 7. SUMMARY OF THERMODYNAMICALLY FEASIBLE METAL REDUCTANTS

START'G MAT'L	FEASIBLE METALS	
	FOR ALL MAT'LS	SPECIFIC TO MAT'L
SiO_2	IIA, IIIB, IVB, Al, R.E.'s[a]	Li, Ga
SiF_4	IIA, IIIB, IVB, Al, R.E.'s	IA
$SiCl_4$	IIA, IIIB, IVB, Al, R.E.'s	IA, V, Cr, Mn, Zn, Cd
$SiBr_4$	IIA, IIIB, IVB, Al, R.E.'s	IA, V, Cr, Mn, Zn, Cd, Sn, Pb, Ta[b], Fe[b]

a R.E.'s = rare earths

b ~0 to 10 kcal/mol at high temperatures

Table 8. Materials cost analysis for MG-silicon

Item	Unit Cost ($)*	Cost ($/kg Si)**	% MG-Si Price***
Quartzite	8.00/ton	0.012	1.2
Wood Chips	10.00/ton	0.008	0.8
Pet. Coke	21.00/ton	0.006	0.6
Met. Coal	28.00/ton	0.008	0.8
Electrode	0.10/lb	0.034	3.4
Electricity	0.012/kwh	0.166	16.6
		0.234	23.4

* Dow Corning figures.

** Yield data from Fairchild (2).

*** Mg-Si = $1.00/kg.

Table 9. Prices of Various Silicon-Containing Materials

Raw Si Material	Selling Price ($/lb)	Selling Price ($/kg Si)	Relative Price ($/kg Si)	Comments
SiO_2 (quartzite)	0.004	0.024	1	arc furnace material
Si (metallurgical)	0.45	1.00	42	
SiF_4 (as 23% H_2SiF_6)	0.034*	1.63	68	fertilizer industry by-product
$SiCl_4$ (tech. grade)	0.135*	1.79	75	epitaxy use
$SiHCl_3$ (silicone grade)	0.45	4.78	200	
$SiHCl_3$ (semi. grade)	0.68	7.22	300	
Si (solar grade)	4.54	10.	420	JPL goal
$SiCl_4$ (semi. grade)	2.00	26.	1100	epitaxy use
Si (semi. grade)	31.8	70.	2900	average
SiH_2Cl_2 (semi. grade)	20.	160.	6700	epitaxy use
SiH_4 (semi. grade)	340.	860.	36000	epitaxy use

* Chemical Marketing Reporter (4/28/75); others are Dow Corning selling or determined prices.

Table 10. Prices of Materials for Reacting with Various Silicon Compounds

Reductant or Intermediate for Silicon Cmpd.	Selling Price ($/lb)	Selling Price* ($/kg Si*)	Relative Price* ($/kg Si*)
C (Mixture)**	0.008	0.100	1
H_2**	1.22	0.38	4
Cl_2	0.0575	0.64	6
Al	0.335	0.95	10
Na	0.225	1.62	16
Mg	0.82	3.13	31

* For reaction equivalent of reducing four silicon compound bonds.

** Dow Corning determined price; other prices from Chem. Mark. Rept. (4/28/75).

Table 11. Reactions Identified as Feasible for Preparing Silicon After Thermodynamic and Raw Material Economic Screening

No. Reactions	1975 Raw Mat'l. Cost For Reaction ($/kg Si)	Reaction Type
2	0.12 for C 0.97 for Al	$SiO_2 \xrightarrow{C^* \text{ or } Al} MG\text{-}Si$
8	0.12 min. to 2.06 max.	$SiO_2 \xrightarrow{MG\text{-}Si,\ Al,\ C,\ or\ Mg} SiO \xrightarrow{Al,\ C,\ H_2\ or\ Mg} Si$
1	1.00 - 2.63 (assuming 0-100% SiF_4 recycle)	$MG\text{-}Si \xrightarrow{SiF_4} 2SiF_2 \xrightarrow[-SiF_4]{} Si$
1	1.14	$SiO_2 \xrightarrow{C\ \&\ Cl_2} SiCl_4 \xrightarrow{H_2} Si$

* Commerical Arc Furnace Process

Table 12. Comparison of Impurities in Various Grades of Silicon

Impurity (ppma)	Purchased MG-Si(4)	Upgraded MG-Si*	Upgraded MG-Si**	Proposed SoG-Si(12)
Al	1570	<10	8	≤1
B	44	42	5	≤0.01
Cr	137	<5	<0.01	≤5
Cu	<50	13	0.05	≤5
Fe	2070	5	<0.05	≤25
Mn	70	<5	<0.01	≤5
Ni	47	<5	<0.03	≤5
P	28	18	2	≤0.01
Ti	163	<6	0.02	≤5
V	100	<6	<0.01	≤5

* Combined slagging and acid leaching technique; analysis by emission spectroscopy.

** Acid leaching followed by one Czochralski pull; analysis by spark-source mass spectroscopy.

Table 13. Results of Semi-quantitative Spectrographic Analysis

Range of Concentration	Metallurgical Grade Si	Transported Si A	Transported Si B
Major (10%)	Si	Si	Si
Near Major (5-25%)			
Minor (1-10%)			
Near Minor (0.5-5%)			
Low (0.1-1%)	Fe,Al		
Near Low (0.05-0.5%)			
Very Low (0.01-0.1%)	Ti,Ca	Al	Al
Strong Trace (0.005-0.05%)	Mn,Cr,V	Fe,Na	Fe,Na
Trace (0.01%)	Mg,Ni,Cu,B,Zr	Mg,Ba,Cu,Ti, Mn,Zr,Ca	Mg,Cu,Ti,Ba, Mn,Zr,Ca
Not Detected*	Li,Ba,Na,K,Sb, As,Pb,W,Ge,In, Bi,Cb,Be,Mo,Sn, Cd,Ag,Zn,Co,Sr	B,Sb,As,Pb, W,Ge,In,Ni, Bi,Cb,Be,Mo, Sn,V,Cd,Ag, Zn,Co,Cr,Sr, Li,K	B,Sb,As,Pb, W,Ge,In,N, Bi,Cb,Be,Mo, Sn,V,Cd,Ag, Zn,Co,Cr,Sr, Li,K

*See Table 14 for limits of detection.

Table 14. Approximate Limits of Detection for Various Elements Under Semi-Quantitative Emission Spectrographic Analysis (From National Spectrographic Laboratories Listing).

	%		%		%
Ag	0.001	Ni	0.002	Cs	0.05
Al	0.001 - 0.005	Pb	0.005	Rb	0.1
As	0.01	Sb	0.01 - 0.005	Tl	0.01
Be	0.0005	Si	0.001	Ta	0.05
B	0.001	Sn	0.001 - 0.005	Th	0.5
Bi	0.002	Sr	0.001 - 0.005	P	0.5
Ca	0.001	Ti	0.001 - 0.005	Ga	0.01 - 0.005
Cb/Nb	0.005 - 0.01	V	0.001 - 0.005	Pd	0.005
Cd	0.01	W	0.01 - 0.05	Au	0.001 - 0.005
Co	0.005	Zn	0.01	Hf	0.005 - 0.01
Cr	0.002 - 0.005	Zr	0.001	In	0.005
Cu	0.0005	Ba	0.005	Ir	0.005
Fe	0.001	Li	0.0001	Pt	0.001 - 0.005
Ge	0.001	K	0.001	Re	0.01 - 0.05
In	0.005	Na	0.0005	Rh	0.005
Mg	0.0005	Hg	0.001	Ru	0.005
Mn	0.001	Te	0.05	Os	0.001
Mo	0.001 - 0.005				

Note: These limits were determined for a graphite matrix. Detection limits will vary somewhat with the matrix of the sample.

TABLE 15. FLUORIDE TRANSPORT OF IMPURITIES AT 1500°K

ELEMENT	FLUORIDE FORMATION REACTION	$\Delta G_{R,T}$ Kcal/mole	Fluoride Melting Point, °K	Fluoride Boiling Point, °K	Comments
Al	$4Al+SiF_4 \rightarrow 4AlF(g)+Si$	-12	(g)	(g)	Probable transport as AlF, conversion to AlF_3 and al during deposition.
	$4/3Al+SiF_4 \rightarrow 4/3AlF_3(s)+Si$	-23	-	1549 (SP)	
Fe	$Fe+SiF_4 \rightarrow FeF_2(\ell)+SiF$	+62	1373	2100	Formation of significant amounts of fluoride not likely.
	$2Fe+SiF_4 \rightarrow 2FeF_2(\ell)+Si$	+92	1373	2100	
	$4/3Fe+SiF_4 \rightarrow 4/3FeF_3(g)+Si$	+109	--	1200(SP)	
Ca	$Ca+SiF_4 \rightarrow CaF_2(s)+SiF_2$	-51	1691	2807	Fluoride formation probable, transport below 1500°K not favorable.
	$2Ca+Si_4 \rightarrow 2CaF_2(s)+Si$	-134	1691	2807	
	$4Ca+SiF_4 \rightarrow 4CaF(g)+Si$	(+)	(g)	(g)	
Ti	$Ti+SiF_4 \rightarrow TiF_2(g)+SiF_2$	+12	(g)	(g)	Fluoride transport probable.
	$2Ti+SiF_4 \rightarrow 2TiF_2(g)+Si$	-8	(g)	(g)	
	$4/3Ti+SiF_4 \rightarrow 4/3TiF_3(g)+Si$	-22	--	1310(SP	
Cr	$Cr+SiF_4 \rightarrow CrF_4(g)+SI$	+144	550	570	Significant fluoride formation not probable.
	$Cr+SiF_4 \rightarrow CrF_2(\ell)+SiF_2$	+41	1375	2400	
	$2Cr+SiF_4 \rightarrow 2CrF_2(\ell)+Si$	+60	1375	2400	
	$4/3Cr+SiF_4 \rightarrow 4/3CrF_3(\ell)+Si$	+71	1373	1700	
Mn	$Mn+SiF_4 \rightarrow MnF_2(\ell)+SiF_2$	+37	1129	2300	Significant fluoride formation not probable.
	$2Mn+SiF_4 \rightarrow 2MnF_2(\ell)+Si$	+42	1129	2300	
	$4/3Mn+SiF_4 \rightarrow 4/3MnF_3(\ell)+Si$	+79	1350	1600	
V	$V+SiF_4 \rightarrow VF_4(g)+Si$	+43	--	600(SP)	Significant fluoride formation not probable.
	$V+SiF_4 \rightarrow VF_2(\ell)+SiF_2$	+56	1400	2500	
	$2V+SiF_4 \rightarrow 2VF_2(\ell)+SiF_4$	+80	1400	2500	
	$4/3V+SiF_4 \rightarrow 4/3VF_3(\ell)+Si$	+51	1400	1700	
B	$B+SiF_4 \rightarrow BF_2(g)+SiF_2$	+41	(g)	(g)	Some transport as BF_3 possible.
	$2B+SiF_4 \rightarrow 2BF_2(g)+Si$	+50	(g)	(g)	
	$4/3B+SiF_4 \rightarrow 4/3BF_3(g)+Si$	-2	171	197	
Cu	$Cu+SiF_4 \rightarrow CuF_2(\ell)+SiF_2$	+103	1043	1727	Fluoride transport unlikely
Mg	$Mg+SiF_4 \rightarrow MgF_2(s)+SiF_2$	-21	1536	2500	Fluoride formation probable, transport below 1500°K not favorable.
	$2Mg+SiF_4 \rightarrow 2MgF_2(s)+Si$	-74	1536	2500	
Ni	$Ni+SiF_4 \rightarrow NiF_2(\ell)+SiF_2$	+75	1300	1900	Singificant fluoride formation at probable.
	$2Ni+SiF_4 \rightarrow 2NiF_2(\ell)+Si$	+118	1300	1900	
P	$P+SiF_4 \rightarrow PF_2(g)+SiF_2$	+75	(g)	(g)	Significant fluoride formation not probable.
	$2P+SiF_4 \rightarrow 2PF_2(g)+Si$	+118	(g)	(g)	
	$4/3+SiF_4 \rightarrow 4/3PF_3(g)+Si$	+155	122	172	
Zr	$Zr+SiF_4 \rightarrow ZrF_4(s)+Si$	(-)	-	1200(SP	Transport as ZrF probable.
	$2Zr+SiF_4 \rightarrow 2ZrF_2(s)+Si$	-30	1800	2500	
	$4/3Zr+SiF_4 \rightarrow 4/3ZrF_3(g)+Si$	-25	1600	2400	

TABLE 16: Fluoride Transport Of Impurities at 1700°K

ELEMENT	FLUORIDE FORMATION REACTION	$\Delta G_{R,T}$ Kcal/mole	Fluoride Melting Point, °K	Fluoride Boiling Point, °K	COMMENTS
Al	$4Al+SiF_4 \rightarrow 4AlF(g)+Si$	-41	(g)	(g)	Fluoride transport probable.
	$4/3Al+SiF_4 \rightarrow 4/3AlF_3(g)$	-21	-	1549 (SP)	
Fe	$Fe+SiF_4 \rightarrow FeF_2(\ell)+SiF_2$	+59	1373	2100	Fluoride formation not favored.
	$2Fe+SiF_4 \rightarrow 2FeF_2(\ell)+Si$	+95	1373	2100	
	$4/3+SiF_4 \rightarrow 4/3F_3(g)+Si$	+115	-	1200(SP)	
Ca	$Ca+SiF_4 \rightarrow CaF_2(\ell)+SiF_2$	-51	1691	2807	Transport as CaF probable,
	$2Ca+SiF_4 \rightarrow 2CaF_2(\ell)+Si$	-125	1691	2807	formation of other fluorides
	$4Ca+SiF_4 \rightarrow 4CaF(g)+Si$	(-)	(g)	(g)	also likely.
Ti	$Ti+SiF_4 \rightarrow TiF_2(g)+SiF_2$	+3	(g)	(g)	Fluoride transport probable.
	$2Ti+SiF_4 \rightarrow 2TiF_2(g)+Si$	-17	(g)	(g)	
	$4/3Ti+SiF_4 \rightarrow 4/3TiF_3(g)+Si$	-25	-	1310 (SP)	
Cr	$Cr+SiF_4 \rightarrow CrF_4+Si$	(+)	550	570	Limited data on ΔG, formation of
	$Cr+SiF_4 \rightarrow CrF_2+SiF_2$	(+)	1375	2400	fluorides probably not favored.
	$2Cr+SiF_4 \rightarrow 2CrF_2+Si$	(+)	1375	2400	
	$4/3Cr+SiF_4 \rightarrow 4/3CrF_3+Si$	(+)	1375	1700	
Mn	$Mn+SiF_4 \rightarrow MnF_2(\ell)+SiF_2$	(+)	1129	2300	Same as above, anticipate transport
	$2Mn+SiF_4 \rightarrow 2MnF_2(\ell)+Si$	(+)	1129	2300	not likely.
	$4/3Mn+SiF_4 \rightarrow 4/3MnF_3(g)+Si$	(+)	1350	1600	
V	$V+SiF_4 \rightarrow VF_4(g)+Si$	(+)	--	600 (SP)	Same as above
	$V+SiF_4 \rightarrow VF_2(\ell)+SiF_2$	(+)	1400	2500	
	$V+SiF_4 \rightarrow 2VF_2(\ell)+Si$	(+)	1400	2500	
	$4/3V+SiF_4 \rightarrow 4/3VF_3(g)+Si$	(+)	1400	1700	
B	$B+SiF_4 \rightarrow BF_2(g)+SiF_2$	+32	(g)	(g)	Some transport as BF_3 possible.
	$2B+SiF_4 \rightarrow 2BF_2(g)+Si$	+41	(g)	(g)	
	$4/3B+SiF_4 \rightarrow 4/3BF_3(g)+Si$	-1	171	197	
Cu	$Cu+SiF_4 \rightarrow CuF_2(\ell)+SiF_2$	+100	1043	1727	Fluoride transport not likely.
Mg	$Mg+SiF_4 \rightarrow MgF_2(\ell)+SiF_2$	-16	1536	2500	Some transport as MgF_2 probable.
	$2Mg+SiF_4 \rightarrow 2MgF_2(\ell)+Si$	-55	1536	2500	
Ni	$Ni+Si_4 \rightarrow NiF_2(\ell)+SiF_2$	+75	1300	1900	Fluoride formation not favored.
	$2Ni+SiF_4 \rightarrow 2NiF_2(\ell)+Si$	+118	1300	1900	
P	$P+SiF_4 \rightarrow PF_2(g)+SiF_2$	+73	(g)	(g)	Fluoride formation not favored
	$2P+SiF_4 \rightarrow 2PF_2(g)+Si$	+123	(g)	(g)	
Zr	$Zr+SiF_4 \rightarrow ZrF_4(g)+Si$	(-)	-	1200 (SP)	Limited $\Delta G_{R,T}$ data, anticipate
	$2Zr+SiF_4 \rightarrow 2ZrF_2(g)+Si$	(-)	1800	2500	some transport as ZrF_4 and
	$4/3Zr+SiF_4 \rightarrow 4/3ZrF_3(\ell)+Si$	(-)	1600	2400	possibly ZrF_3.

Table 17

Electrolysis of silicon dissolved in molten solvent electrolyte.

Reference Number	Electrolyte	Remarks
12	SiO_2-KOH	Platinum rod was used as cathode and platinum crucible was used as anode. Cathodic silicon deposit was obtained as shiny metallic flakes.
13	SiO_2-NaCl-$AlCl_3$	Aluminum was deposited along with silicon. It was removed by dissolving in HCl.
14	SiO_2-NaF-KF	Impure silicon deposits were obtained at the cathode.
15	SiO_2-NaOH-K_2CO_3 or SiO_2-NaOH-Na_2CO_3	Potassium and sodium were obtained as impurities along with silicon.
16	SiO_2-SrO_2-$SrCl_2$-SrO	Electrolyte was stirred to keep SrO in suspension and silicon deposited along with strontium.
17	SiO_2-NaCl-Na_3AlF_6-Al_2O_3	Electrolysis was carried out in the temperature range 700-1000 °C. A silicon-aluminum alloy was obtained as the deposit.
18	SiO_2-LiF-Li_2O	Electrolysis was carried out at 950 °C. Cathode deposit consisted of a silicon-lithium alloy with traces of iron.
19	SiO_2-CaF_2-$CaCl_2$-$CaCO_3$	Electrolysis yielded calcium silicide as the cathodic deposit.
20	SiO_2-Al_2O_3-$NaHCO_3$	Silicon was obtained as the cathodic deposit free of aluminum.

Table 17 (continued)

Reference Number	Electrolyte	Remarks
21	Na_2O-SiO_2 K_2O-SiO_2	Cathodic silicon deposits was obtained with low current efficiencies.
	SiO_2-MO (where M represents Ca, Br, or Sr)	Cathodic deposits yielded silicon alloys of the type MSi_2.
22	SiO_2-LiO_2-TiO_2-LiF SiO_2-CaO-TiO_2-CaF_2 SiF_4-2KF-TiO_2	Silicon deposits with titanium and alkaline earth silicides resulted on electrolyses.
23	SiO_2-Na_2O-NaF SiO_2-Na_2O-KF SiO_2-Al_2O_3-AlF_3 SiO_2-MgO-MgF_2	Silicon deposits with respective metallic silicides were obtained.
24	SiO_2-Na_3AlF_6-NaF SiO_2-Al_2O_3-AlF_3-Na_3AlF_6	Crystalline silicon as the cathodic deposit. Silicon-aluminum alloy was obtained on electrolysis.
25	SiO_2-LiO-GeO_2	Electrolysis resulted in Ge-Si alloy.
26	SiO_2-Na_3AlF_6	Cathodic silicon after purification analysed 99.7-99.99%.
27	Na_2SiO_3-NaF	Electrolysis at 1100 °C yielded molybdenum silicide. Molybdenum was used as cathode.
28	SiO_2-Na_3AlF_6	Silicon deposit was obtained in the form of a pasty ball and was separated by leaching out the electrolyte. The silicon crystals obtained were further treated as required for electronic use.

Table 17 (continued)

Reference Number	Electrolyte	Remarks
29	Na_3AlF_6-SiO_2-Al	A possible production of silicon aluminum alloys was discussed.
30	Na_3AlF_6-SiO_2 Na_3AlF_6-SiO_2-AlO_3	At current densities less than 0.2 amps/cm^2, silicon was deposited at the cathode. At higher current densities, silicon and aluminum were deposited.
31	Na_3AlF_6-SiO_2	Pure silicon was produced by anodic dissolution of copper-silicon, copper-silicon-iron, and aluminum-silicon-iron anodes.

Table 18

Comparison of Electrolysis and Arc-Furnace Production of Silicon

Process	Arc-Furnace	Electrolytic
Capacity (Kg Si/Hr.)	1000-2000	0.1
Silicon Purity Wt. %	98	99.7-99.99
Energy Consumption KWH/Kg Si	12	34

Table 19

Silicate Containing Electrolytes

Reference Number	Electrolyte	Remarks
32	K_2SiF_6-KCl	Electrolysis yielded cathodic silicon deposits along with trace amounts of potassium.
33	K_2SiF_6-NaCl	Electrolysis at 700 °C yielded pear shaped deposit up to 10% by weight.
34	Na_2SiF_6-Na_2CrO_4-CrF_2	Chromium silicon alloy was deposited at the cathode.
	Na_2SiF_6-MnF_2-MnO_2	Manganese-silicon alloy was obtained on electrolysis.
	K_2SiF_6-TiO_2	Resulted in titanium silicide in the form of $TiSi_2$.
35	K_2SiF_6-KBF_4	Electrolysis resulted in boron-silicon alloy.
36	K_2SiF_6-KCl-NaCl	Electrolysis yielded cathodic silicon deposits.
37	K_2SiF_6-KCl K_2SiF_6-NaCl K_2SiF_6-KCl-NaCl	Studied the mechanism of silicon deposition in the temperature range 750-805 °C.
38	K_2SiF_6-KCl-NaCl-KF	Silicon deposit with trace impurities as potassium and sodium.
39	K_2SiF_6	No deposit was obtained due to decomposition of K_2SiF_6.
	K_2SiF_6 - Na_2SiF_6	Si deposit was obtained along with Na and K.
40	NaCl-KCl-K_2SiF_6-Na_2TiF_6	Silicon with titanium silicide along with trace impurities of sodium & potassium.

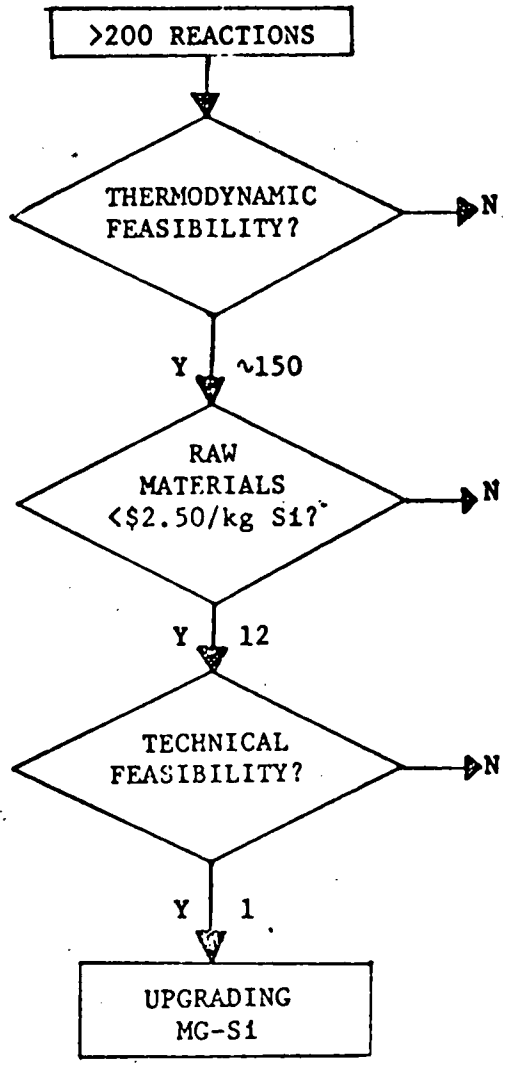

Figure 3. Screening Steps Used to Select the Most Probable Process for Producing Solar-Grade Silicon.

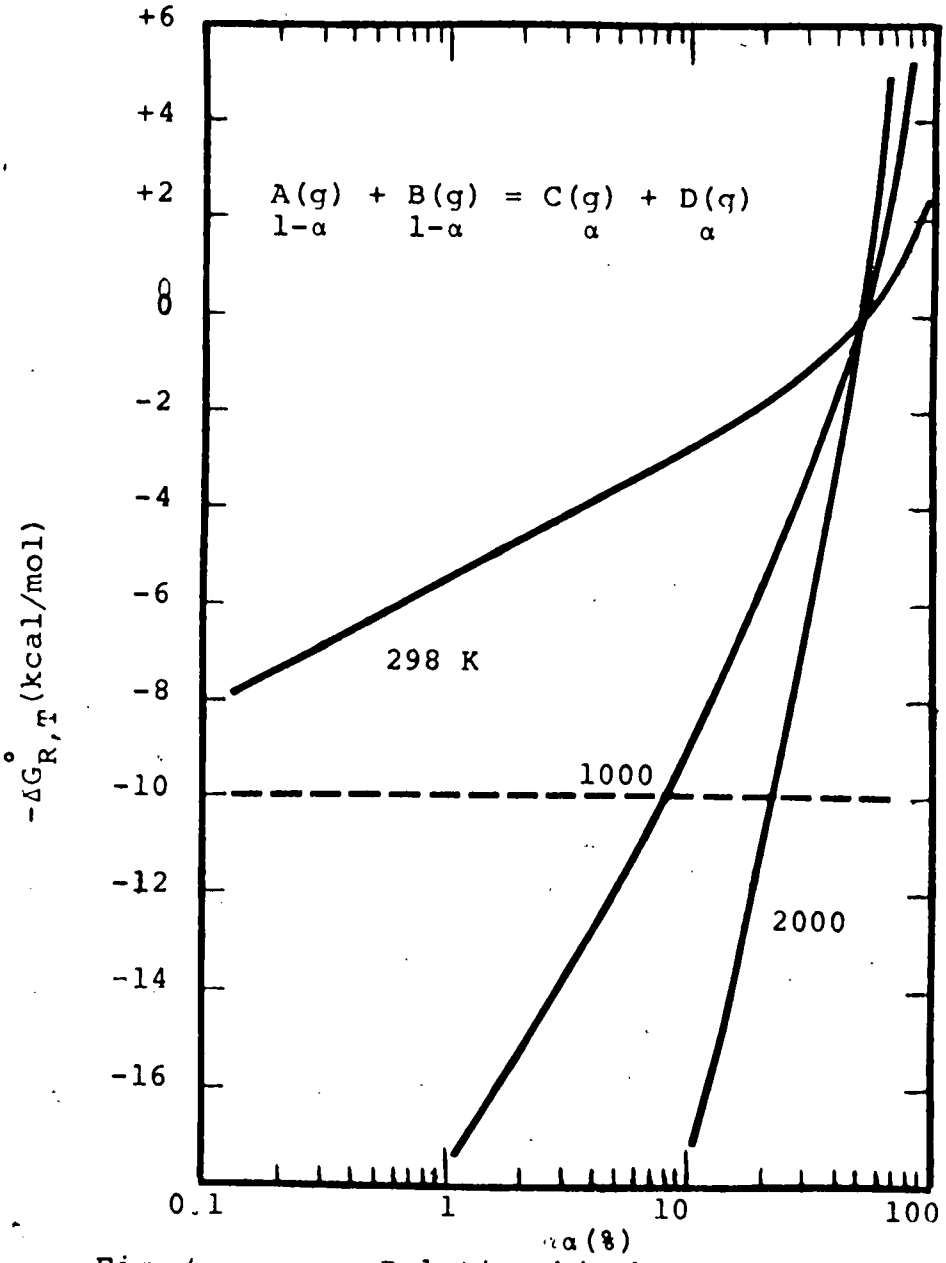

Fig. 4. Relationship between free energy change and degree completion of a specific reaction at different temperatures.

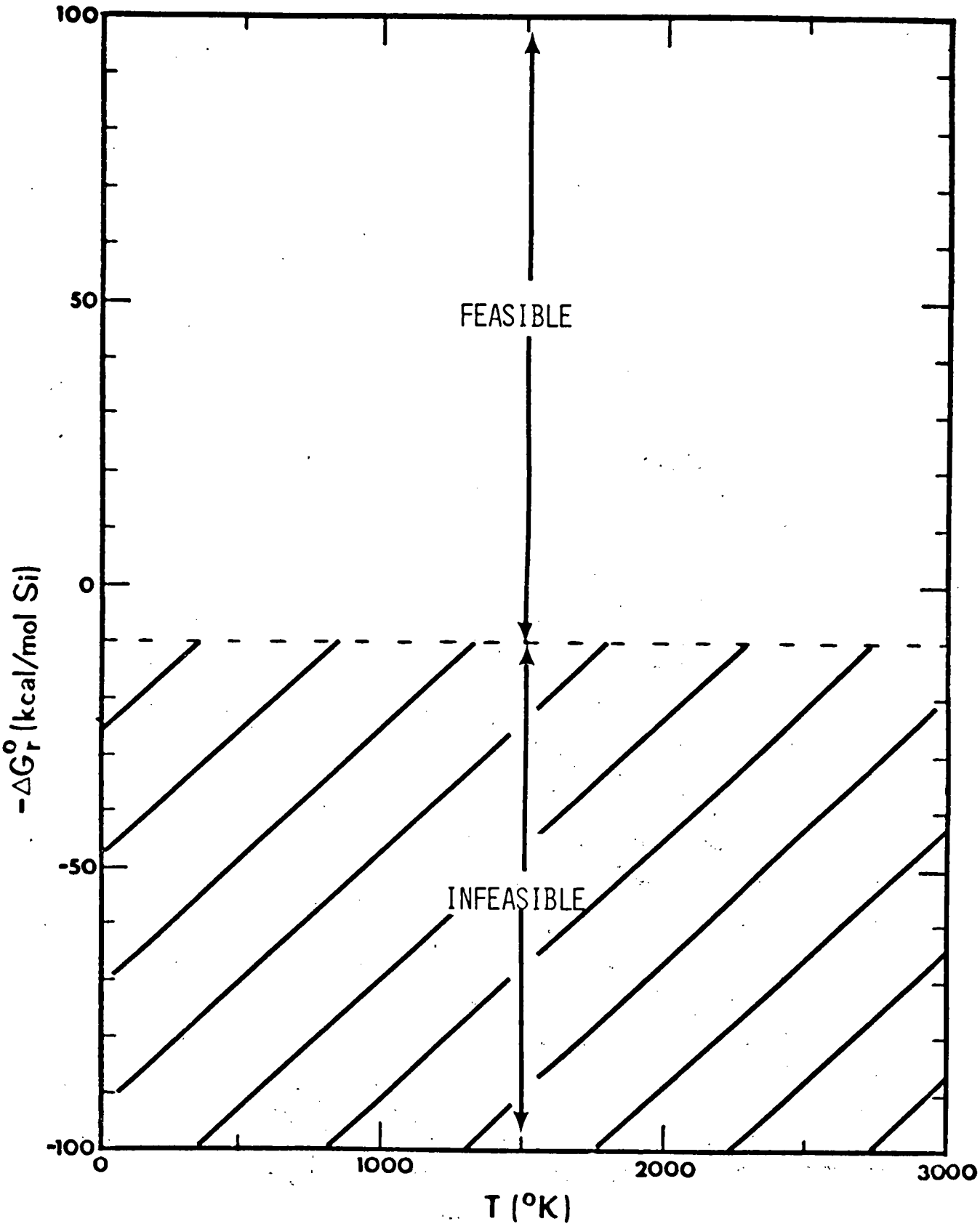

Fig. 5. General coordinate system for the thermodynamic screening of proposed chemical reactions

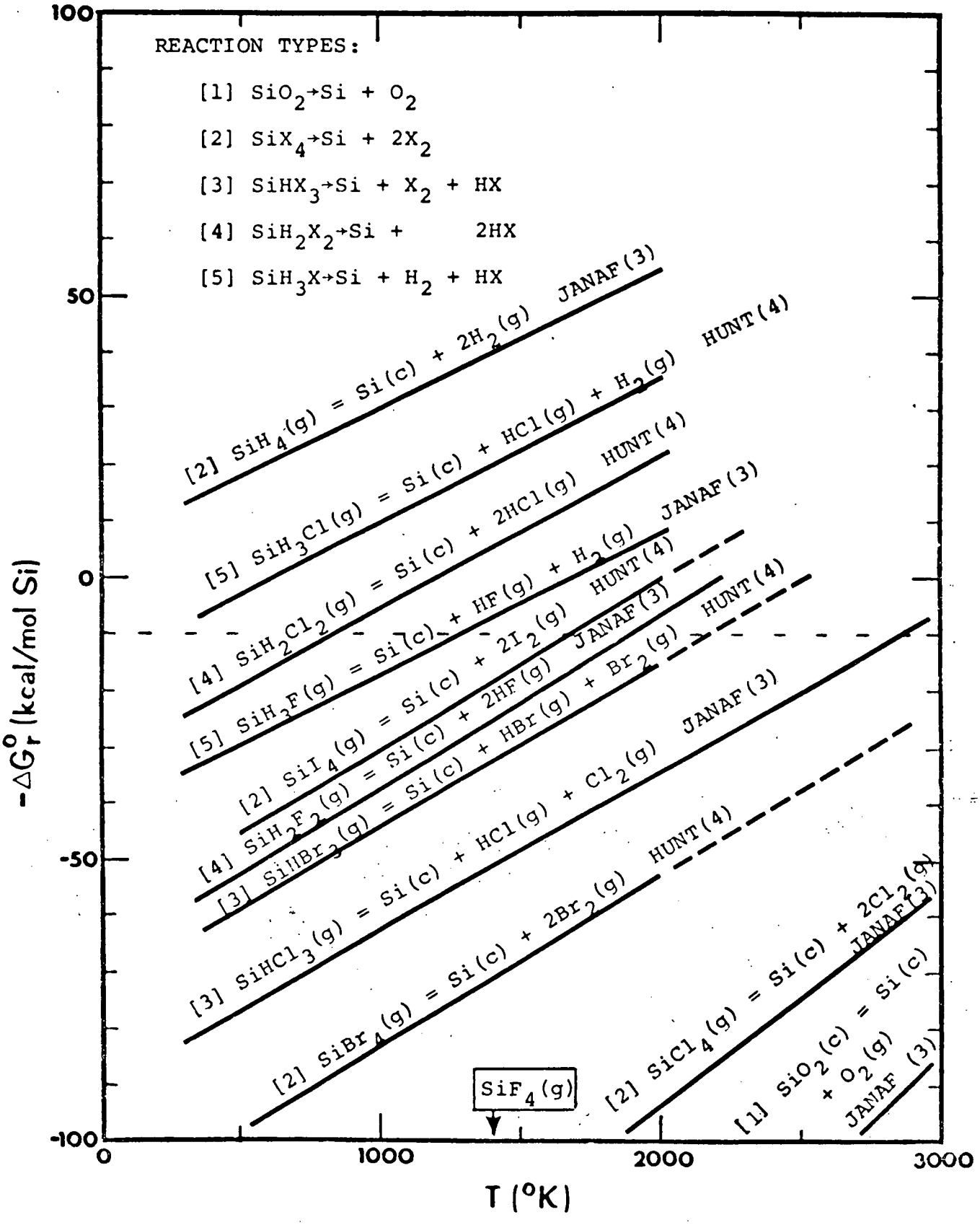

Fig. 6. Pyrolysis reactions for the production of silicon

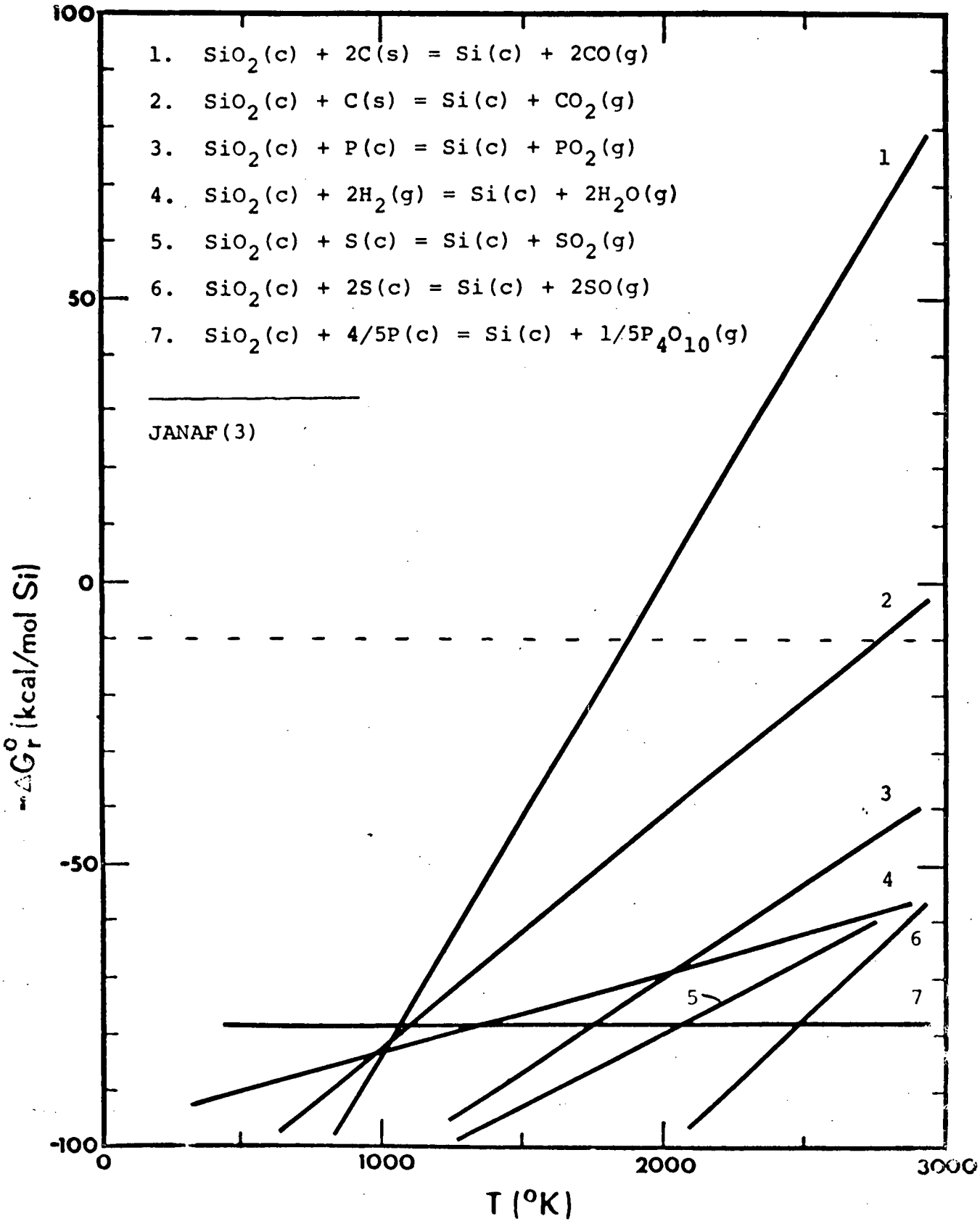

Fig. 7. Silicon synthesis by the reduction of silica with nonmetals.

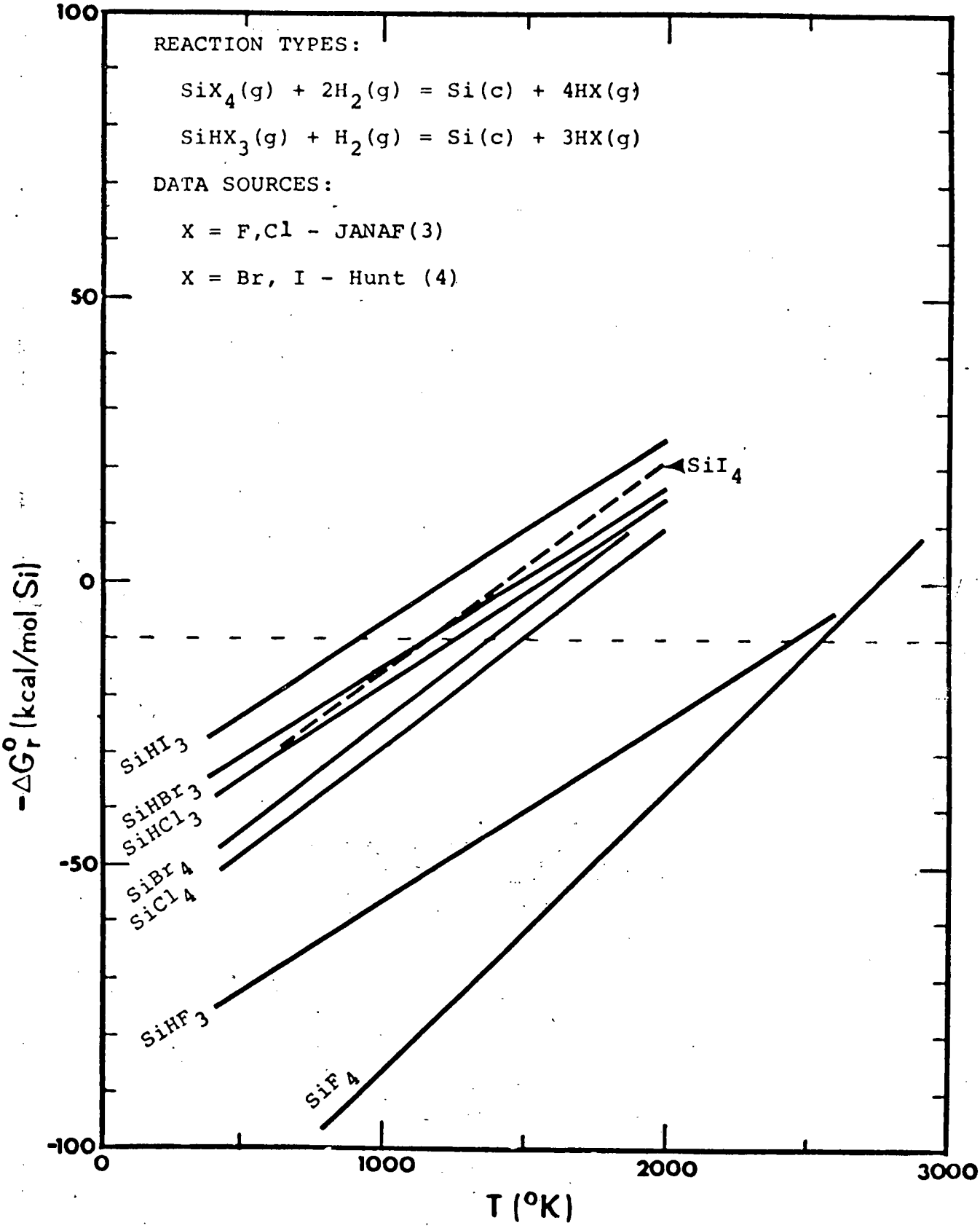

Fig. 8. Silicon synthesis by the hydrogen reduction of tri- and tetrahalosilanes

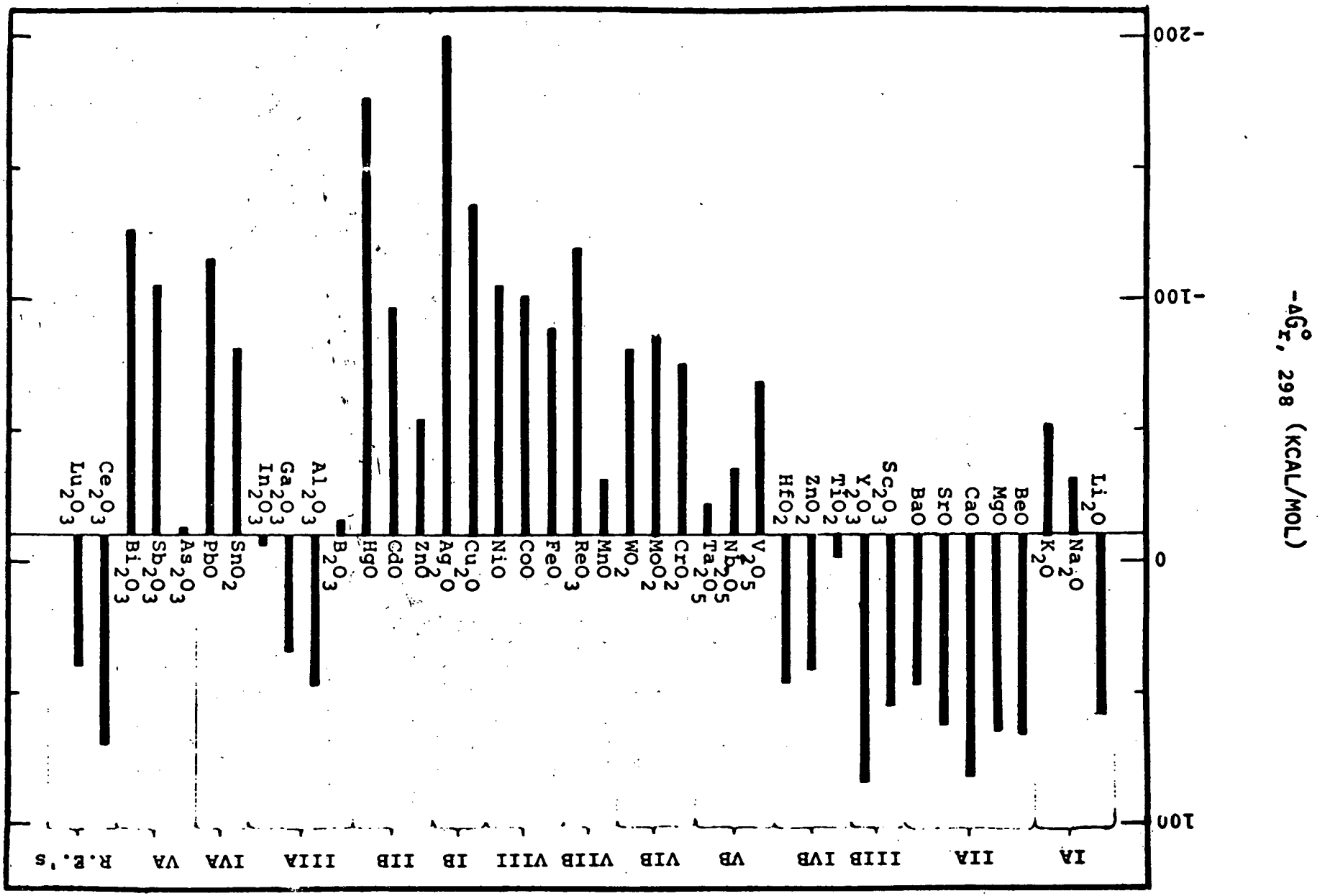

Fig.9. Silica reduction by metals according to the general reaction

$$SiO_2(s) + 4/nM(s) = Si(s) + \begin{cases} 2/nM_2O_n(s), & n = \text{odd} \\ 4/nMO_{n/2}(s), & n = \text{even} \end{cases}$$

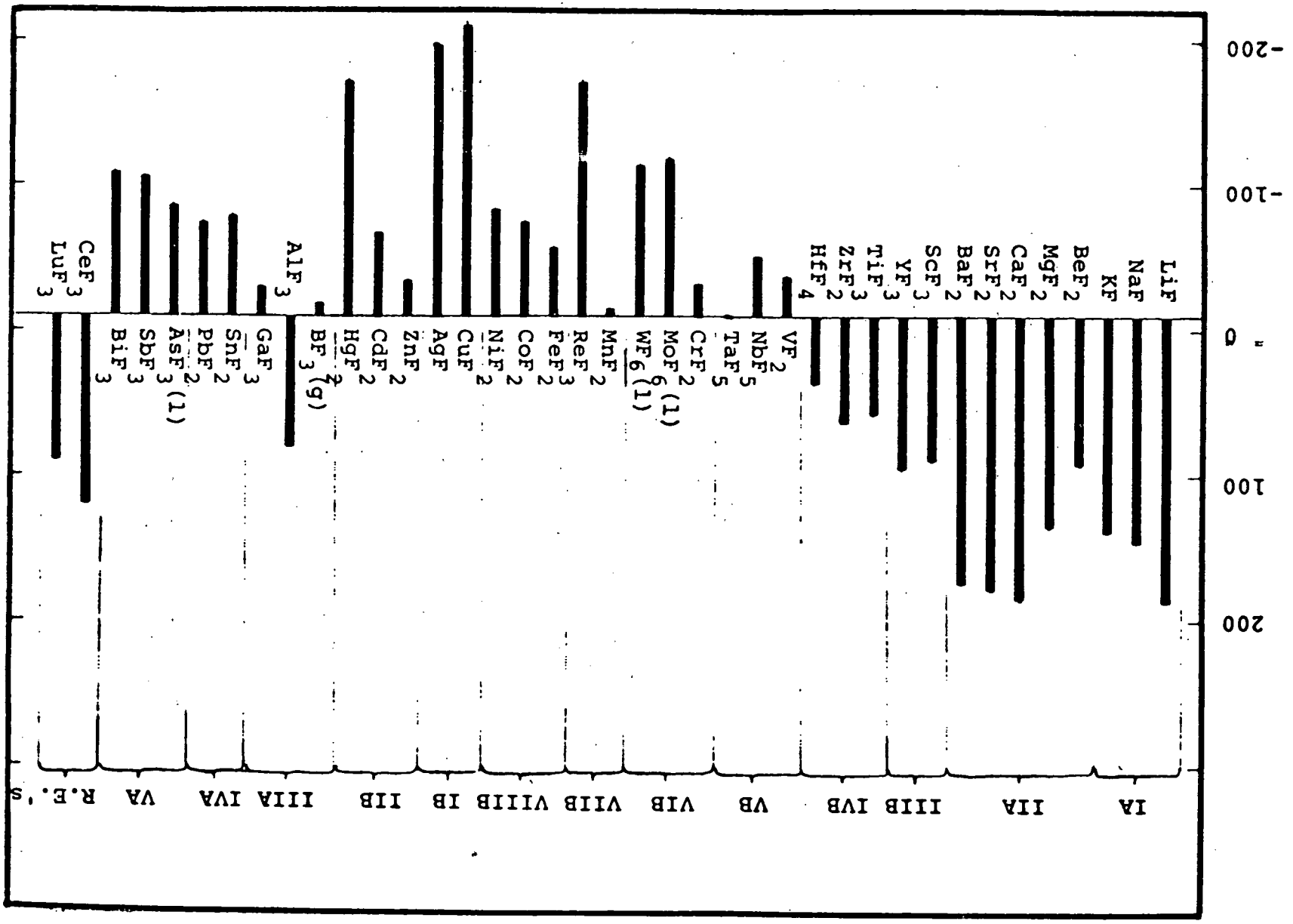

Fig. 10. The reduction of silicon tetrafluoride by metals according to the general reaction $SiF_4(g) + 4/nM(s) = Si(s) + 4/nMF_n(s)$

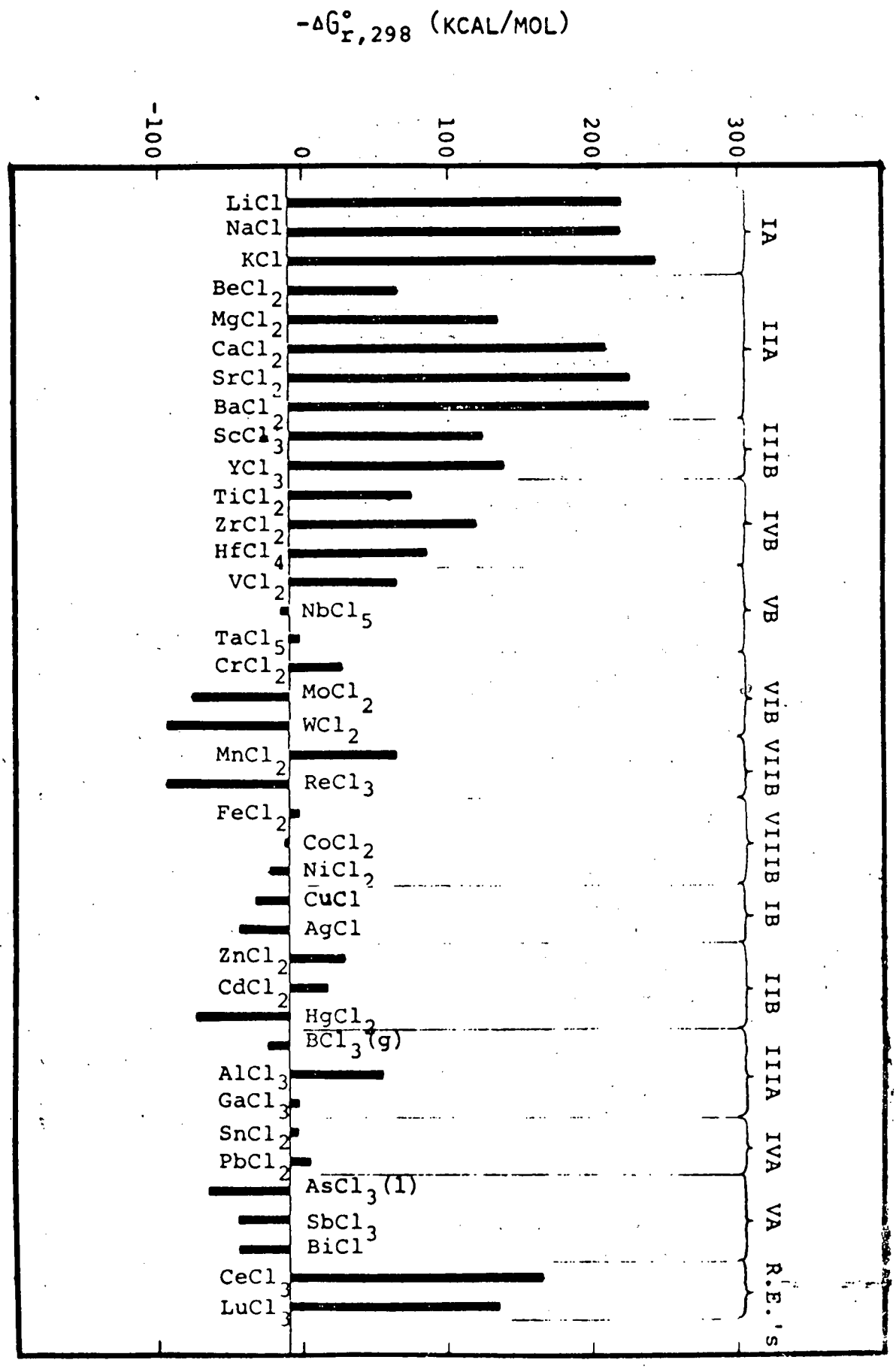

Fig. 11. The reduction of silicon tetrachloride by metals according to the general reaction $SiCl_4(g) + 4/nM(s) = Si(s) + 4/nMCl_n(s)$.

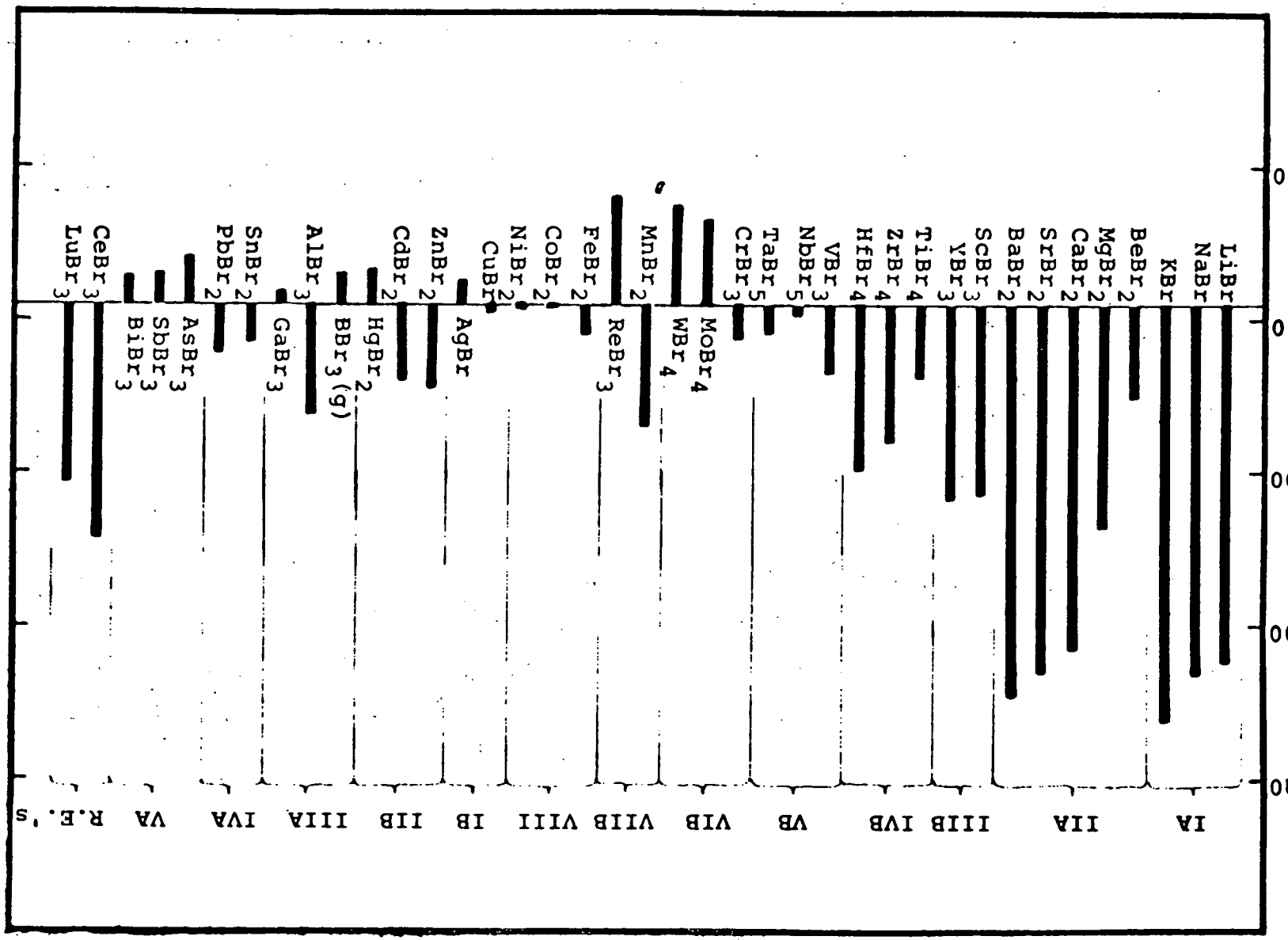

Fig 12. The reduction of silicon tetrabromide by metals according to the general reaction $SiBr_4(g) + 4/nM(s) = Si(s) + 4/nMBr_n(s)$.

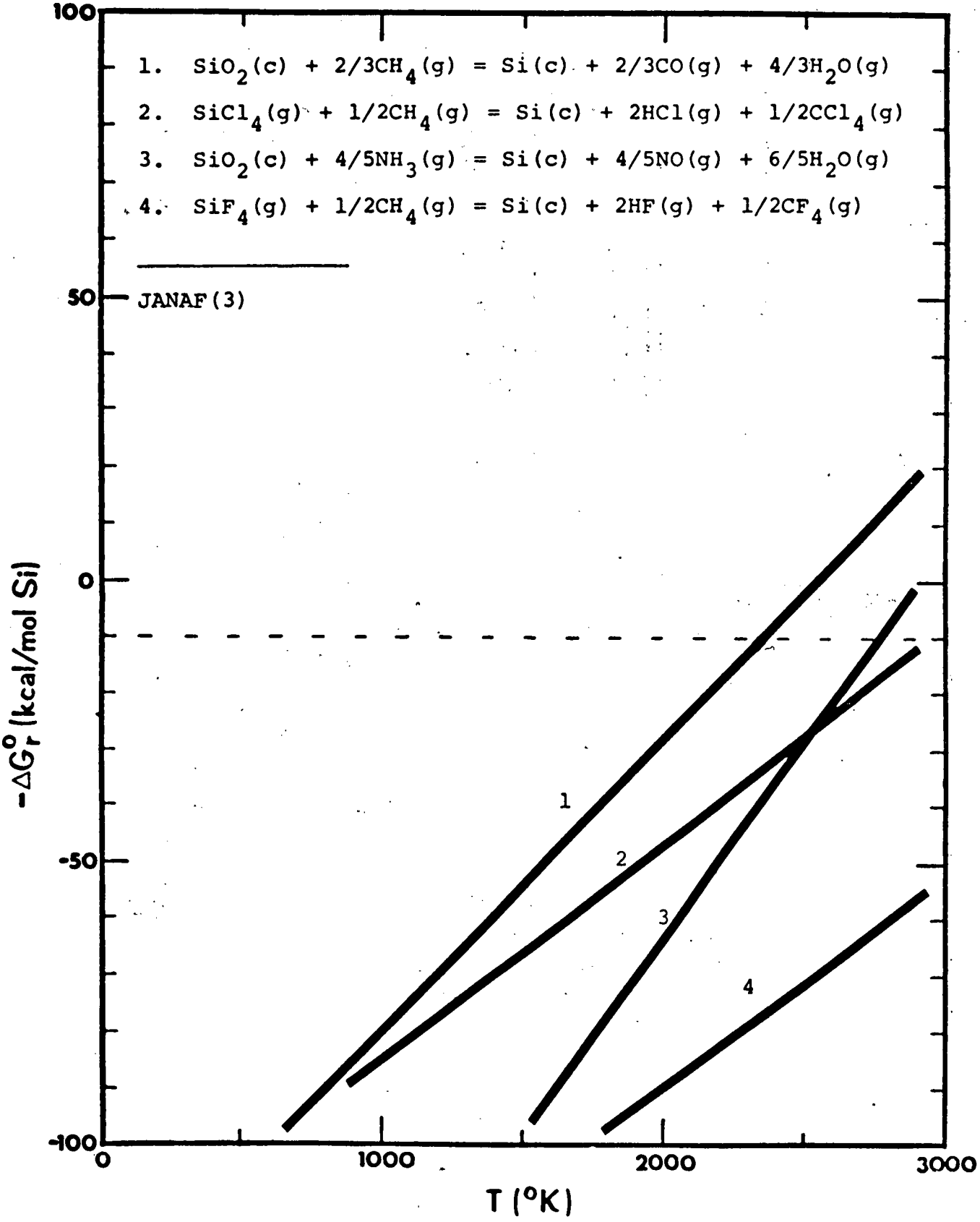

Fig. 13. Silicon from the reduction of SiO_2, SiF_4, and $SiCl_4$ by the compounds CH_4 and NH_3.

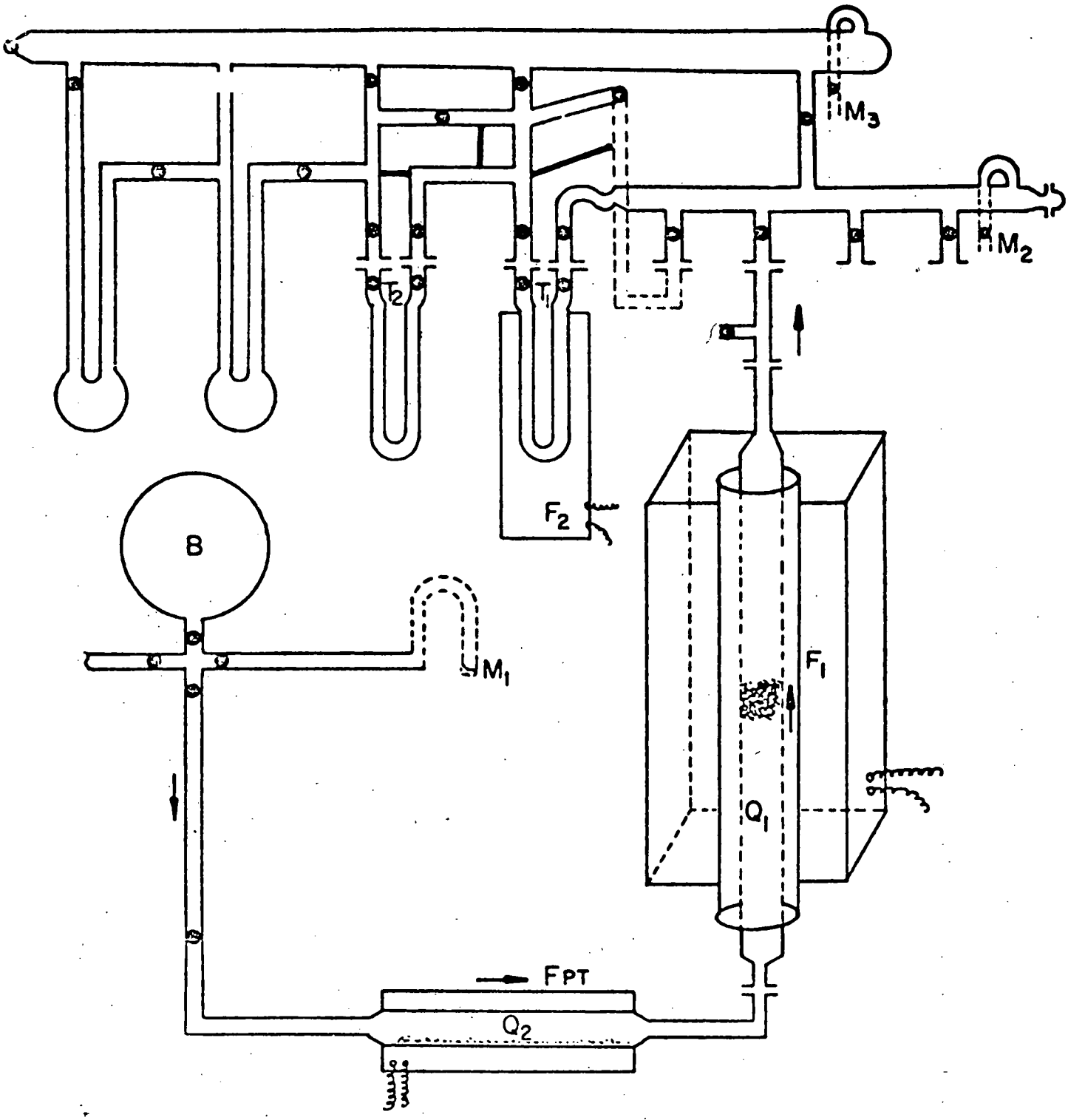

Figure 14. Experimental Silicon Fluoride Transport System

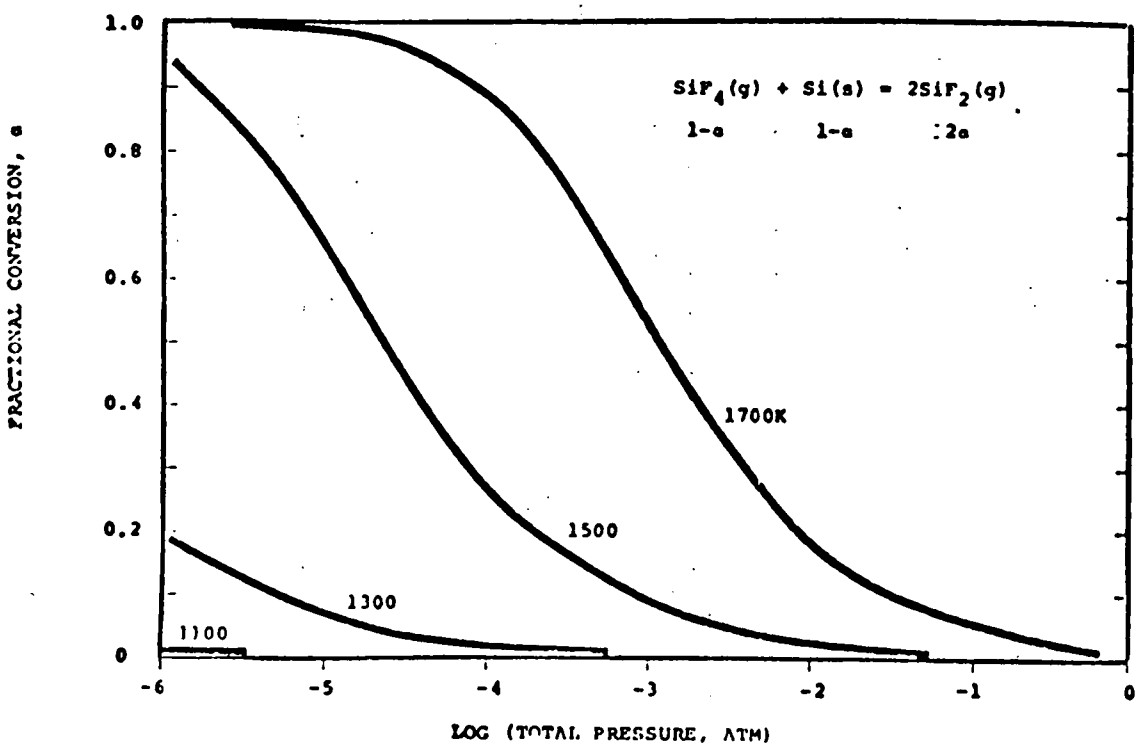

Fig 15. FRACTIONAL CONVERSION OF SiF_4 TO SiF_2 AS A FUNCTION OF TEMPERATURE AND TOTAL PRESSURE

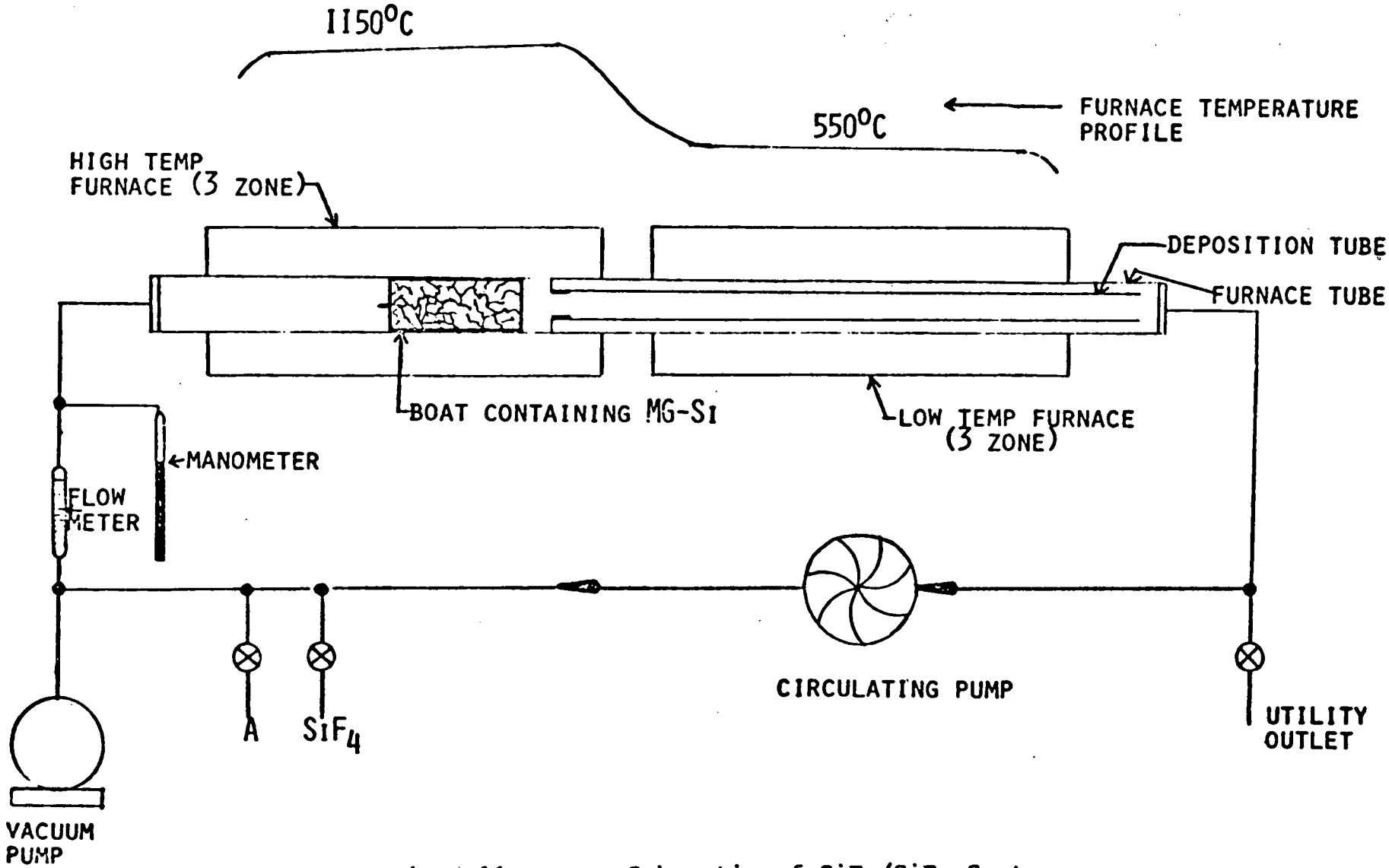

Fig. 16. Schematic of SiF_2/SiF_4 System

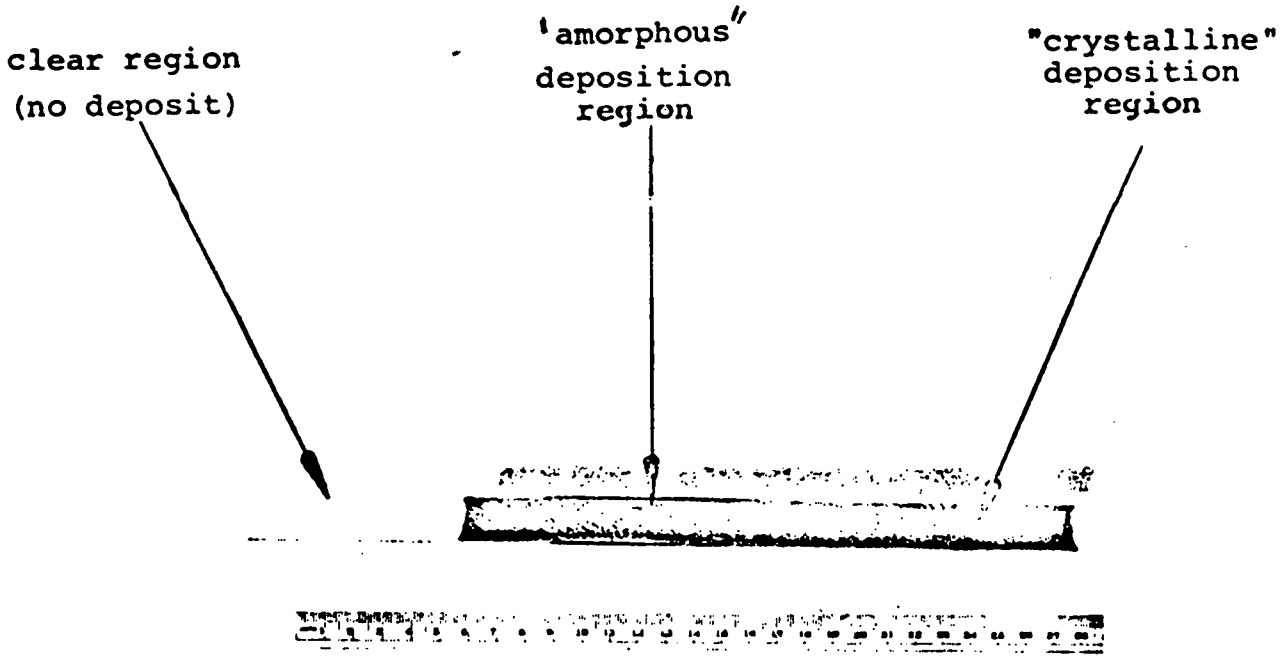

Figure 17. Cross Section of Input End of a Deposition Tube

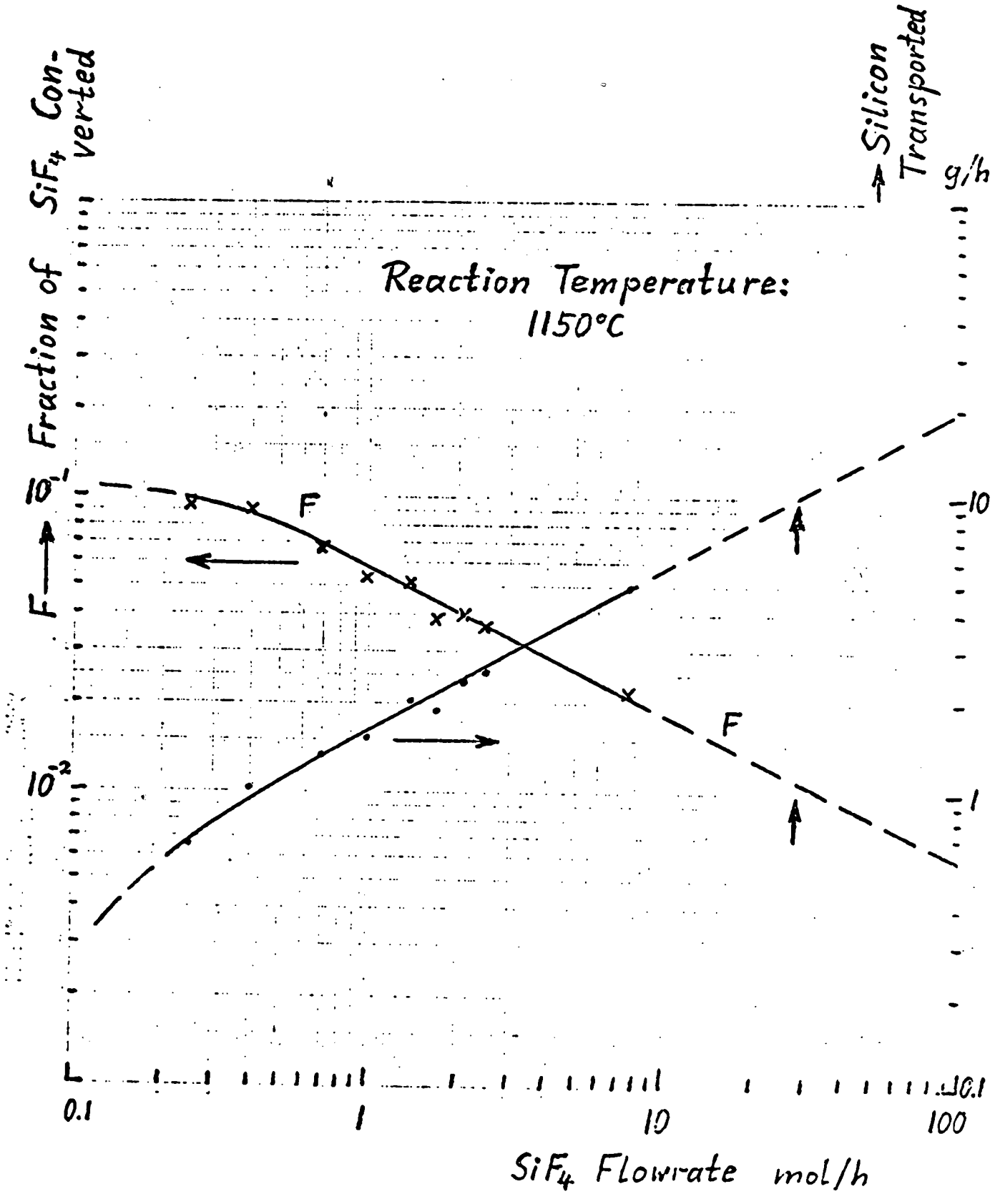
Reaction Temperature:
1150°C
Fraction of SiF_4 Converted
Silicon Transported
g/h
F
F
10^{-1}
10^{-2}
10
1
0.1
0.1
1
10
100
SiF_4 Flowrate mol/h

Fig. 18

III. THE FORMATION OF SILICON SHEET

A. General

The work of this area is concerned with the formation of purified silicon into thin large area sheets of single crystal silicon. As a practical matter, it is highly probable that a polycrystalline sheet consisting of crystallities with a minimum linear dimension of the order of 3 mm or greater will allow the formation of photovoltaic cells and arrays with acceptable efficiencies (Ref. 56). If a sheet formation technique does not yield sheet of adequate crystallinity, but is attractive from the point of view of some of the other criteria (e.g. cost, speed, etc.), then the use of a separate recrystallization step (see section IV of this report) may be justified.

The specific goals of this area are:

Geometry - 1 meter wide, 100 micrometers thick
Production Rate - 20 meters (at nominal width) per hour
Energy Investment - 150 kWh or less per square meter
Morphology - Single crystal or large grain polycrystal
Cost - less than $5.00 per square meter

For the convenience of the following discussion, the potential sheet growth processes have been categorized as either solid, liquid, or vapor processes as determined by the type of phase change involved. Tables 20-22 provide a listing of the sheet formation processes which have been considered during the program.

Table 20 shows the three solid sheet formation processes considered and gives brief comments with regard to the listed assessment factors. Hot rolling is of considerable interest because of its potential as a high speed operation. Hot rolling of sheet metals is performed at speeds up to 60 mph, well in

excess of the speed (20 meters per hour) specified as the goal for this program. A literature search disclosed reports of reasonable ductility in polycrystalline silicon bars at elerated temperatures (57) and limited success in an attempt to hot roll silicon by C.L. Kolbe (58, 59). A report of the successful hot rolling of germanium by M.S. Abrahams (60) provided further evidence of the basic feasibility of hot rolling diamond cubic materials. Despite the above mentioned work, it was found that an extensive lack of quantitative data on the mechanical properties of polycrystalline silicon at elevated temperatures and high strain rates existed. This lack posed a major obstacle to the attempt to arrive at a difinitive assessment of the feasibility and potential capabilities of both the hot rolling and extrusion processes. The existing body of data was found to be insufficient to answer such key questions as: what rolling and extrusion speeds are possible, what thickness reduction per pass through the rolls can be realized, and what degree of crystallinity can be realized with rolled or extruded silicon? A research program was initiated at the University to acquire the necessary data to answer these questions. Significant progress has been made in this area and the results to date are very encouraging. A detailed review of this work and its current status is given in Section III-B.

Extrusion, like rolling, is a potentially high speed process and shares similar materials selection problems. It also would yield material with a fine grain structure, requiring recrystallization. Impurity inclusion may be a somewhat more severe problem than with rolling, however, the form of the input silicon usable by this process would probably have a wider range.

Kolbe's work (58) is the only experimental study of silicon extrusion uncovered by the literature search. The test samples used in his experiments consisted of zone refined single crystal and cast polycrystal rods with diameters of 0.75"-1.25" and lengths of 0.188"-2.060". The samples were encased in thick

molybdenum jackets which provided support for the silicon and aided in maintaining the temperature during the deformation. The jacketed samples were heated in a furnance in a hydrogen atmosphere for periods of 1/2 to 3.4 hour to bring them to equilibrium at the desired temperature. The molybdenum jacket was removed by oxidation after the process.

Extrusions were performed at temperatures of 1300°, 1325°, and 1350°C with a maximum ram load of 300 tons. The diameter of the billets prior to extrusion was 2-1/16". Most of the extrusions were through a 0.75" x 1.50" inch rectangular die, while a few samples were extruded through a 1.0" inch die. X-ray examination of the extruded samples indicated that extrusions made at 1325°C and 1350°C were free of cracks while some of those done at 1300°C had cracked regions. The majority of the extrusions were made at a ram speed of 6" per second.

The field of silicon ribbon growth techniques is currently the subject of considerable interest and activity (61, 62). The third process listed in Table 20 is the formation of large area silicon sheets by alloy-bonding a number of such ribbons together. A metal film would be deposited onto the edges of the ribbons after which they would be butted together to form a sheet and alloy bonded through the application of heat and lateral pressure. The proper selection of the metal to be used in the alloying will allow the use of the bond area as an isolation/interconnection region for the cells making up the array. Should the ribbon growth techniques, such as the EFG process, prove to be feasible as large scale, low cost manufacturing processes, then the ribbon alloying technique will warrant serious consideration. It is felt that the experimental feasibility of the alloying process can be established with a relatively moderate effort.

The sheet formation processes listed in Table 21 involve a phase transition from the liquid to the solid state. Two of the processes which fall into this catagory have received con-

siderable attention as potential processes for lowering silicon solar cell manufacturing costs. The dendritic growth process was extensively investigated by Westinghouse (Ref. 63) in the nineteen sixties and work on this process have recently been initiated at the University of South Carolina (62). Wide variations in the physical dimensions of the dendritically grown material, caused by difficulties in controlling the temperature gradient in the vicinity of the dendrites and other growth parameters, considerably reduced the economic and technical attractiveness of this process, and the development of the technology to overcome these difficulties was never completed.

The Edge-Defined-Growth (EFG) process, presently under investigation by Tyco (Ref. 61), is a promising example of the processes which use shaping dies to control the geometry of the sheet or ribbon as it is pulled from a silicon melt. The process is particularly attractive because it can yield single crystal material. The development of the EFG process is presently hindered by the interaction between the die material and the molten silicon which results in die erosion and silicon contamination problems. A number of die material combinations are under investigation which, hopefully, will eliminate (or at least reduce to manageable proportions) this problem. This is clearly the developmentally most advanced sheet or ribbon growth technique at this time, and can be considered as a good possibility for incorporation into the low cost solar array fabrication concept.

The other processes shown in Table 21 have been the subject of brief studies in the past, but have not received major developmental attention. In particular, W.R. Grace & Co. (Ref. 64) investigated sheet casting, and, to a lesser extent, the pulling of silicon sheet from a binary melt as part of a one year government sponsored program. In the casting experiments, molten silicon was floated on liquid metals (primarily lead).

Polycrystalline films were obtained which, because of surface tension effects, were lens shaped and relatively thick. Films of this type might be suitable as starting material for the hot rolling process.

The growth of silicon from a binary melt is attractive because of the potential for low temperature growth and the consequent reduction of materials interaction problems. The feasibility of the basic process for silicon (Refs. 64 and 65) and other semiconductors (Ref. 66) is well established, and the technique has recently found wide application for III-V compounds in the experimental fabrication of devices, particularly LED's. The major concern in the present application would be to develop techniques which will allow reasonable growth rates without the inclusion of large amounts ($>10^{-5}$) of the other melt-constituent. Techniques involving the circulation of the solvent are under consideration. This process was initially felt to be of sufficient potential to warrant a small scale experimental investigation, however, further investigation lead to the conclusion that some of the other processes were more promising and the work on this process was suspended. This work is discussed in Section III-C.

Processes involving the vaporization of silicon or the use of silicon compounds in vapor form are shown in Table 22. One of the less extensively explored reactions in the area of chemical vapor deposition uses silicon fluoride as the transport medium. This reaction also has potential for purifying silicon. Work on an experimental program to investigate this process is described in Section II. In general, deposition rates for chemical vapor deposition depend upon the particular chemical species, pressures, and temperatures used. Chemical vapor deposition processes have been intensively investigated during the last decade or so. Table 23 lists some of the reactions which have been considered. The thermodynamics of these processes was discussed in Section II above. In general, minimum reaction temperatures increase as one

proceeds from the iodides up through the fluorides. Silicon deposition rates of the order of micrometers per minute have been realized for reactions such as the pyrolisis of silane (Ref. 67) and the hydrogen reduction of silicon tetrachloride (Ref. 68). Deposition rates of this order over a fairly large area would yield acceptable sheet growth rates for the present program goals.

The V-L-S process uses an alloy melt as an interface between the growing crystal sheet and the vaporized silicon compound. A temperature gradient is maintained across the melt such that the surface in contact with the vapor is hotter than that in contact with the growing crystal. The vaporized compound dissociates at the hotter surface, and the resulting elemental silicon is incorporated into the melt and diffuses through the melt to the growing surface where it is deposited. The process is very similar to that of pulling a crystal from a binary melt with the silicon compound vapor acting as the silicon source to replenish the material removed from the solution during growth. The growth rate for this process is controlled by a number of factors, including the mass transport rate of the reactant compound(s) to the surface of the melt, the rate of the reaction at the melt surface which results in the freezing of the elemental silicon, and the diffusion rate of the silicon through the melt to the solidifying surface. The latter will probably be the major growth rate limiting factor.

Vacuum deposition of thin silicon films using sputtering and electron beam evaporation techniques has been studied by a number of workers. Fang, et.al. (Ref. 69) of Boston College are currently investigating this process for solar applications. The interaction of the deposited silicon with the substrate material poses serious problems here as elsewhere.

B. SILICON DEFORMATION BY ROLLING

1. Introduction

In order for a material to be rollable several conditions must be met. First, the material must undergo substantial reduction in thickness by rolling without cracking. Cracking normally occurs first along the edges of the strip, since this is where the local stresses are tensile rather the compressive. To evaluate the rolling limit imposed by edge cracking, we are determining the "forming limit diagram" for polycrystalline silicon. Such diagrams have proven extremely useful in metal working applications, and it is hypothesized that they will also be applicable to silicon. During the plastic deformation of a metal in a forming process, the onset of fracture is determined by the maximum tensile strain and the maximum compressive strain at the point of initiation of the fracture. For the purposes of the analysis, the range of values of these two strains are plotted on a "forming limit diagram" (Fig. 19) on which they form a line. The diagram is then used in the following manner: If the forming process is such that during deformation the strain coordinates of all points in the material are such that the resultant falls below the line, then the material will not fracture. If, however, the resultant at some point falls above the line, then the part will fracture. For example: during rolling the edge of the sheet is subjected to both compressive tensile strains. If in Figure 19 (for cold drawn 1045 steel) the tensile strain is 0.8 and the compressive strain is -0.8, then the resultant point will lie above the forming limit curve and fracture will occur. The forming limit diagram for a material is a function of temperature, strain rate, and crystallographic texture, hence silicon forming limit diagrams will have to be determined for a range of these parameters. Despite some reservations concerning its applicability in the case of silicon, the forming limit diagram technique is felt to be sufficiently promising to justify an investigation.

The diagram is determined by hot uniaxial compression of samples as illustrated in Figure 20. During high temperature compression, the sample deforms from the shape shown on the left side of Figure 20 to that shown on the right. As a result of this deformation w_o increases to w and h_o decreases to h. The maximum tensile strain is then given by $\ln(w_{max}/w_o)$ and the maximum compressive strain by $\ln(h_{max}/h_o)$. The values of these two strains are then plotted on the forming limit diagram. Different ratios of these strains are produced by using cylinders with different initial height to diameter ratios.

A uniaxial compression rig was built and installed in an Instron test unit, in which silicon can be deformed at various temperatures and strain rates. The experiments to date have been performed on samples cut from as-formed polycrystalline logs of semiconductor grade silicon obtained from Dow Corning. Prior to testing the samples exhibit the oriented fine needle like crystal structure typical of these logs. It has been observed that the crystallographic texture changes after plastic deformation and annealing at approximately 1300°C. This observation is of considerable importance as will become apparent in the detailed discussion of these results. An x-ray diffraction technique has been used in the studies of textural changes in the polysilicon which clearly demonstrates the occurance of recrystallization.

The compression measurements also provide the stress as a function of strain rate and temperature, which determines the force and power that must be supplied to the rolling mill in a rolling operation.

2. Uniaxial Compression Experiments.

The test rig consists of two push rods made of graphite (Poco HPD-1), the upper one is mounted on the Instron machine cross head, which can be moved at a constant speed (0.02" - 2"/min.) The bottom rod rests on a load cell, the output of which is connected to a single pen strip chart recorder. A quartz tube

sealed at both ends by water cooled Viton "O" rings serves as a chamber through which Argon gas can be circulated. The top and bottom ends of the push rods are water cooled. Fig. 21 shows the arrangement of various parts of the rig. The platens were made of a Ta-10%W alloy. Pyrolytic graphite discs (2 and 6 in Fig. 21) considerably reduced the conductive heat losses. Initially, temperature measurements were made with an optical pyrometer. Very recently we have been successful in using a Pt' Pt-10Rh-thermocouple for accurate temperature ($\pm 3^{o}C$) measurements. This has been verified by checking the melting point of high purity (99·999%) copper inside the graphite susceptor.

A 10 KVA induction unit was found adequate for heating a silicon sample inside a graphite susceptor to temperatures as high as $1400^{o}C$.

Samples (0.325" dia., 0.500" length) of two major orientations (Fig. 22) were core drilled from a polylog, one containing the long grains normal to the compression axis (i.e. compression axis parallel to polylog axis) and the other containing the long grains parallel to the compression axis (i.e. compression axis normal to the polylog axis). They were uniaxially compressed following mechanical and chemical polishing.

A total of 10 samples have been plastically deformed to observe the effect of temperature, orientation and strain rate on the deformation behavior. The yield strength (0·02% offset) dropped from 21·2 KPSI at $1285 \pm 20^{o}C$ to 4·3 KPSI at $1350 \pm 20^{o}C$ (see Table 23 and Fig. 23). Attempts to conduct tests at temperatures higher than $1350^{o}C$ were unsuccessful due to a strong reaction of the silicon with the platens under high pressure. Increasing the strain rate by one order of magnitude raised the yield strength and work hardening coefficient by about 12%.

The stress strain curves for samples 7 and 10 show a strong yield drop (Fig. 25), a characteristic which is very similar to that of single crystal silicon. This behavior is consistant with the idea that the needle like grains have a particular crystallographic orientation (in this case (110), verified later). Such a strong yield drop giving a highly non-homogeneous deformation makes this orientation unsatisfactory for rolling into a sheet.

To obtain an estimate of the rate of softening at the deformation temperature the following experiments were performed. Sample #1 (see Figure 23) was deformed to approximately 10% strain, unloaded and immediately reloaded. Since the flow stress upon reloading is the same as it was before unloading, there is no appreciable softening occurring in times of the order of a minute or so. This same sample was then deformed to a total strain of approximately 20% (see Figure 23), unloaded, held at the deformation temperature, 1350°C, without load for ½ hour and then reloaded again. It can be seen from Figure 23 that plastic flow following this annealing treatment begins at a much lower stress. This suggests that recovery and recrystallization are not occurring at a rate sufficient to soften the silicon while the deformation is being carried out at this strain rate. Similar observations at a strain rate an order of magnitude higher are shown in Fig. 24. These findings show that in a rolling operation the polysilicon will be "cold rolled" even though the rolling temperatures are as high as 1350°C.

3. Texture and Recrystallization of Polycrystalline Silicon.

The polylogs grown by the CVD technique consist of long needle shaped (dia~10μ, length~1cm) crystals growing radially outwards from the central "slim rod". The photomicrographs (see for example Fig. 10, in the July 1975 Progress Report) showing such

a structure, the strong anisotropic plastic deformation showing ellipticity in the cross sections of cylindrical samples and a strong yield drop for samples when compressed along the long grains indicated that the long grains have a preferred crystallographic orientation.

The changes in mechanical properties on annealing shown in Figs. 23 and 24, and the change in the microstructure following deformation and annealing (Figs. 9 and 10 in the July 1975 Report) strongly suggested that recrystallization has occured. To determine the crystallographic texture of the polylog and to verify the occurence of recrystallization we have used a standard x-ray diffraction (reflection) technique for texture determination.

A thin square sample (1/8" x 1" x 1") was cut from a polylog near the outside diameter center such that the long grains were in the plane of the slice ("A" in Figure 26). The sample was mounted on the goniometer of a siemens texture diffractometer unit. The Schultz (Ref. 71-73) reflection method was used where the sample rotates both around the axis normal to its plane (BB' in Fig. 27) and around an axis in the plane (AA' in Fig. 27). This allows one to trace a spiral on the stereographic projection and plot intensities of a particular reflection.

To see the effect of deformation and annealing a thin sample was prepared in the following way:

i) cylinder 0.5" x 0.5" of CVD material was prepared, with the long grains normal to compression axis.

ii) The sample was compressed (Argon atmosphere), at 1350°C, by 70% at a strain rate $\sim 10^{-3}$ sec^{-1}, and annealed for 1/2 hr. at the same temperature.

iii) The sample was hot pressed again by 25% (total $\Delta\ell/\ell \sim 90\%$) at 1350°C at a strain rate $\sim 10^{-4}$ $sec.^{-1}$.

iv) The sample was annealed at 1300°C for 5 hrs. in an innert atmosphere (Ar gas).

The sample was mechanically and chemically polished and a grain size of 20 to 30 μm was measured using an optical microscope. The Schultz method was used as described above to find the texture. The sample was then annealed at 1350°C for another 5hrs. to see if any changes in the texture earlier determined had occurred.

Fig. 28 shows the results before deformation and after deformation and annealing, using (111), (220) and (400) reflections. The long axis of the grains is shown by the arrow pointing in the North-South direction on each pole figure. It is clear from the upper pole figures that the samples have an extremely strong (110) fiber texture; the preferred growth direction of the elongated radial grains is the (110) crystallographic direction, with random rotations about this direction.

Diffraction from the same sample after annealing at 1350°C for 5 hrs without deformation resulted in no qualitative change in the fiber texture. The large grain size, however, made it difficult to plot the exact intensities, therefore, the plots are not included in this report.

Sample B_7' after deformation and annealing clearly shows a cube texture (100) (bottom of Fig. 28). This proves the occurance of recrystallization following plastic deformation and annealing. Details on the effect of rate and degree of deformation on annealing and the minimum time and temperature required for recrystallization will be the subject of future work on this subject.

Further annealing at 1350°C for 5 hrs did not change the cube texture significantly. The only effect was the growth of grains to a size of about 1 mm from an initial size of 20-30μ.

4. Conclusions

The results to date can be summarized as follows:

(a) The rolling of polysilicon at 1350°C will be a "cold working" operation rather than a "hot working" process, since recrystallization will not occur during the rolling process

(b) The best polylog orientation for rolling seems to be the one where compressive loads are along the polylog axis.

(c) It can be stated unequivocally that recrystallization occurs in polysilicon following plastic deformation and annealing at about 1350°C.

(d) considerable mechanical softening occurs in ½ hr. at 1350°C (for sheet thickness ~½") after compressive strains of the order of 20%

C. GROWTH OF SILICON FROM BINARY ALLOY SOLUTIONS

An extensive study of the known characteristics of the alloys of silicon with the various elements was conducted. Table 24 lists elements whose alloys with silicon have been studied along with various characteristics pertinent to their use in the solution growth process. The temperature and solubility data appearing in this table is taken from Hanson and other binary alloy catalogues (74). The impurity level data is taken from various silicon properties sources (75). Table 25 lists elements whose binary alloys with silicon are not well characterized in the literature. A study of properties such as those listed in Table 24 has led to their classification as shown in Table 26. Solution whose compatibility with the high speed growth and high purity requirements of the overall process is questionable

generally fall into one of three catagories. In the first catagory (I in Table 26) are alloys which exhibit very low melting points (highly desireable), but also have very low silicon content at the low temperatures. These solutions will probably yield very slow growth rates; even with special techniques such as melt circulation. In the second catagory (II) the solutions are characterized by high silicon content, but their melting points are relatively high. Many of the alloy co-constituents in this catagory also have high solid solubilities in silicon at or near the alloy melting point. In the third catagory are solutions with moderate melting points and high silicon content but whose constituents are known to be electrically active or lifetime killers in silicon. The majority of the potential candidates fall into one of these catagories. A large number of the remaining candidate alloy solutions have not been characterized (lower right portion of Table 26). Binary solutions of silicon with the two materials shown in the lower left portion of the Table would appear, on the basis of the published data, to hold some potential for the production of solar grade silicon at reasonable rates. Sulfur should actually be placed in the uncharacterized catagory, however, a highly speculative phase diagram for the S-Si system was found. (Ref. 76, Vol. X). The diagram was based on extremely limited data, but, if it is born out, sulfur would have to be considered a possible candidate. The palladium alloy melts at 879^{o}C and has a silicon liquid solubility of >50% at temperatures slightly above this. Its solid solubility is reported to be less than 3 x 10^{16} cm^{-3} in this temperature range. These properties certainly make it of interest. Unfortunately, little useful information on its behavior as an impurity in silicon has been found to-date.

Concurrently with the materials survey, a brief experimental study of binary solution growth was conducted using the tin-silicon system. The experiments were conducted with a two zone rocking furnace using a 960°C dissolution temperature and deposition temperatures ranging from 300°C to 870°C. Evidence of epitaxial growth was obtained, however, as the results of the study of tabulated materials properties indicated that this process was not as attractive as some other candidates, this work was terminated. Further experimental work on the binary solution growth of silicon is probably not warranted until such time as significant new information is acquired which indicates a reasonable prospect of successful process development for one or more of the elements.

D. REFERENCES - SECTION III

56. Heliotek Division of Textron Electronics, Inc.
"High Efficiency Silicon Solar Cells", Final Report (August 1964), Contract DA36-039-SC-90777.

57. Lillie, D. W.; Trans. Met. Soc. AIME, April 1958, p. 249.

58. Kolbe, C. L.; "Hot Extrusion and Rolling of Silicon", General Electric Research Laboratory Report #63-RL-3221 M Schenectady, New York (January 1963).

59. U. S. Patent 3,243,274 (March 29, 1966).

60. Abrahams, M. S.; Trans. Met. Soc. AIME 230, 888 (1964).

61. Mobil Tyco Solar Energy Corporation
"Large Area Silicon Sheet Growth By EFG", 1st Quarterly Report (December 1975), JPL Contract No. 954355.

62. R. B. Hilborn, Jr. and R. B. Faust, Jr., University of South Carolina, Quarterly Report for Period 10/ 1/75-12/31/75, Dated 12/12/75, JPL Contract No. 954344.

63. Westinghouse Corp.
"Dendritic Silicon Solar Cell Optimization and Fabrication", Final Report (1967), Contract AF33(615)-3223.

64. W. R. Grace & Co.
"Investigation of Thin Sheets of High Quality Single Crystal Silicon", 1st Report (1960), Contract DA36-039-SC-85242.

65. Wagner, R. S.; Jour. Appl. Phys. 38, 1554 (1967).

66. Nelson, H.; RCA Review 24, 603 (December 1963).

67. Bhola, S. R. and Mayer, A.; RCA Review 24, 511 (December 1963).

68. Tung, S. K.; Metallurgical Soc. Conferences, Vol. 15, p. 84; Edited by John B. Schroeder; Interscience Publishers, New York, 1961.

69. Fang, P.; "Low Cost Silicon Solar Cells for Large Electrical Power Systems - Growth of Silicon Layers on Steel Substrates", presented at the Solar Energy Research Information Meeting of NSF-RANN Grantees, March 15-16, 1973, at the University of Pennsylvania, Philadelphia, Pennsylvania.

70. Kuhn, H. A., Lee, P. W., and Erturk, T.; Jour. Mat. Engr. and Tech., October 1973, p. 213.

71. Barrett, C. S.; "Structure of Metals", 3rd Edition, McGraw-Hill, 1966, p. 201.

72. Cullity, B. D.; "X-Ray Diffraction", Wesley, 1956, p. 290.

73. Schultz, L. G.; Jour. Appl. Phys. 20, 1030 (1949).

74. Hansen, M.; "Constitution of Binary Alloys", Second Edition, McGraw-Hill Book Company, New York, 1958.

Elliott, R. P.; "Constitution of Binary Alloys, First Supplement", McGraw-Hill Inc., New York, 1965.

Shunk, F. A.; "Constitution of Binary Alloys, Second Supplement, McGraw-Hill Book Company Inc., New York, 1969.

75. Wolf, H. F.; "Semiconductors", John Wiley & Sons, Inc. New York, 1971.

76. Padnos, B. N. et al.; "Integrated Device Technology, Vol. X", Technical Report ASD-TDR-63-316, Vol. X
Air Force Contract AF33(615)-1998, Project No. 4159, Task No. 415906.

TABLE 20: SOLID STATE SHEET FORMATION PROCESSES

PROCESS	ASSESMENT FACTORS				
	Speed	Temperature Range	Probable Resultant Morphology	Anticipated Problem Areas	Comments
Hot Rolling	mph for metals, unkown for Si	>1300°C	fine grain to large grain polyxtal	1. roller and bearing materials.	experiments demonstrate deformability. rate parameters under study.
Extrusion	ram speed of 6 in/sec reported.	>1000°C	fine grain polyxtal	1. die erosion. 2. Silicon Contamination.	not as attractive as rolling.
Alloy Ribbons	Probably limited by ribbon growth rate.	Probably <1000°C	ribbons are singlextal	1. control of alloying over large areas.	basic feasibility should be easily demonstrateable.

TABLE 21: LIQUID TO SOLID SHEET FORMATION PROCESSES

PROCESS	ASSESSMENT FACTORS				
	Speed	Temperature Range	Probable Resultant Morphology	Anticipated Problem Areas	Comments
Growth from Elemental Melt	cms/min.	1420°C	single crystal	1. die materials for EFG. 2. temp. control for dendritic.	several techniques being evaluated by contemporary investigators. EFG most advanced.
Growth from Binary Melt	solvent dependent, diffusion limited.	<1420°C	potential for single crystal.	1. growth rate. 2. solv. contamination.	evaluation of potential alloys indicates other processes more promising.
Casting	cms/min.—m/min.	1420°C	fine grain to large grain polycrystal	1. control of thickness. 2. contamination from substrate.	early experimental studies not encouraging. newer concepts could alter this.

TABLE 22: VAPOR TO SOLID SHEET FORMATION PROCESSES

PROCESS	ASSESMENT FACTORS				
	Speed	Temperature Range	Probable Resultant Morphology	Anticipated Problem Areas	Comments
Chemical Vapor Deposition	10 m/min, but large areas.	300°-1200°C	fine grain polyxtal to singlextal	1. growth rate. 2. suitable substrate 3. silicon purity.	SiF_4 transport process studied experimentally.
Vapor - Liquid - Solid Process	Species dependent, diffusion limited	< 1420°C	large-grain or singlextal	1. growth rate. 2. Solvent contamination.	rates and temperatures vary with alloy elements.
Vacuum Evaporation	net rate of cms/min conceiveable for large area deposition	1420°C	amorphous or fine grain	1. substrate contamination.	experimentally evaluated by several investigators. film electrical characteristics generally poor.

TABLE 23

Sp. No.	Orientation (angle between compression axis and polylog axis)	Strain Rate Sec^{-1}	Temperature ^{o}C	Yield Strength 0.02% offset Kpsi (upper yield point for 7 and 10)	Plastic Strain $\frac{\Delta \ell}{\ell}$ (%)
1.	0	$6{\cdot}6 \times 10^{-4}$	1350±20	4.30	47
2.	0	$6{\cdot}6 \times 10^{-3}$	1350±20	4.80	45
3.	0	$6{\cdot}6 \times 10^{-3}$	1350±20	4.75	41.6
4.	0	$6{\cdot}6 \times 10^{-3}$	1350±20	4.82	50*
5.	0	$6{\cdot}6 \times 10^{-3}$	1350±20	4.70	55*
6.	0	$6{\cdot}6 \times 10^{-4}$	1285±20	21.20	17
7.	90	$6{\cdot}6 \times 10^{-4}$	1285±20	32.50	8
8.	0	$6{\cdot}6 \times 10^{-4}$	1300±20	12.40	8
10.	90	$6{\cdot}6 \times 10^{-4}$	1300±20	27.00	9

*Samples developed large cracks on the cylindrical surface.

TABLE 24 Attributes of Elements Relevant to Their Use in the Solution Growth Process

Co-Constituent of Binary Melt	Minimum Feasible Deposition Temperatures	Maximum %Si in Melt at Prospective Dissolution and Deposition Temperatures	Solid Solubility in Silicon at Temperature (cm^{-3})	Impurity Levels in Silicon (eV relative to Conduction or Valence band)	Capture Radius for Thermal Carriers in Silicon (Angtroms)	Comments
Silver (Ag)	841°C	1300°C - 58% 1200°C - 33% 1100°C - 24% 1000°C - 18% 850°C - 12%		DO·31eV (+V) AO·21ev(-C)	21 Å	Deep level Recombination Centers
Aluminum (Al)	578°C	1300°C - 76% 1200°C - 65% 1100°C - 54% 1000°C - 45% 600°C - 13%	$\sim 10^{19}$	AO·057 (+V)	7 Å	
Arsenic (As)	1074°C	1300°C - 80% 1200°C - 70% 1100°C - 60%	1×10^{21}	DO·049eV (-C)	8 Å	
Gold (Au)	371°C	1300°C - 82% 1200°C - 70% 1100°C - 60% 1000°C - 53% 400°C - 32%	1×10^{17} 8×10^{16} 3×10^{16} 1×10^{16}	DO·33eV (+V) AO·54eV (-C)	21 Å 26 Å	Deep level Recombination Centers
Barium (Ba)	1021°C	1300°C - 96% 1200°C - 92% 1100°C - 86% 1050°C - 78%				
Beryllium (Be)	1090°C	1300°C - 80% 1200°C - 56% 1100°C - 37% 1090°C - 35%				
Bismuth (Bi)	264°C	1300°C - 12% 1200°C - 11% 1100°C - 11% 1000°C - 10% 300°C - 5%	1×10^{18} 4×10^{17}	DO·069eV (-c)		

TABLE 24 (continued)

Co-Constituent of Binary Melt	Minimum Feasible Deposition Temperatures	Maximum %Si in Melt at Prospective Dissolution and Deposition Temperatures	Solid Solubility in Silicon at Temperature (cm^{-3})	Inpurity Levels in Silicon (eV relative to Conduction or Valence band)	Capture Radius for Thermal Carriers in Silicon (Angtroms)	Comments
Calcium (Ca)	981°C	1300°C - 88% 1200°C - 80% 1100°C - 74% 1000°C - 62%				
Copper (Cu)	558°C	1300°C - 79% 1200°C - 65% 1100°C - 53% 1000°C - 42% 600°C - 25%	1×10^{18} 1×10^{18} 8×10^{17} 4×10^{17} 4×10^{16} @ 800°C	AO·49eV (+V) DO·24eV (+V)	14 Å 9 Å	
Iron (Fe)	1200°C	1300°C - 84% 1200°C - 73%	3×10^{16} 1×10^{16}	DO·55eV (-C) DO·40eV (+V)	7 Å	Deep level Recombination Centers
Gallium (Ga)	30°C	1300°C - 67% 1200°C - 50% 1100°C - 30% 1000°C - 20% 200°C - 0%	3×10^{19} 3×10^{19} 2×10^{19} 2×10^{19}	AO·065eV (+V)	7 Å	
Indium (In)	156°C	1300°C - 36% 1200°C - 13% 1100°C - 9% 1000°C - 5% 600°C - 0%		AO·16eV (+V)	21 Å	
Lithium (Li)	650°C	1300°C - 74% 1200°C - 63% 1100°C - 57% 1000°C - 52% 700°C - 46%	4×10^{19} 5×10^{19} 4×10^{19} 4×10^{19} 2×10^{19}	DO·033eV (-C)		Deep level Recombination Centers

TABLE 24 (continued)

Co-Constituent of Binary Melt	Minimum Feasible Deposition Temperatures	Maximum %Si in Melt at Prospective Dissolution and Deposition Temperatures	Solid Solubility in Silicon at Temperature (cm^{-3})	Impurity Levels in Silicon (eV relative to Conduction or Valence band)	Capture Radius for Thermal Carriers in Silicon (Angtroms)	Comments
Magnesium (Mg)	950°C	1300°C - 83% 1200°C - 72% 1100°C - 63% 1000°C - 56%		DO·11eV (-C) DO·25eV (-C)		
Manganese (Mn)	1142°C	1300°C - 80% 1200°C - 72% 1180°C - 70%		DO·53eV (-C)		Deep level Recombination Centers
Nickel (Ni)	994°C	1300°C - 82% 1200°C - 74% 1100°C - 65% 1000°C - 60%	5×10^{21}	AO·21eV (+V) AO·35eV (-C)	5 Å	Deep Level Recombination Centers
Phosphorus (P)	1131°C	1300°C - 80% 1200°C - 72% 1131°C - 68%	1×10^{21} 1×10^{21} 1×10^{21}	DO·045eV (-C)	5 Å	
Lead (Pb)	327°C	1300°C - 2% 1200°C - 1% 1100°C - <1% 1000°C - <1%				
Palladium (Pd)	870°C	1300°C - 88% 1200°C - 80% 1100°C - 72% 1000°C - 65% 900°C - 58%	3×10^{16}			
Platinum (Pt)	984°C	1300°C - 86% 1200°C - 78% 1100°C - 72% 1000°C - 70%		DO·31eV (+V)		Deep level Recombination Centers

TABLE 24 (continued)

Co-Constituent of Binary Melt	Minimum Feasible Deposition Temperatures	Maximum %Si in Melt at Prospective Dissolution and Deposition Temperatures	Solid Solubility in Silicon at Temperature (cm^{-3})	Impurity Levels in Silicon (eV relative to Conduction or Valence band)	Capture Radius for Thermal Carriers in Silicon (Angtroms)	Comments
Rhenium (Re)	1125°C	1300°C - 95% 1200°C - 92% 1125°C - 90%				
Antimony (Sb)	630°C	1300°C - 65% 1200°C - 18% 1100°C - 10% 1000°C - 7% 650°C - 0%	6×10^{19} 5×10^{19} 4×10^{19} 4×10^{19}	DQ·043eV (-C)	15 Å	
Tin (Sn)	232°C	1300°C - 3.8% 1200°C - 1.8% 1100°C - 0.8% 1000°C - 0.4% 700°C - 0%	4×10^{19} 4×10^{19} 4×10^{19} 3×10^{19}			
Strontium (Sr)	1000°C	1300°C - 96% 1200°C - 91% 1100°C - 85% 1000°C - 75%				
Zinc(Zn)	420°C	1300°C - NA 1200°C - NA 1100°C - 4% 1000°C - 1% 600°C - 0%	6×10^{16} 3×10^{16} 1×10^{16} 3×10^{15}	AO·55 (-C) AO·30 (+V)		
Sulfur(s)	750°C	1250°C - 90% 1050°C - 80% 750°C - 70%	1×10^{16} 3×10^{15}	DO·18 (-C)		

TABLE 24 (continued)

Co-Constituent of Binary Melt	Minimum Feasible Deposition Temperatures	Maximum %Si in Melt at Prospective Dissolution and Deposition Temperatures	Solid Solubility in Silicon at Temperature (cm^{-3})	Impurity Levels in Silicon (eV relative to Conduction or Valence band)	Capture Radius for Thermal Carriers in Silicon (Angtroms)	Comments
Boron (B)	-	-	$8x10^{21}$ @ 1375° $1x10^{21}$ @ 1300°C $6x10^{20}$ @ 1100°C	AO·049eV (-C)	24 Å	Forms stable alloys and solid solutions
Carbon (C)	-	-	$3x10^{18}$ @ 1410°C			Forms stable alloys and solid solutions
Cerium (Ce)	1240°C	1350°C - 90% 1250°C - 82%				
Cobolt (Co)	1260°C	1350°C - 81% 1275°C - 66%				
Chromium (Cr)	1335°C	1400°C - 93% 1335°C - 85%		AO·37 (+V) AO·53 (-C)		
Germanium (Ge)	-	-				Complete solid miscibility
Hafnium (Hf)	1325°C	1400°C - 96% 1325°C - 90%				
Mercury (Hg)	-	-		AO·36 (-C) AO·31 (-C) DO·33 (+V) DO·25 (+V)		Hg vapor above 375°C
Molybdenum (Mo)	1410°C	1410°C - 97%		DO·33 (-C) AO·30 (+V)		

TABLE 24 (continued)

Co-Constituent of Binary Melt	Minimum Feasible Deposition Temperatures	Maximum %Si in Melt at Prospective Dissolution and Deposition Temperatures	Solid Solubility in Silicon at Temperature (cm^{-3})	Impurity Levels in Silicon (eV relative to Conduction or Valence band)	Capture Radius for Thermal Carriers in Silicon (Angtroms)	Comments
Niobium (Nb)	1300°C	1400°C - 99% 1300°C - 95%				
Oxygen (O)	1350°C	1400°C - 99% 1350°C - 78%	1.5×10^{18} @ 1410°C	DO·16 (-C) AO·35 (+V) AO·38 (-C)	17 Å	
Plutonium (Pu)	1232°C	1400°C - 99% 1300°C - 90% 1232°C - 84%				
Tantalum (Ta)	1385°C	1385°C - 99%	reported very low			
Thorium (Th)	1400°C	1400°C - 97%				
Titanium (Ti)	1330°C	1400°C - 98% 1330°C - 86%				
Uranium (U)	1315°C	1400°C - 97% 1315°C - 86%				Solid solutions formed
Vanadium	1400°C	1400°C - 97%				
Tungsten (W)	1400°C	1400°C - 99%		AO·37 (-C) DO·34 (+V)		
Yttrium	1215°C	1400°C - 98% 1300°C - 87% 1215°C - 82%	less than 10^{19}			
Zirconium (Zr)	1300°C	1400°C - 97% 1300°C - 91%	reported less than 5%			

Table 25 Materials Whose Silicon Alloy Systems are not Well Characterized

Cadmium	(Cd)	Praseodymiom	(Pr)
Cesium	(Cs)	Rubidium	(Rb)
Iridium	(Ir)	Rhodium	(Rh)
Potassium	(K)	Ruthenium	(Ru)
Lanthanum	(La)	Scandium	(Sc)
Nitrogen	(N)	Selenium	(Se)
Sodium	(Na)	Samarium	(Sm)
Neodymium	(Nd)	Tellurium	(Te)
Neptunium	(Np)	Thallium	(Tl)
Osmium	(Os)	Ytterbium	(Yb)

Table 26

CANDIDATE MATERIALS FOR SILICON SOLUTION GROWTH

I M.P. $\leq 600^{o}C$ LIQ. SOL'Y. $\leq$ 5% AT M.P.	II M.P. $\geq 950^{o}C$ LIQ SOL'Y. HIGH	III M.P. $\leq 950^{o}C$; LIQ. SOL'Y. HIGH ELECTR. ACTIVE OR LIFETIME KILLER
BI IN PB SN ZN	AS CR NI TH B FE O TI BA HF P U BE HG PT V C MG PU W CA MN RE Y CE MO SR ZR CO NB TA	AG AL AU CU GA LI SB

$600^{o} \leq$ M.P. $\leq 950^{o}C$ LIQ. SOL'Y. HIGH, NEUTRAL	SI ALLOYS NOT CHARACTERIZED
S (?) PD	CD N PR SE CS NA RB SM IR ND RH TE K NP RU TL LA OS SC YB

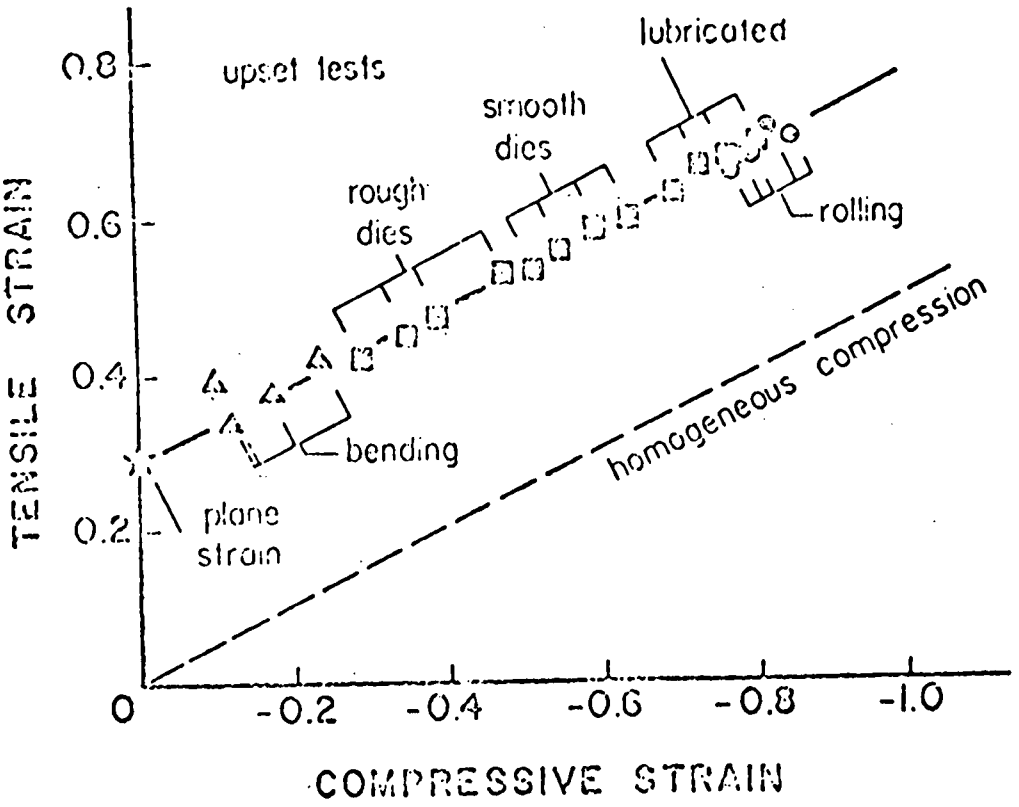

Figure 19. Relationship Between Tensile and Compressive Surface Strains at Fracture (Room Temperature) for Cold-Drawn 1045 Steel. Intercept is 0.28

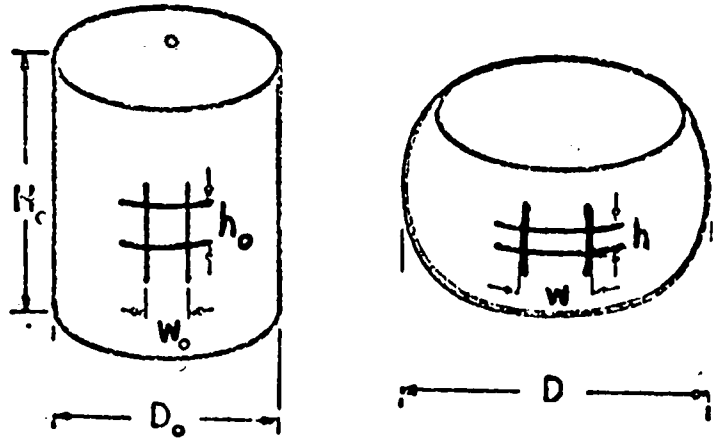

AXIAL STRAIN $\varepsilon_z = \ln(h/h_o)$

HOOP STRAIN $\varepsilon_\theta = \ln(w/w_o)$ or $\ln(D/D_o)$

Figure 20. Schematic Illustration of the Upset Test on Cylindrical Specimens. Surface Principal Strains are Calculated from Grid Displacement.

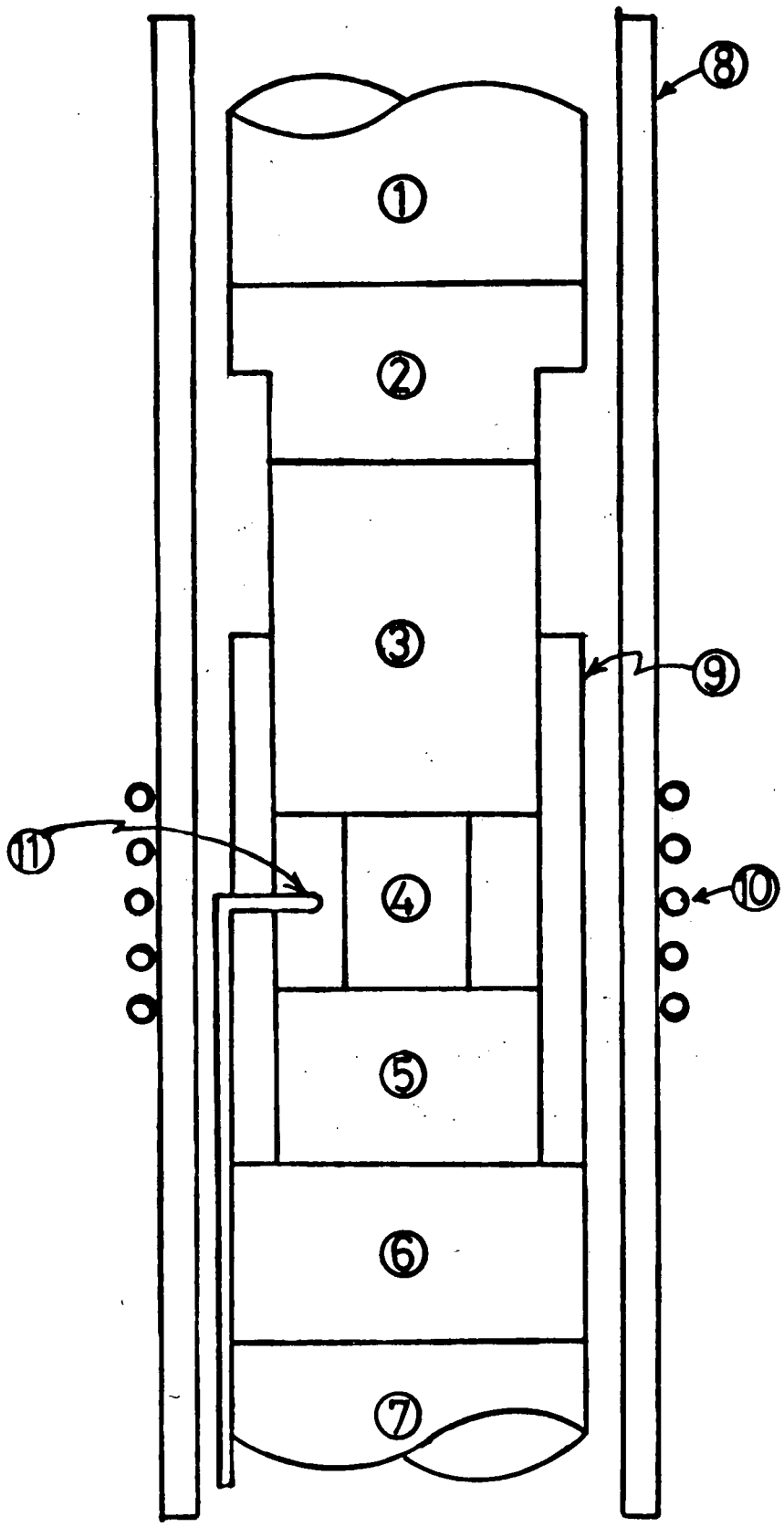

Figure 21. Schematic of Compression Rig
(see Key overleaf)

KEY TO FIGURE 21.

(1) Top push rod to crosshead

(2) Pyrolytic graphite button

(3) Top platen made of Ta-10%W

(4) Silicon sample

(5) Bottom platen made of Ta-10%W

(6) Pyrolytic graphite disc

(7) Bottom push rod to load cell

(8) Quartz tube

(9) Graphite suscepter

(10) R. F. Heater coil

(11) Thermocouple

Figure 22. Schematic Of Polylog From Which Samples Of Two Different Orientations Are Core Drilled

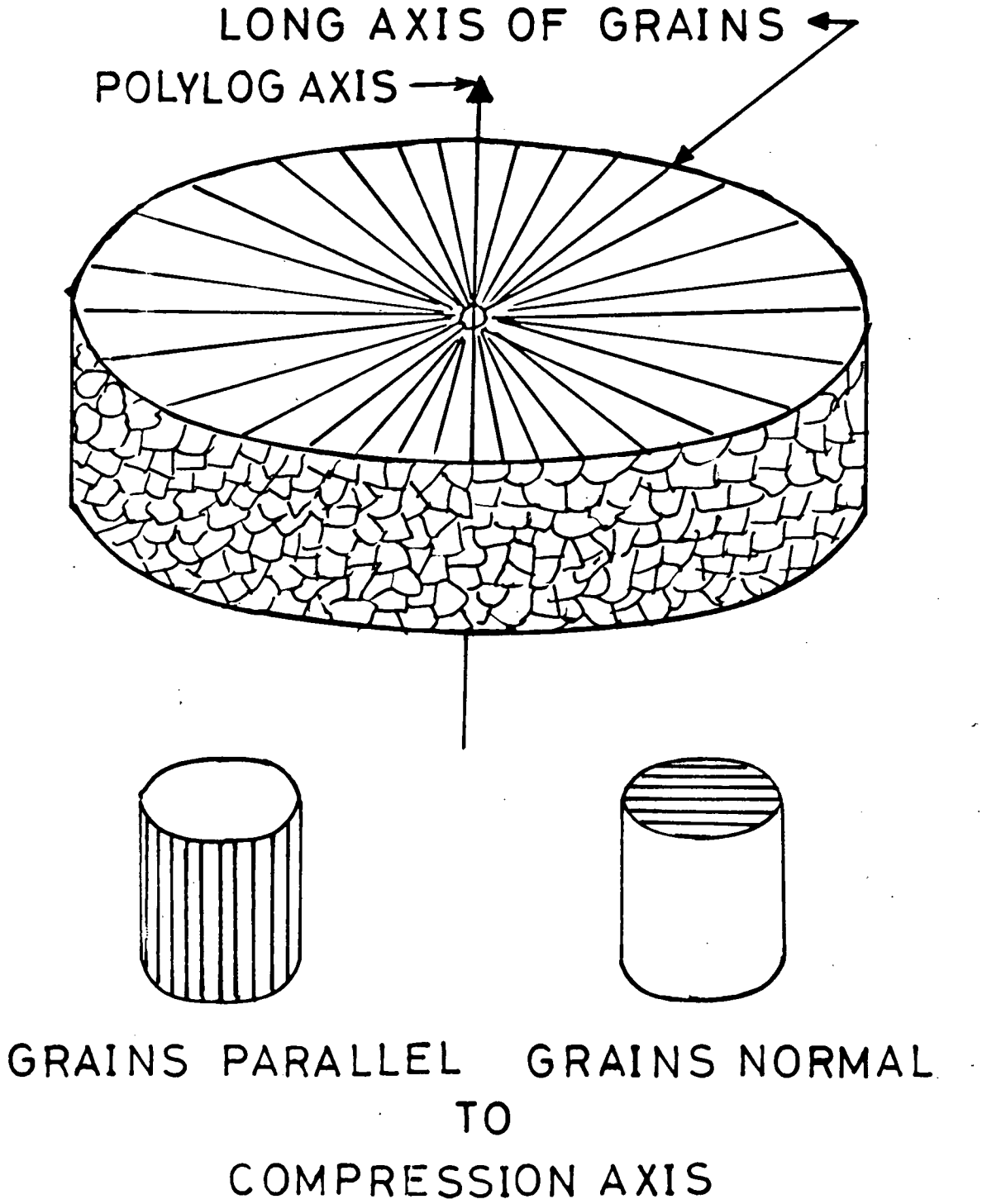

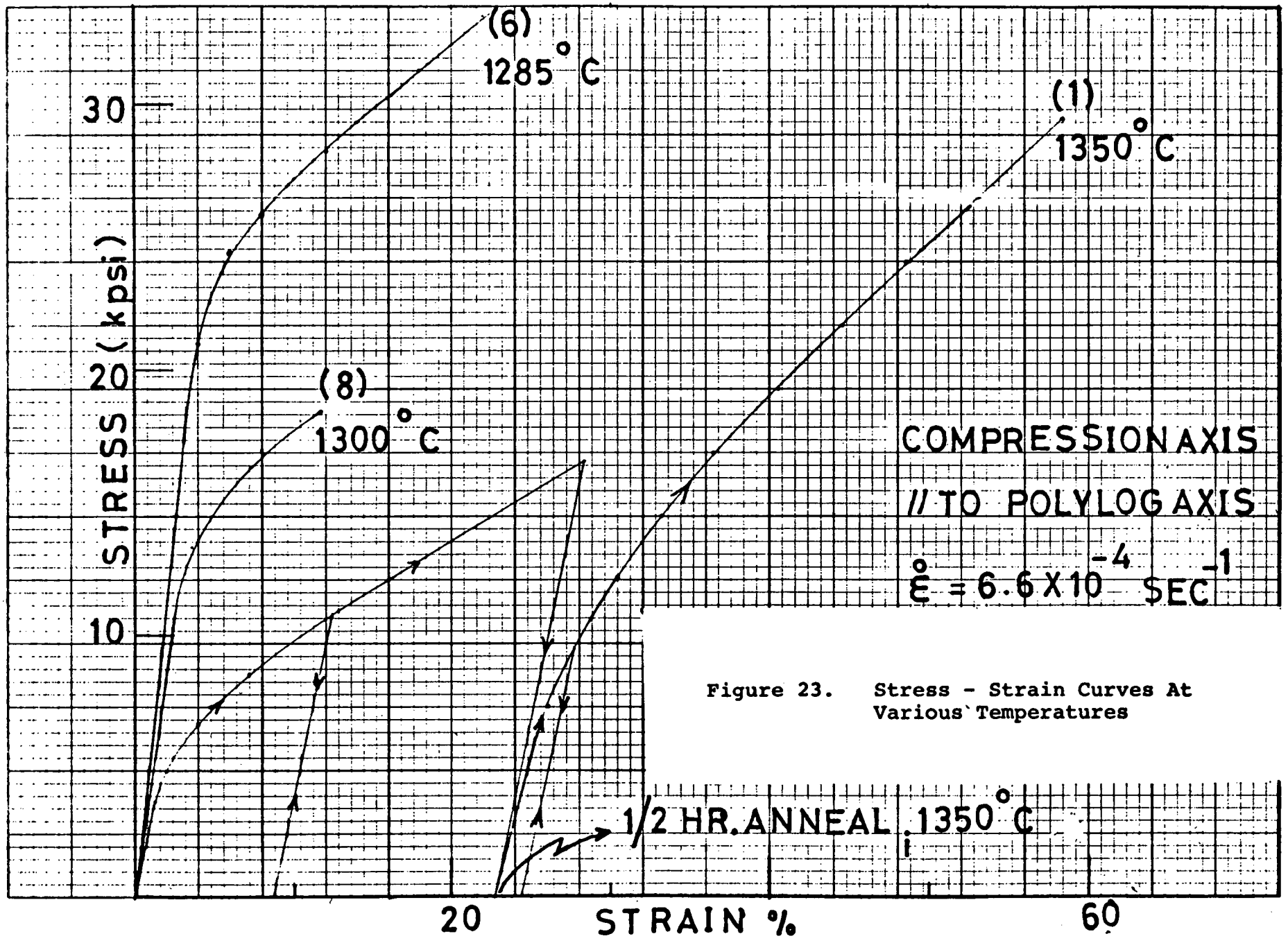

Figure 23. Stress - Strain Curves At Various Temperatures

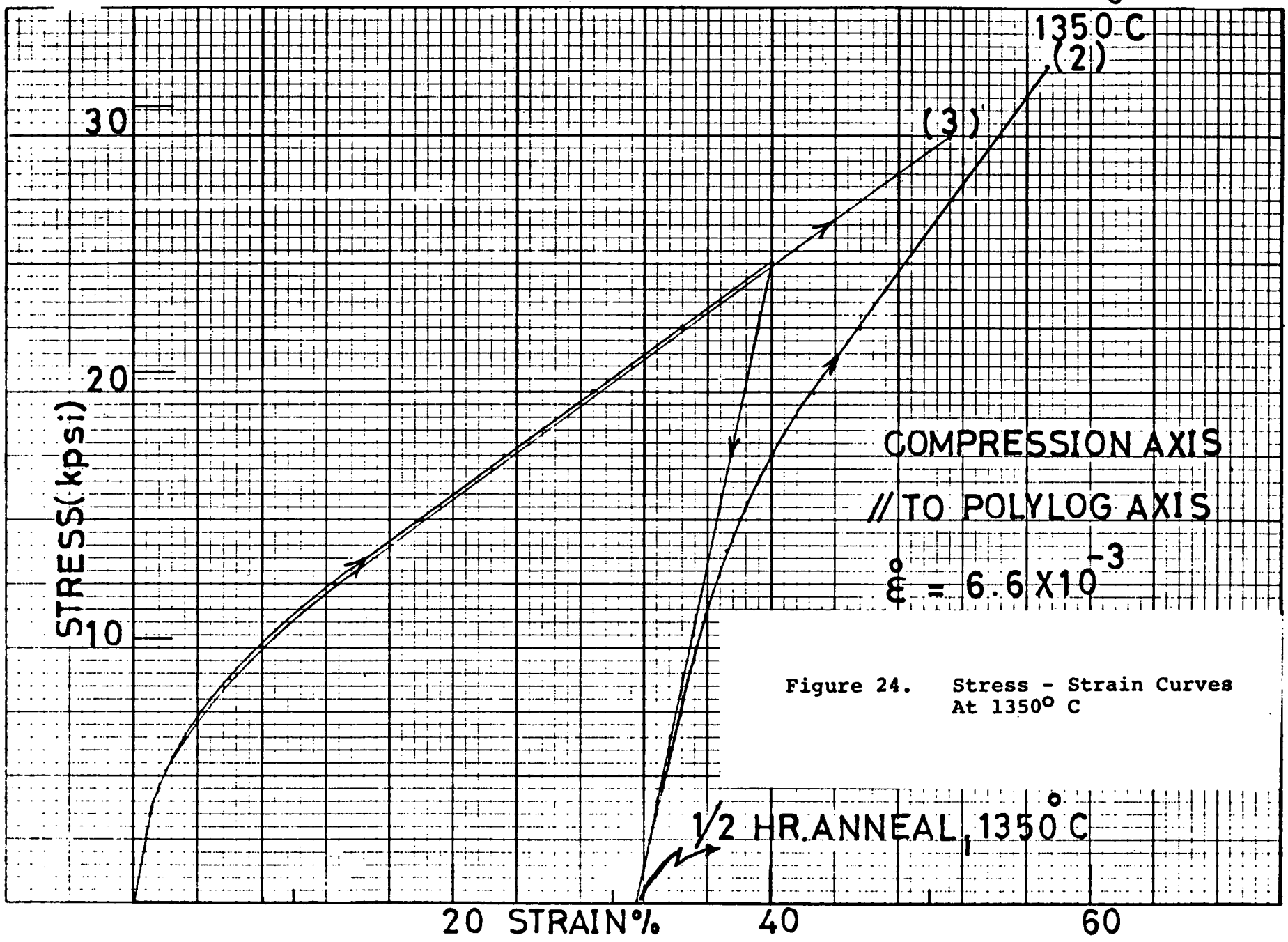

Figure 24. Stress - Strain Curves At 1350° C

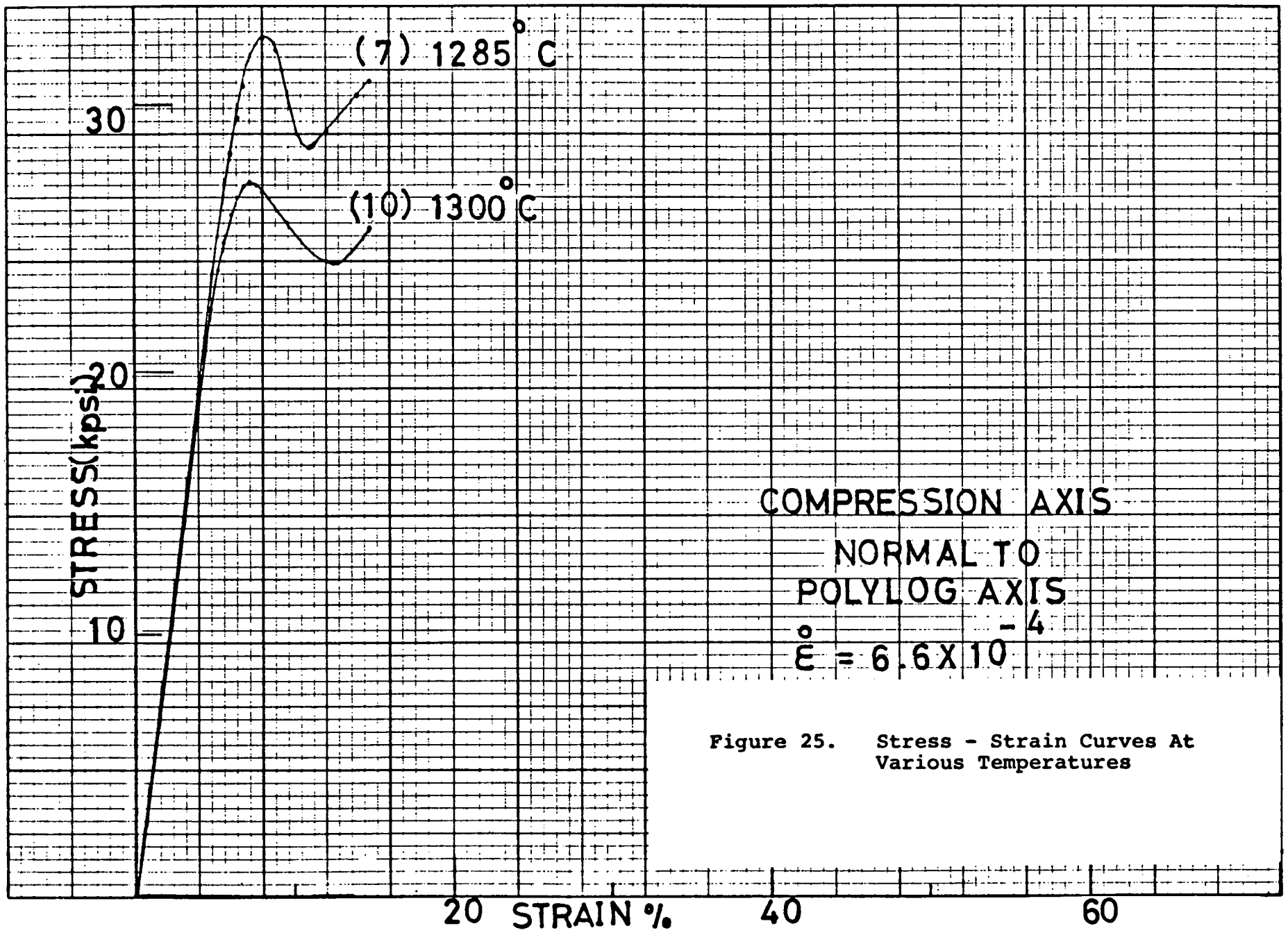

Figure 25. Stress - Strain Curves At Various Temperatures

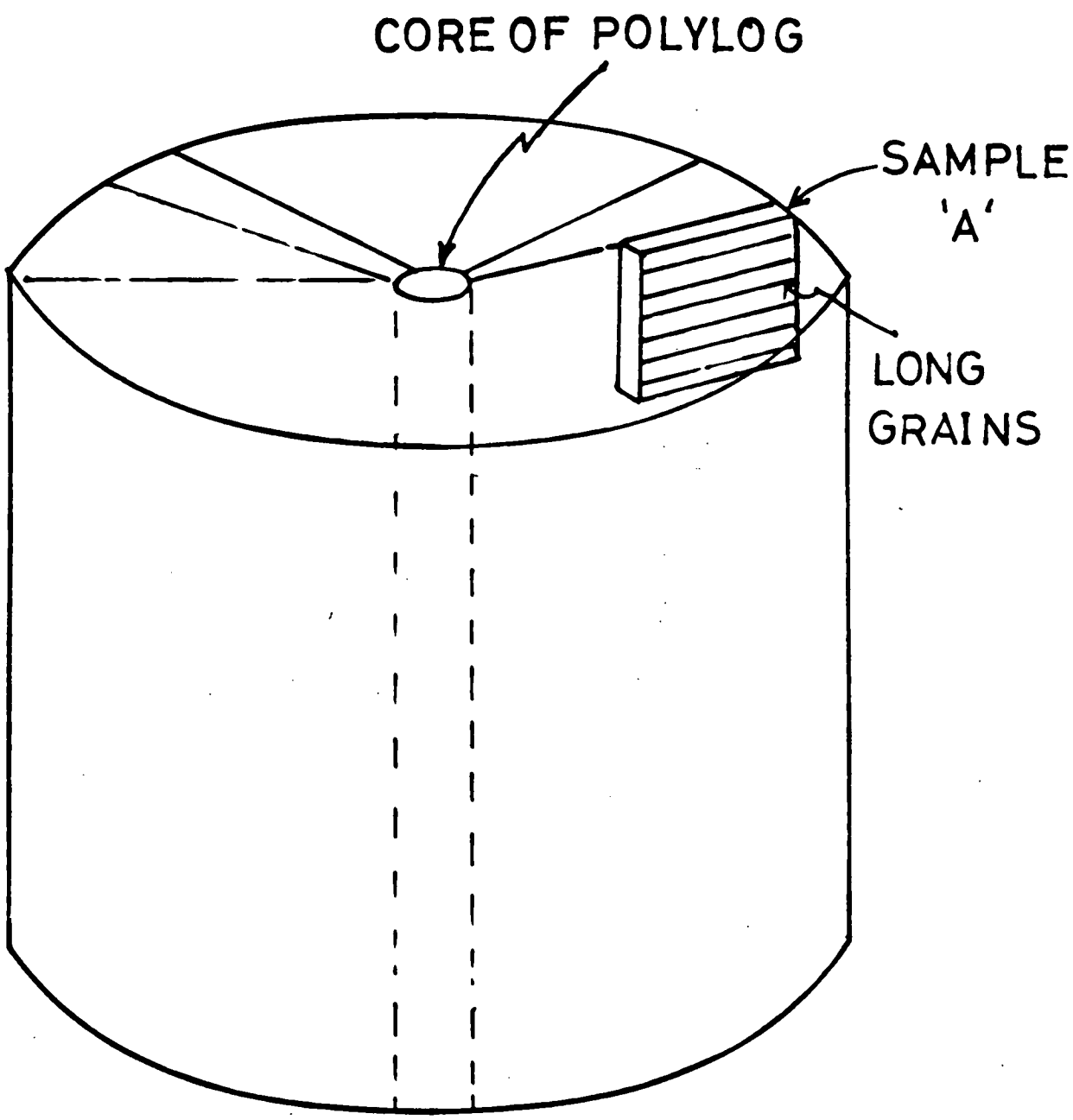

Figure 26. Sample 'A' Cut From The Polylog For Texture Determination

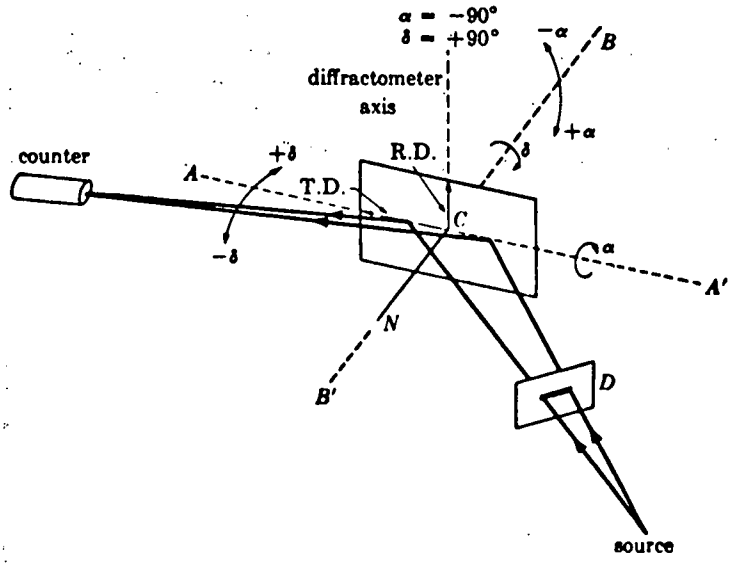

FIG. 27. Reflection method for pole-figure determination.

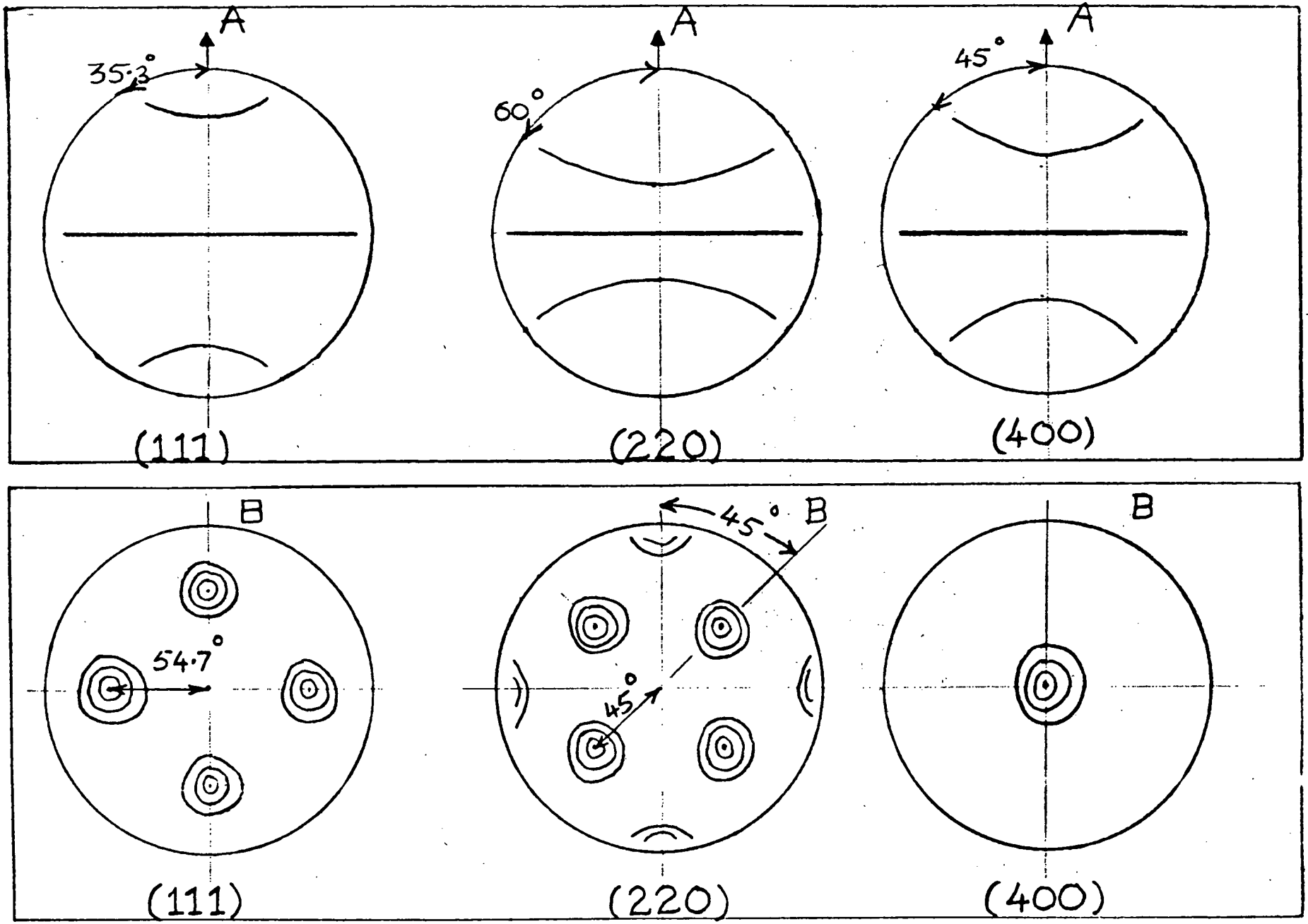

Figure 28. (111), (220), and (400) Reflections (see Key overleaf)

KEY TO FIGURE 28.

A. Fiber texture; <110> along the long axis of the grains in CVD material

B. Cube texture; (110) {001} showing evidence of recrystallization in a plastically deformed and annealed sample (B'_7)

IV. MORPHOLOGY ENHANCEMENT IN POLYCRYSTALLINE SILICON SHEET

A. General

Many of the processes for forming silicon sheet have a high probability for resulting in either amorphous or fine grain polycrystalline material. In the event that such a process is selected as the most acceptable technique for use in the overall array fabrication process, it will be necessary to enhance the morphology of the sheet by recrystallization in order that reasonable solar cell efficiencies and yields can be obtained. Recrystallization techniques fall into two general categories, those which involve the melting or dissolution of the silicon and those involving the motion of grain boundaries without any apparent melting. Recrystallization techniques evaluated during the course of this program are shown in Table 27.

Processes falling into the category of grain boundary propagation without phase change are generally called annealing and consist of supplying sufficient energy, by heating and/or other means, to the crystal to enable the propogation of the grain boundaries with a resultant coalescence of individual grains and a subsequent increase in the average grain size.

A review of the literature indicates that the probability of achieving significant grain growth by a simple isothermal annealing process is extremely low due to the extreme stability of the fine grained polycrystalline structure in silicon and the consequent difficulty in propagating grain growth. Any annealing technique will probably be relatively slow, necessitating stacking of sheet sections in ovens for extended periods. It is also likely that a successful annealing technique will probably yield a large grained polycrystalline structure rather than single crystal.

Little or no published information on the application of the other two annealing techniques listed in Table 27 (thermal-cycle and strain annealing) to silicon recrystallization was found. This

lack of knowledge led to the conclusion that some experimental evaluation would be required in these areas before a sound judgement as to their feasibility and applicability to the array fabrication process could be reached. As a result, research efforts were planned and implemented in these areas. The results of these efforts are reported in detail in section IV-C below.

Table 27 also shows two recrystallization techniques which involve a liquid to solid phase transition - the zone melting technique and the traveling solvent technique. These two are closely related, both consisting of moving a narrow molten zone through the polycrystalline sheet to achieve recrystallization. Both also have the potential for producing single crystal sheet.

In the traveling solvent technique a thin layer of an element which forms a binary alloy with silicon having a melting point lower than elemental silicon is used to achieve a low temperature molten zone (77). This technique offers some potential for lowering contamination from surrounding materials due to the lowered temperature. In addition, the height of the molten zone is determined by the amount of the solvent element present. Hence it should be possible to maintain relatively narrow zones; an important factor in controlling sheet geometry. The major difficulties of this process are the probable contamination of the recrystallized sheet by the solvent and growth rates limited by the diffusion of the silicon atoms through the molten alloy. No experimental investigation of sheet recrystallization by this technique was made during this phase of the program, however, studies of silicon sheet growth from binary solutions, the results of which are also relevant to this process, were performed. A discussion of the results of these studies appears in section III-C above.

The traveling molten zone (without solvent) technique was felt to be the most attractive recrystallization process because the basic technique is well established and has been used commercially in zone refining. It's speed potential is adequate and contamination problems should be minimal. The major unknown is the ability

to achieve a sufficiently narrow zone to ensure the maintenance of sheet geometry. An experimental program was initiated to establish feasibility in this area. This work is discussed in the following section.

B. Traveling Molten Zone Recrystallization

1. Theoretical Analysis

One of the important tasks in the investigation of molten zone recrystallization has been to analytically characterize the maximum zone travel speed and the required energy input. During the course of this program, an attempt has been made to compute the temperature distribution of a silicon sheet containing a molten zone to a more accurate degree than achieved in previous computations (78, 79) which made use of some relatively coarse approximations. The determination of this distribution leads to the maximum velocity.

All analyses of crystal growth from the melt, including Czochralski crystal pulling, start with the heat transport considerations:

a.) the heat transport in unit time $\dot{Q}$, away from the liquid-solid interface occurs by conduction through the solid:

$$\dot{Q} = A_c k_s \frac{dT}{dx} ; \qquad (1)$$

where

A_c = cross sectional area of crystal at location x

= πr^2 for circular ingots (r=radius)

= ab for rectangular ingot
(ribbons, sheets)
(a = width of sheet
b = thickness of sheet)

k_s = thermal conductivity of solid crystal

x = coordinate parallel to longitudinal crystal axis

T = absolute temperature here referring to crystal

Note: Equ. 1 is strictly correct only for the case of a planar liquid-solid interface oriented normal to the x-direction, but will, for most practical cases, be a good approximation. For the general case, the area of an isotherm would have to be taken with the temperature gradient normal to it rather than to the crystal cross section.

b.) The heat dissipated to the environment of the crystal from a crystal surface element of thickness dx:

$$\dot{dQ} = C_s d_x \left[\sigma(\varepsilon T^4 - \alpha T_{ar}^4) + U(T - T_a)\right] ; \qquad (2)$$

where

C_s = circumferential dimension of crystal
= $2\pi r$ for circular ingots
= 2 (a+b) for rectangular ingots

σ = Stefan-Boltzmann constant

ε = emittance of crystal at temperature T

α = effective absorptance of crystal at temperature T for radiation of black body at temperature T_{ar}

T_{ar} = equivalent black body radiation temperature of environment at temperature T_a

U = heat transfer coefficient for conduction and convection through the gas envelope of the crystal to the environment at temperature T_a.

c.) the heat flux contributed by the molten zone per unit time:

$$\dot{Q} = k_1 A_1 \frac{dT}{dx_1} + L \frac{dm}{dt} ; \qquad (3)$$

where

k_l = thermal conductivity of the liquid material

A_l = area of an isotherm on the liquid side near the liquid-solid interface (see note at equ. 1).

L = latent heat of fusion of material

$\frac{dm}{dt}$ = mass of material solidified per unit time

it is

$$\frac{dm}{dt} = \rho \cdot A_c \cdot v; \qquad (4)$$

with

v = travel velocity of liquid-solid interface relative to solidified crystal

ρ = density of liquid material

A few observations are in order at this point:

1. A little reflection reveals, that the total heat flow away from the liquid-solid interface is determined by the total energy dissipation of the crystal to its environment. As soon as there is a liquid-solid interface, there has to be a cross section of the crystal at the melting temperature T_m. Consequently, depending on the heat transfer parameters of the environment, a certain temperature distribution along the entire crystal will be established which in turn, determines the amount of heat dissipated to the environment. This dissipation is dependent only on the crystal geometry and the environment, once a steady state with a melt interface has been established. In particular, this dissipation is independent of any additional melting or freezing at the interface.

2. In the extreme case, all the energy flux dissipated to the environment by the grown crystal originates from the latent heat of fusion, that is from solidifying material. This means that no heat is transferred by conduction, from the melt to the liquid-solid interface. The first term on the right hand side of equ. 3 would, under these conditions be zero, which means that there will be a zero temperature gradient in the melt adjacent to the liquid-solid interface. Any temperature gradients in the melt farther away from the interface have to be maintained through the heat input from an energy source and the dissipation from the melt surfaces to the environment.

3. The maximum growth velocity is determined by the condition discussed in the preceding point and can be increased only by improved heat transfer to the environment.

Earlier attempts at solution of the problem, including our own, were based on deriving, from equ. 1 and 2 a second order, nonlinear differential equation for T(x).

$$\frac{\dot{dQ}}{dx} = A_c \left[k_s \frac{d^2T}{dx^2} + \frac{dk_s}{dT} \left(\frac{dT}{dx}\right)^2\right] \quad ; \qquad (4)$$

Introducing this into equation (2) yields:

$$\frac{d^2T}{dx^2} + \frac{1}{k_s} \frac{dk_s}{dT} \left(\frac{dT}{dx}\right)^2 - \frac{C_s}{K_s A_c} \left[\sigma(\varepsilon T^4 - \alpha T_{ar}^4) + U\,(T-T)_a\right] = 0; \qquad (5)$$

From the solution $T(x)$, $\frac{dT}{dx}$ could be obtained and with it, from equ. 3, the maximum growth velocity.

In all of these computations, the assumption has been made that the crystal on both sides of the molten zone is long enough to reach essentially environmental temperature T_a before the point at which it is clamped in a holder.

To make the solution tractable, the earlier computations made a number of simplifying assumptions, (78):

1. $\varepsilon(T)$ = constant
2. T_{ar} = 0 (space environment)
3. U = 0 (vacuum environment)
4. $k_s = k_{sm}\frac{Tm}{T}$; an approximation to Si behaviour
5. $\frac{dk_s}{dT}$ = 0; to permit analytical solution.

where

ν_{max} = maximum possible growth velocity

T_m = melting temperature of material

k_{sm} = thermal conductivity of solid material just below melting point.

With assumptions 1 to 3 and 5, equ. 5 reduces to:

$$\frac{d^2T}{dx^2} - \frac{C_s}{A_c}\frac{\sigma\varepsilon}{k_s}T^4 = 0; \qquad (6)$$

or, including assumption 4:

$$\frac{d^2T}{dx^2} - \frac{C_s}{A_c}\frac{\sigma\varepsilon}{k_{sm}T_m}T^5 = 0; \qquad (6a)$$

where:

$$\frac{C_s}{A_c} = \frac{2}{r} \quad \text{for the cylindrical ingot}$$

and:

$$\frac{C_s}{A_c} = 2\left(\frac{1}{b} + \frac{1}{a}\right) \quad \text{for the rectangular ingot}$$

$$\approx \frac{2}{b} \text{ for } \frac{a}{b} >> 1.$$

Equation (6a) can be integrated once by use of the substitution

$$y = \frac{dT}{dx}$$

to yield:

$$ydy = \frac{C_s}{A_c} \frac{\sigma\varepsilon}{k_{sm} T_m} T^5 dT;$$

and

$$\frac{dT}{dx} = \sqrt{\frac{C_s}{A_c}} \sqrt{\frac{1}{k_{sm}}} \sqrt{\frac{1}{3}} T_m^{5/2} \qquad (7)$$

or, by use of equ. 1, 3, and 3a, with $\frac{dT}{dx}_1 = 0$:

$$v_{max} = \frac{1}{\rho L} \sqrt{\frac{C_s}{A_c}} k_{sm} \sigma\varepsilon \sqrt{\frac{1}{3}} T_m^{5/2};$$

This is the relationship obtained by Runyan (78) for the cylindrical ($\frac{C_s}{A_c} = \frac{2}{r}$), and the rectangular ingot, [$\frac{C_s}{A_c} = 2\left(\frac{1}{b} + \frac{1}{a}\right)$], respectively.

It was felt that the simplifying assumptions made are too coarse to permit general application of the results. In particular, the conflict between assumptions 4 and 5 was found objectionable but assumptions 2 and 3 are also significant deviations from most real situations.

The first attempts were to solve the more general differential equation (equ. 5) including the second term, but still with $T_a \equiv U \equiv 0$. Integration could be done only by use of numerical methods, as described in the 3rd Semi-Annual progress report. The accuracy of the result was, however, questioned, and a second integration using a different numerical method was carried out. Its results were equally unsatisfying, and a search for a more accurate numerical method, with reasonable computer usage, has remained fruitless. The search for a better numerical method has led, however, to a new analytical solution. The solution method is based on the recognition that the function T(x) is not really the function of primary interest; it is in fact $\dot{Q}(T)$ which is required. This leads to expression of equ. 2 as

$$\frac{d\dot{Q}}{dx} = \frac{d\dot{Q}}{dT}\frac{dT}{dx} ;$$

and, with substitution from equ. 1:

$$\frac{dT}{dx} = \frac{1}{A_c K_s}\ \dot{Q} ;$$

to seperation of variables in equ. 2;

$$\dot{Q}\ d\dot{Q} = C_s A_c k_s [\varepsilon\sigma\ (T^4 - T_a^4) + U(T-T_a)]\ dT; \qquad (9)$$

The solution to this equation is:

$$\dot{Q}^2(T) = \dot{Q}^2(T_o) + 2\ C_s A_c \int_{T_o}^{T} k_s\ [\sigma(\varepsilon T^4 - \alpha T^4) + U(T-T_o)]\ dT; \qquad (10)$$

In the general case, the quantities k_s, ε, α, and U are functions of the temperature, T. For certain cases, these functions are of simple analytical form, such as k_s = const, or $k_s = k_{sm} \cdot \frac{T_m}{T}$, and ε, α, and U = const, permitting direct integra-

tion. In other cases, these quantities may have more complicated temperature relationships. In this case, integration by parts, if necessary piecewise for different temperature ranges, leads to the required answer:

$$\dot{Q}^2(T) = \dot{Q}^2(T_o) + 2\,A_c\,C_s$$

$$\cdot\{\sigma T^4\,k_s\varepsilon dT\Big|_{T_o}^{T} - 4\sigma T^3\,dT\,k_s\varepsilon dT\Big|_{T_o}^{T}$$

$$+12\sigma T^2 \int dT \int dT \int k_s\,\varepsilon dT\Big|_{T_o}^{T}$$

$$-24\sigma T \int dT \int dT \int dT \int k_s\,\varepsilon dT\Big|_{T_o}^{T}$$

$$+24\sigma \int dT \int dT \int dT \int d + \int k_s\,dT\Big|_{T_o}^{T}$$

$$-T_a{}^4\sigma \int_{T_o}^{T} k_s\alpha dT + T\int k_s\,UdT\Big|_{T_o}^{T} - \int dT \int k_s\,UdT\Big|_{T_o}^{T} -$$

$$T_a \int_{T_o}^{T} k_s\,UdT\}; \qquad (10a)$$

For the case k_s = const and ε = const, with $T_a = T_o = 0$ and $U = 0$, the answers from the older approximation method and from equ. 10 are identical, since

$$\frac{dk_s}{dT} = 0: \qquad \nu_{max} = \frac{1}{\rho L}\sqrt{\frac{C_s}{A_c}\,K_s\varepsilon\sigma}\sqrt{\frac{2}{5}}\,T_m{}^{5/2}; \qquad (11)$$

It is seen, that this answer, as will other following ones using different approximations differs from that of equ. 8 only by the magnitude of a constant factor, which here is $\sqrt{\frac{2}{5}}$ as compared to $\sqrt{\frac{1}{3}}$ in equ. 8.

For the case corresponding to that treated by the previous authors, that is, using assumptions

1. to 4., including

$$k_s = k_{sm} \frac{T_m}{T},$$

but excluding assumption 5. which means using equ. 10, the maximum growth velocity becomes

$$\nu_{max} = \frac{1}{\rho L} \sqrt{\frac{C_s}{A_c} k_{sm} \varepsilon\sigma \sqrt{\frac{1}{2}}} T_m^{5/2}; \quad (12)$$

Thus, inclusion of the second term in equ. 5 yields a growth velocity a factor of $\sqrt{\frac{3}{2}}$ larger than the approximation method, for this particular case of $k_s(T)$.

A more accurate approximation for k_s involves expanding it as a power series in T and fitting the coefficients to the experimental values (22) by the least squares method:

$$k_s = C_1 \left(\frac{T}{T_m}\right)^4 + C_2 \left(\frac{T}{T_m}\right)^3 + C_3 \left(\frac{T}{T_m}\right)^2 + C_4 \left(\frac{T}{T_m}\right) + C_5 \quad (13)$$

Using this approximation for k_s in equ. 10a, under, otherwise, the same conditions applied to obtain the solution (equ. 12) above, yields the maximum velocity

$$\nu_{max} = \frac{1}{\rho L} \sqrt{\frac{C_s}{A} k_{sm} \varepsilon\sigma \sqrt{\frac{1}{2.20}}} T_m^{5/2} \quad (14)$$

Because of the nature of this new solution it is no longer very difficult to take into account a non zero ambient temperature. The maximum velocity may now be written as

$$\nu_{max} = \frac{1}{\rho L} \sqrt{\frac{C_s}{A_c} k_{sm} \varepsilon\sigma \sqrt{\frac{1}{D}}} T_m^{5/2}$$

where $$D = \frac{1}{.414 - \left(\frac{T_o}{T_m}\right)^4 (7.09) + \left(\frac{T_o}{T_m}\right)^5 g\left(\frac{T_o}{T_m}\right)}$$

with: $g(\frac{T_o}{T_m}) = 10.784(\frac{T_o}{T_m})^4 - 42.607(\frac{T_o}{T_m})^3$

$$+67.986\ (\frac{T_o}{T_m})^2 - 56.307(\frac{T_o}{T_m}) + 26.821$$

To compare these values for a silicon sample 3 cm wide and .05 cm thick and with an emissivity of .7 the values of ν_{max} are, for

$$T_o = 0^oK, \nu_{max} = 3.96 \text{ meters/hour}$$

for

$$T_o = 300^oK, \nu_{max} = 3.94 \text{ meters/hour}$$

It is apparent that very little can be gained by cooling the environment of the system below 300^oK. Both of these values are about 15% larger than the values obtained from the older rough approximation (equ. 8).

$$\nu_{max} = 3.43 \text{ m/hr.}$$

The temperature distribution in the silicon sample can be determined from a fairly straight forward treatment of the above equations. Combining equations 1 and 10 yields

$$\frac{dT}{dx} = \frac{1}{A_c K_s}\left[\dot{Q}^2(T_o) + 2C_s A_c \int_{T_o}^{T} k_s\{\sigma(\varepsilon T^4 - \alpha T_a^4) + U(T-T_o)\}\right]^{\frac{1}{2}}$$

or, seperating the variables

$$\int dx = \int \frac{A_c k_s\, dT}{\left[\dot{Q}^2(T_o) + 2C_s A_c \int_{T_o}^{T} k_s\{\sigma(\varepsilon T^4 - \alpha T_a^4) + U(T-T_o)\}\right]^{\frac{1}{2}}}$$

For a sample with a width of 3 cm and a thickness of 0.05 cm and again assuming $\alpha=\varepsilon=0.7$, $T_o=T_a = 300^oK$, $\dot{Q}(300) = 0$, and k_s given by equation 12 we can perform the numerical integration to obtain X(T). The results of such an integration are shown in Figure 29.

The above calculations assume samples of infinite length. During the past quarter, the theoretical analysis of the temperature distribution in a traveling molten zone sample has been extended to allow consideration of finite samples whose ends are attached to clamps as in our present experimental setup. Since the clamps have a larger surface area they will cool faster than the sample. Let the sample have a length $2X_o$ and for the clamps, assume a cross-sectional area of A_{cg}, a surface area of C_{sg}, a thermal conductivity of k_{sg} and an emissivity of ε_g. For the clamp (i.e. for $X \geq X_o$) then, we have

$$\dot{Q}^2(T) = 2\, C_{sg}\, A_{cg}\, \sigma\varepsilon_g \int_{T_o}^{T} k_{sg}\, (T^4-T_a^4)\, dt$$

In the sample assuming that all of the heat flowing down the sample flows to the clamp, the equation becomes

$$\dot{Q}^2(T) - \dot{Q}^2(T(X_o)) = 2C_sA_c\sigma\varepsilon \int_{T(X_o)}^{T} k_s(T^4-T_a^4)\, dT$$

The equation for $\dot{Q}(T)$ in the clamp yields a value for $\dot{Q}(T(X_o))$, the heat that flows out of the sample into the clamp. Once again solving for $\dot{Q}(T)$ at T_{max} yields an expression for the maximum growth velocity. In the present experimental set up, the clamp is made of stainless steel which, in the temperature range of interest, has a nearly linear thermal conductivity given by

$$k_{sg} = AT + B\ .$$

It has a rectangular crossection with a width of 7.5 cm and a thickness of 1.5 cm. In order to solve the system of equations, the temperature at the clamp - sample interface is required. This has been used as a variable parameter and the velocity and temperature distribution for several possible values of $T(X_o)$ have been calculated. Once the temperature distribution is known the position of the interface is found from the value of $T(X_o)$ used. The results are given in Table 28. It is seen that the clamp has a significant effect on the maximum velocity only when it is relatively close to the molten zone. The presence of clamps will not significantly increase the maximum velocity for clamp to molten zone separations larger than about 10 centimeters.

It is also of interest to consider cooling the clamps. Consider a clamp being cooled by liquid nitrogen flowing through coils wrapped around the clamp. In this case, the convection and conduction term U is no longer zero for the clamp. For $X > X_o$ we obtain

$$\dot{Q}^2(T) = 2\, C_{sg}\, A_{cg} \int_{T_o}^{T} k_{sg}\, [\sigma\varepsilon_g(T^4-T_a^4) + U(T-T_\ell)]dT,$$

while the expression for $Q(T)$ is the sample remains the same. To solve the set of equations a value for U is required. The cooling coils can be made symmetric and the temperature differences in the grip will not be very large so, for a first approximation, U will be assumed to be a constant over the temperature range of interest. If the clamp is isolated in a vacuum an equilibrium will be established at a particular temperature such that the incident ambient radiation is exactly balanced by the cooling of the liquid nitrogen. If we assume this equilibrium temperature to be 100^oK then

$$-A_{cg}\, \varepsilon_g \sigma \; [\; (100^oK)^4-(300^o)^4] = A_{cg} U(100^oK-78^oK)$$

For the existing stainless steel clamps this yields

$$U = 1.44 \cdot 10^{-3} \frac{watt}{cm^2 {}^{o}K} .$$

Using this value of U and the previously described geometry, the set of equations can be solved. The results are given in Table 29. Just as for the room temperature clamp, cooling the clamp has a significant impact on the maximum growth velocity only if the grip is close to the molten zone. This will make it extremely difficult to achieve an appreciable increase in the growth velocity through the use of clamps.

Also of interest is the power required to produce and maintain a molten zone. The total power input to the system that is needed to maintain the crystal at the elevated temperature distribution with a molten zone, is equal to the sum of the energy dissipated by the material on each side of the molten zone. This power must be supplied to the molten zone, hence:

$$P_{input} = 2\dot{Q} \Big|_{T=T_{max}} .$$

For the sheet geometry with width 3 cm and thickness of 0.05 cm and assuming a room temperature ambient, the power input needed to maintain the distributions is

$$P_{input} = 138 \text{ W.}$$

Since it is planned to reduce the sample thickness to 0.01 cm and assuming a width of one meter, the corresponding values are

$$v_{max} = 8.76 \text{ m/hr}$$

$$P_{input} = 2040 \text{ W}$$

These power input rates are well within the capabilities of the existing electron beam guns and associated equipment.

For a moving molten zone, the power input to maintain the molten zone is given by the sum of the dissipations of the feed crystal and the grown crystal plus the generally small dissipation from the molten zone itself once the latter has been established. As long as the height of the molten zone is kept constant, the power input to the molten zone is independent of the zone travel velocity, up to the maximum velocity. At higher velocities, the zone height will increase. The power input independence arises from the fact that the total dissipation is constant and that, on the freezing side, more of the dissipated energy is supplied from latent heat rather than conduction, while on the melting side of the zone, an equal amount of latent heat has to be supplied for melting new material to keep the zone height constant, in addition to the energy conducted to the yet unmolten crystal for dissipation to the environment.

2. Experimental Investigations - The Pierce Gun

Previous experimental studies of zone melting of materials in sheet film, and ribbon form have dealt primarily with materials other than silicon (81-83), although brief mention is made of some work with silicon (84). Electron beam zone melting in vacuum is the preferred method for this process. The reactivity of silicon posed problems in the above cited work because the films were substrate supported during melting. Self supporting sheets such as envisioned in this program will not be subject to this problem.

The initial experiments of the present program were perperformed in an existing small electron beam vacuum melting

unit in the Laboratory for Research into the Structure of Matter (LRSM) at the University. The unit was designed for zone melting small diameter metal rods and required some modification to accomodate the sheet geometry. The construction of the unit is similar to that outlined by Lawley (Ref. 85) and is illustrated schematically in Fig. 30. The sample is held rigidly while the electron source is moved along the sample to produce zone travel. The electron source was a tungsten wire filament shaped to the geometry of the sample (see inset, Fig. 30). Several filament shapes and spacings were tested. A 5 kV, 5 kW power supply was used as a high voltage source and a 10 V, 10 A supply was used to supply the filament current. The initial experiments were successful in melting the silicon sheet, however, the adapted system was found to be inadequate for this application from several points of view (particularly provision for electron beam and molten zone control). It was determined that a system designed specifically for this application is required for the continuation of this work.

Accordingly, an appropriate system was designed and built at the University. The apparatus utilizes a "Pierce Gun" type focusing electrode arrangement (86) to produce a well defined rectilinear electron beam of the desired dimensions. Figure 31 illustrates the arrangement of the electron source, focusing electrodes, and the silicon sample. The arrangement is relatively simple and allows adequate spacing between the cathode and the silicon sample to minimize opportunities for contamination. A somewhat similar arrangement has been used with considerable success in the zone refining of high melting point metals (W, Ta, Mo, etc) by G.P. Koutun et al (87). These investigators found the gun to be stable, economical, and essentially contamination free despite heavy outgassing by some of the metal samples. A 10 KeV, 1.5A power supply and other key equipment was

acquired and the apparatus was installed in an existing high vacuum system in the new solar energy laboratory which is housed in the Moore School Building. The system is pictured in Figure 32.

The electron beam unit was made operational, and the initial tests indicated that several modifications of the system were necessary. It was found that the tungsten filament expanded so much upon heating, that it could not be mounted rigidly. The tungsten wire is now attached between two molybdenum fingers. The other end of the fingers are connected by a spring and one of the fingers is free to rotate. Upon heating of the filament, as the tungsten expands the spring tension causes the moveable finger to rotate keeping the tungsten wire taunt. This system successfully keeps the tungsten wire straight. This is not an ideal system, however, since when the molybdenum finger rotates it moves one end of the tungsten wire out of the plane in which it was originally located. This does not influence the dimensions of the resulting beam, but may have an effect upon the efficiency of the system. To alleviate this problem it may be necessary in the future to build a system in which the tungsten filament is only free to move in the direction parallel to its initial alignment.

During operation of the electron beam guns a considerable amount of outgassing has been observed. Localized increases in pressure can lead to intermittent voltage breakdown. Such drastic variations in beam power can not be tolerated for stable crystal growth. The outgassed material tends to collect on the cooler parts of the system. When a coating of this material is deposited on the ceramic voltage insulators they can become

conducting, resulting in a voltage breakdown. The ceramic insulators are being moved farther away from the electron beam area so that less material will be deposited on them. We also believe that moving the high voltage away from the areas, where the electron beam strikes the material, will reduce the outgassing and arcing problem. Therefore, we plan to alter the system so that the filaments and cathodes will be at a high negative potential while the focusing plates and sample will be at ground. Much less material in the chamber will then have a large potential differential with respect to ground. This configuration will also be much easier to adapt to a large scale production unit.

For equal power delivered to the sample, lower applied voltages lead to more heating of the focusing plates. This means that for lower voltages fewer electrons are focused through the exit slit so that the efficiency is lower. It is therefore advantageous to use the highest voltage possible. At present we limited by the voltage break-down problem.

The silicon samples that have been melted were rectangular in cross-section with a width of 1 cm and a thickness of .4 cm. To eliminate the effect of strain, the starting sample consisted of two identical pieces lined up with a gap of approximately 1 mm between them. The guns were used to heat the silicon until it began to glow, then the level of the guns was varied until the top and bottom pieces of silicon were glowing evenly. Finally, the power was increased until the bars melted.

The resultant molten zone was elliptical in cross-section The liquid-solid interface was not horizontal, but was bowed as shown in Figure 33. In the center, the zone was 1 cm high while at the edges it was .5 cm high. The reduction in length of the zone at the edges was probably due to cooling from the ends, since this sample had a large thickness to width ratio. In future experiments with narrower samples the zone should be more nearly horizontal.

C. Annealing

1. Thermal Cycle Annealing

Grain boundaries in silicon are highly immobile and do not readily migrate under the standard isothermal annealing treatment used for a number of other materials. Similar problems have been encountered in attempts to remove dislocation sub-boundaries (e.e. dislocations which have agglomerated into planar arrays) from metallic single crystals by annealing. These sub-boundaries are found to be very stable under isothermal annealing, but migrate rather readily under thermal-cycle annealing (88-90). This fact led to speculation concerning the possible effect of thermal-cycle annealing on fine grain polycrystalline silicon and a small scale experimental investigation was conducted during the earlier part of the program. The process consists of exposing the sample to a continuously varying temperature, ranging from some peak value, normally in the vicinity of typical isothermal annealing temperatures for the given material to a lower (quenching) temperature. The observed annealing effects are attributed to a modification of the grain growth kinetics associated with the introduction of certain types of lattice defects which are in turn caused by the stresses set up by the thermal cycling.

The equipment used in this investigation is shown schematically in Fig. 34 and consisted of a furnace with a controlled temperature gradient and a sample holder contained in a sealed mullite tube which was moved in and out of the furnace in a cyclical manner to achieve the thermal-cycling. The cycle rate ranged from 1 to 2.2 cycles per hour. Most of the experiments were

carried out with the silicon sample in an inert atmosphere (by flowing argon through the mullite tube), although a few used air as the ambient gas. A range of both maximum and minimum temperatures were explored during the course of these experiments.

Temperatures at the high temperature portion of the cycle were varied from 1190°C to 1385°C, while those at the low temperature end were varied from 175°C to 630°C. Annealing times ranged from 4.5 hours to 12.8 days. Control samples were isothermally annealed in an argon atmosphere at temperatures of 1085°C, 1100°C, 1150°C, 1270°C, 1350°C, and 1400°C for periods ranging from 2.5 hours to 12.6 days. The test samples used in these experiments were cut from bulk semiconductor grade silicon blocks grown by CVD. The sample size was 10 mm x 10 mm x 1.6 mm. The grain size in these samples prior to the annealing treatment was approximately 10 micrometers, with the interiors of the grains showing considerable dendritic structure.

The experiments have not yielded spectacular growth, although definite structural changes have been shown to result from these annealing treatments. The changes, in general, consist of a disappearence of the dendritic structure within the individual grains and some localized alterations in the sizes and shapes of the grains. The localized grain size increases might either be attributed to grain boundary migration, under the driving force of the surface tension of the boundary, or to recrystallization due to highly localized plastic deformation resulting from treatment prior to the annealing operation. Since these samples were not subjected to elevated temperatures at any time subsequent to their formation by the CVD process, a plastic

deformation of this type could only have occured during the deposition process. Some of the test results indicate that essentially all of the observed changes occur during the first few temperature cycles, with succeeding cycles contributing little or nothing to the process. Specific attempts were made to slow the recrystallization process (through adjustment of the cycle time and temperature extremes) with the intent of limiting the number of nucleation sites and consequently increasing the size of the grains produced. No significant improvements resulted from these attempts.

The final grain size resulting from these thermal-cycle annealing experiments was of the order of 30 micrometers (initial grain size was 10 micrometers). Typical results are shown in Fig. 35. The isothermally annealed control samples exhibited very much similar changes in grain size, so that the thermal-cycling appears to offer no particular advantage in this regard. The highly localized nature of the observed changes and the small size of the grains resulting from these annealing treatments indicate that this technique, at least in the form studies in these experiments, is not suitable for the purposes and goals of this program.

2. Strain Annealing

Strain annealing combines thermal treatment with the mechanical application of physical stresses to induce grain boundary propagation. It is also a technique which has been used successfully on metals and other materials but has not previously been applied to silicon. Strain annealing requires essentially the same equipment as is used in hot rolling, with the addition of an oven for the thermal treatment. While no

direct experimental investigation of strain annealing for recrystallization was conducted during this phase of the program, the hot rolling studies have yielded some results which reflect very favorably on this process. Considerable grain growth (up to about 1 mm in size) has been observed after compression and subsequent annealing of cylindrical silicon samples at about 1350°C. The grain sizes produced approach the estimated minimum required for adequate solar cell performance. It is felt that these results are promising enough to warrant devoting some attention to this process in the future. A detailed discussion of the recrystallization observed during compression testing appears in section III-B-3 above.

D. REFERENCES - SECTION IV

77. Pfann, W. G.; Trans. AIME 203, 961 (1955); Also Carman, J. N. et al.; Jour. Appl. Phys. 25, 543 (1954).

78. Runyon, W. R.; "Silicon Semiconductor Technology"; Texas Instruments Electronics Series; McGraw-Hill, New York, 1965.

79. Ciszek, T. F.; Jour. Appl. Phys. 47, 440 (1976).

80. Graham, C. D. et al.; "Research and Development of Low Cost Processes for Integrated Solar Arrays", Report # NSF/RANN/SE/GI-29729X/PR/75/2, Third Semi-Annual Report under NSF Grant GI-29729, July 1975.

81. Pfann, W. G. et al.; Jour. Appl. Phys. 30, 454 (1959).

82. Benson, K. K.; "Experimental Results with 'Large-Area Floating Zones'", Metallurgical Society Conferences, Vol. 5, p. 17; Edited by H. C. Gates, Intersciences Publishers, New York (1960).

83. Namba, S.; Jour. Appl. Phys. 37, 1929 (1965).

84. Maserjian, J.; Solid State Electronics, 6, 477 (1963).

85. Lawley, A.; Electronics, 32, 39 (1959).

86. Pierce, J. R.; Appl. Phys. 11, 548 (1940).

87. Koutor, G. P. et al.; Tekhnika Eksperimenta 1, 211 (1966).

88. Bercovici, S. et al.; Scripta Metallurgica, 6, 219 (1972).

89. Fiset, M. et al.; Scripta Metallurgica, 5, 325 (1971).

90. Hasegawa, T. et al.; Jour. Japan Inst. Metals, 33, 1337 (1969).

TABLE 27

SHEET RECRYSTALLIZATION PROCESSES

PROCESSES		ASSESSMENT FACTORS: Speed	Probable Resulting Structure	Temperature Required	Anticipated Problem Areas	Comments
Solid State	Isothermal Anneal	hrs. to days	large grain polyxtal	> 1000°C	1. long anneal periods 2. low success probability	Experiment shows little or no regrowth.
	Thermal-Cycle Anneal	hrs. to days	large grain polyxtal	700°C-1400°C	1. long anneal periods	Experiments indicate insufficient regrowth
	Strain Anneal	mins.-hrs.	large grain polyxtal	>1000°C	1. long anneal periods 2. materials for strain inducing equipment	Significant recrystallization demonstrated.
Liquid to Solid State	Zone Melting	cms/min	Single Crystal	1420°C	1. maintaining sheet configuration	Most attractive process. Experimental studies incomplete.
	Traveling Solvent	diffusion limited	Single Crystal	<1400°C	1. growth rate 2. contamination by solvent	Speed, temperature depend on solvent.

TABLE 28

$T(X_o)$ ^oK	V_{max} (m/hr)	X_o (cm)
300	3.94	∞
320	3.94	13.0
400	4.02	3.6
500	4.38	1.5
700	6.73	.43

TABLE 29

$T(X_o)$ ^oK	V_{max} (m/hr)	X_o (cm)
300	3.94	∞
150	3.98	11.2
250	4.32	3.05

Figure 29
Temperature Distribution

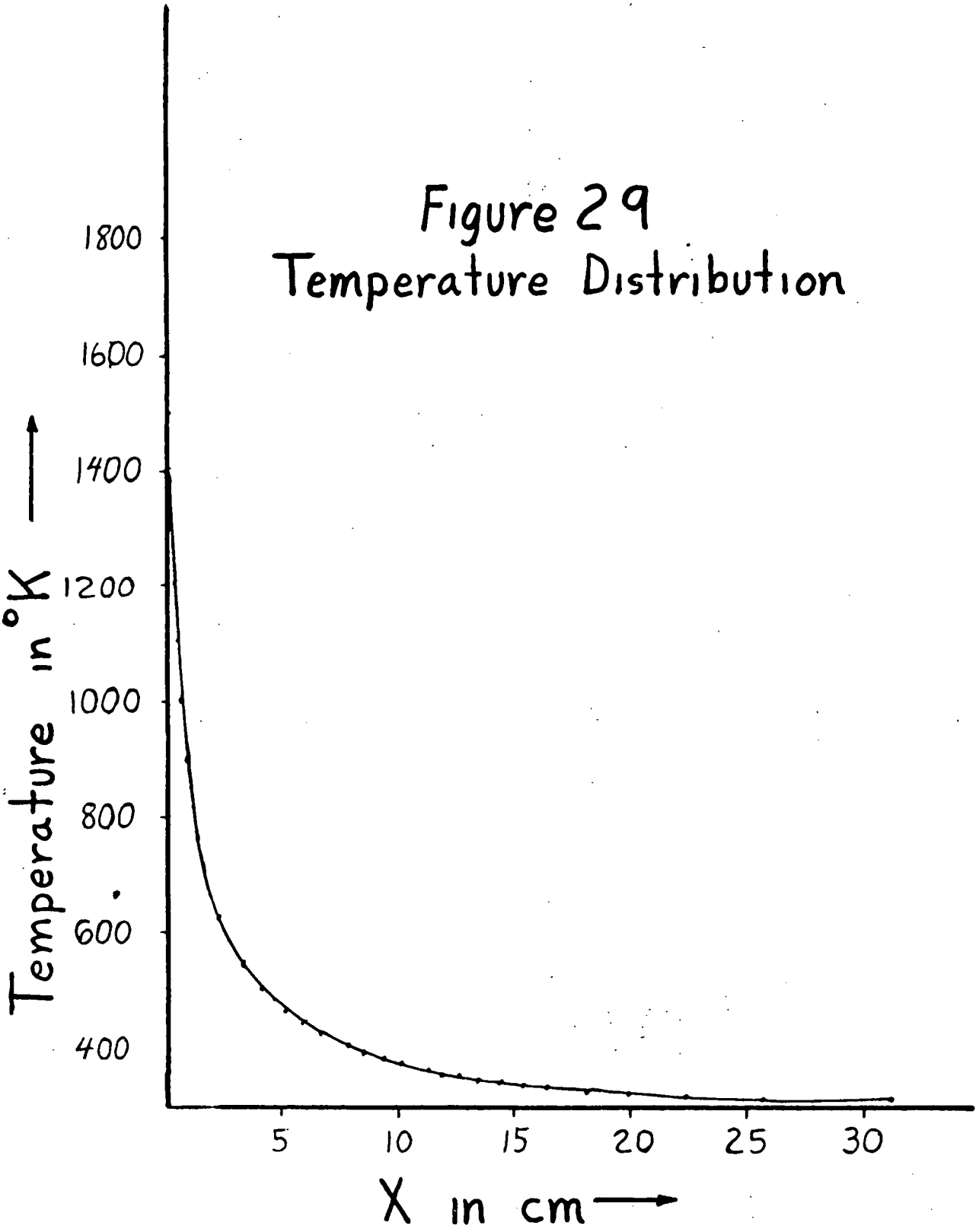

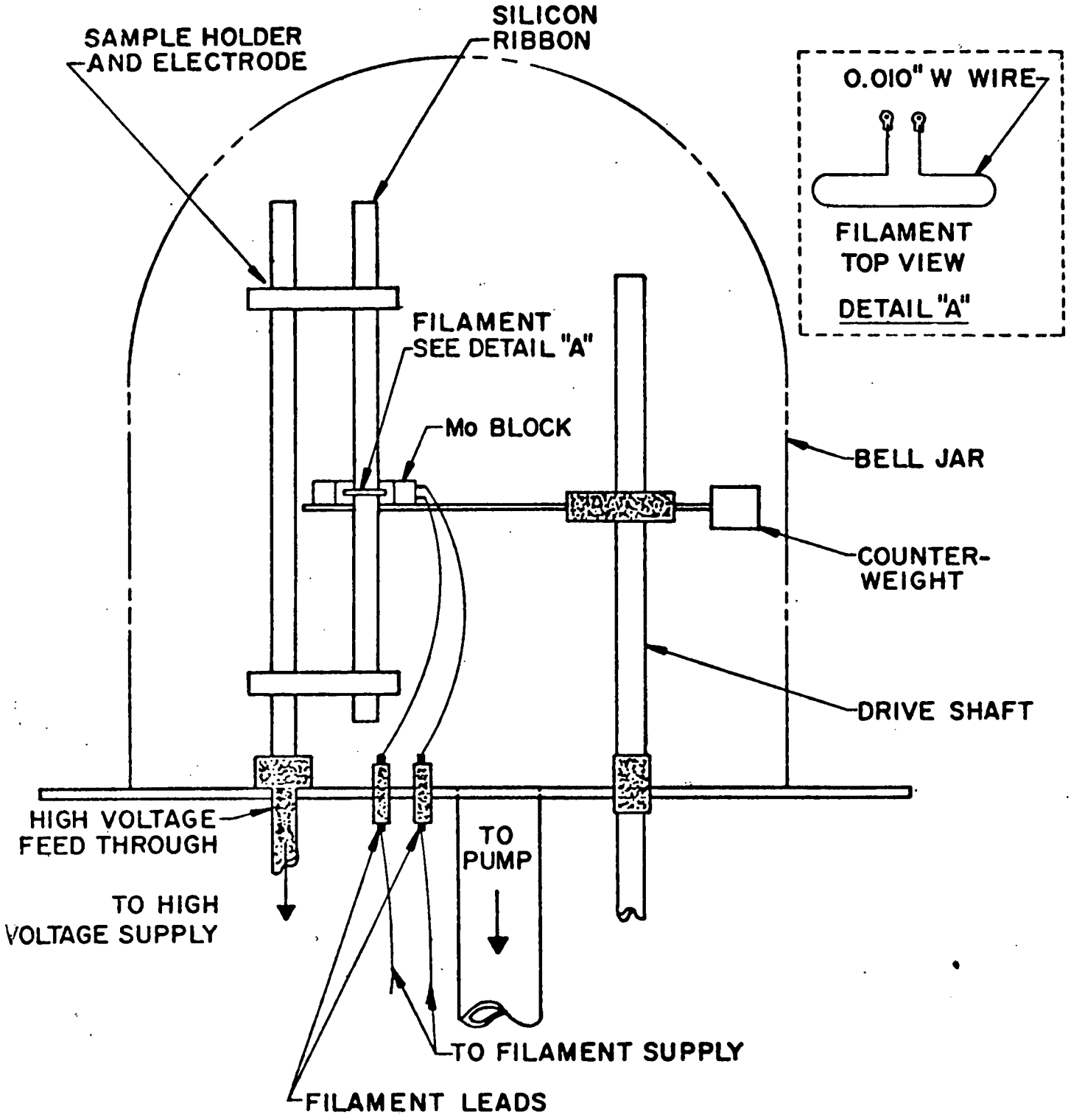

Figure 30. E-BEAM ZONE MELTING

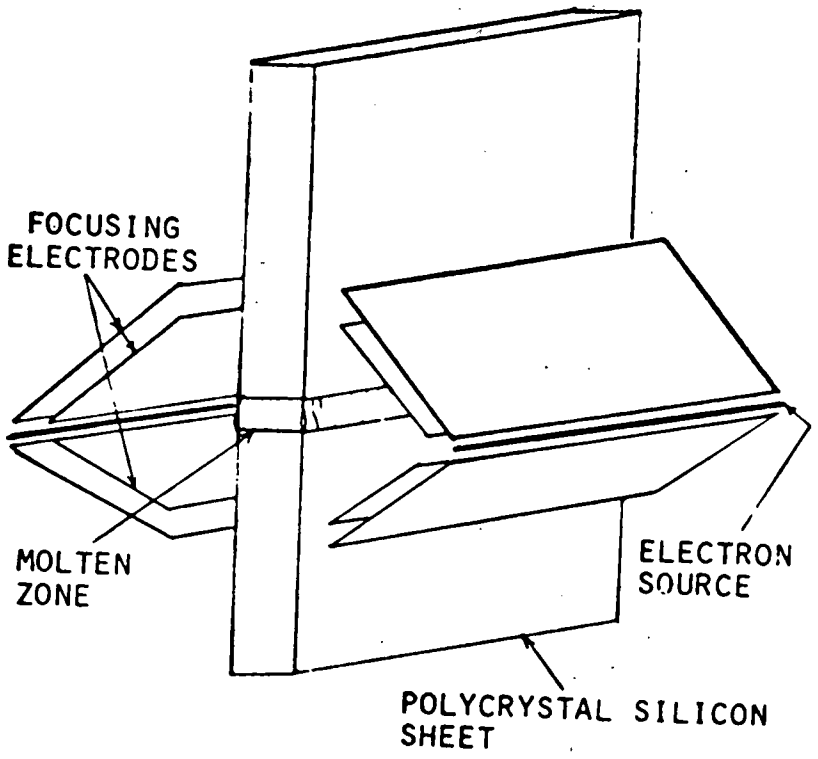

Figure 31. Pierce Gun Electrode and Electron Source Arrangement

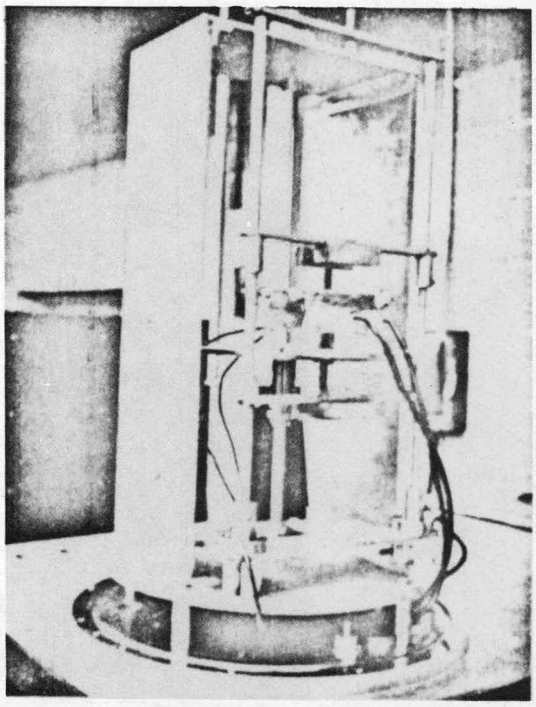

ELECTRON BEAM ZONE MELTING
APPARATUS (PIERCE GUN)

FIGURE 32.

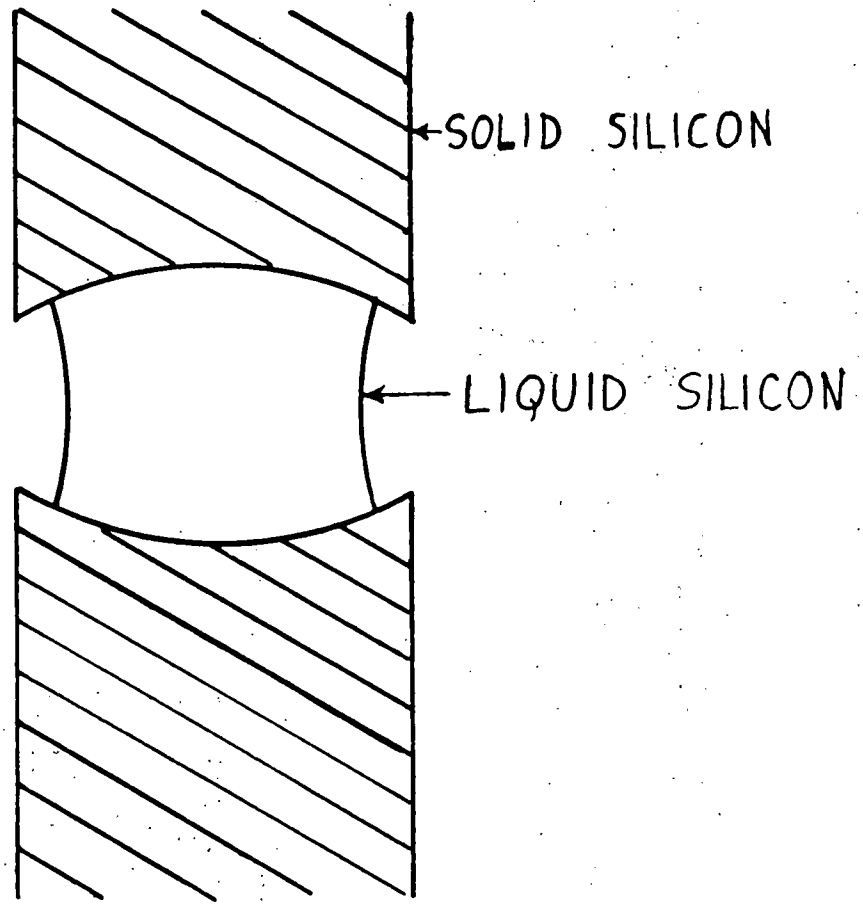

Figure 33. Molten Zone

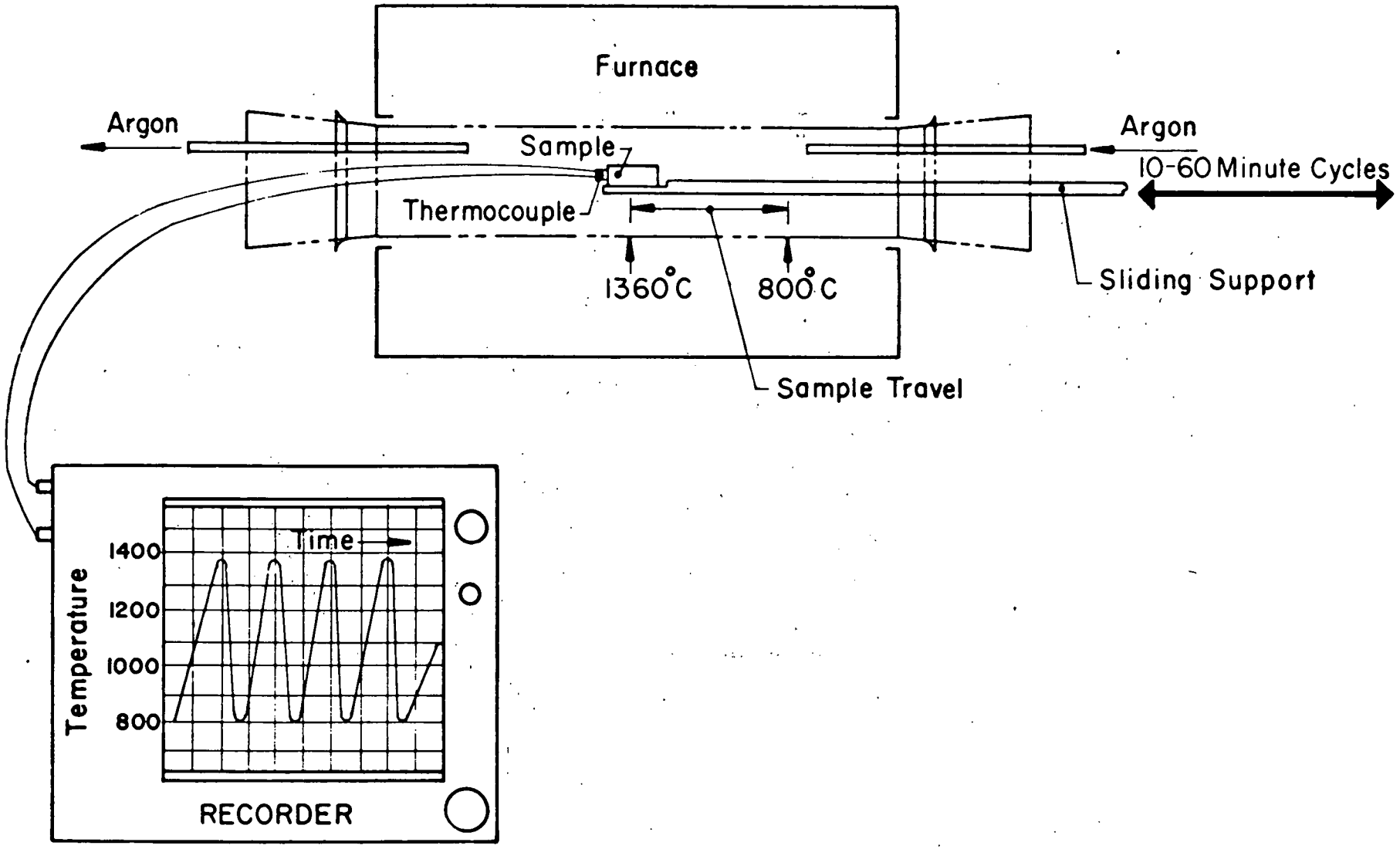

THERMAL CYCLE
GRAIN GROWTH PROCESS

Figure 34.

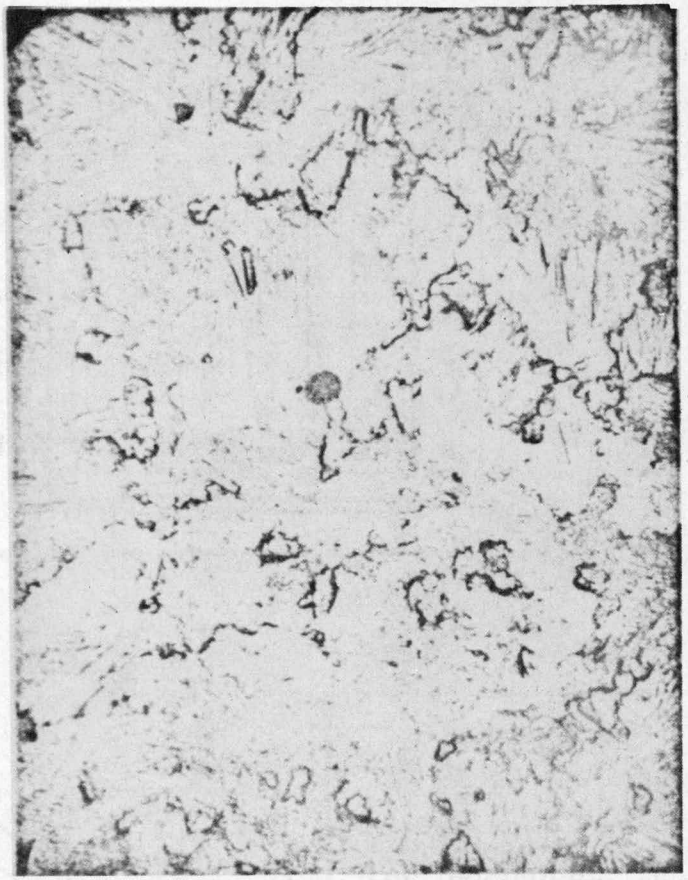

Before Cycle Annealing

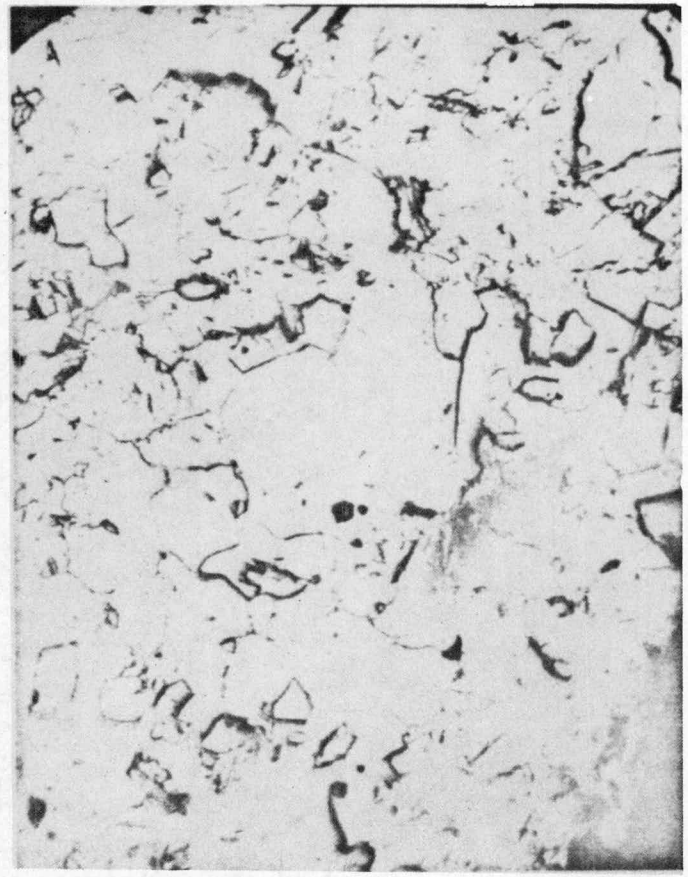

After Cycling- 100 cycles 520-1350°C
(30 min per cycle) 75 cycles 630°C - 1385°
(30 min per cycle)

Figure 35. Typical Thermal Cycle
Annealing Sample

V. TECHNO-ECONOMIC EVALUATION AND COMPARATIVE RATING OF PROCESSES

A. Introduction

Since its inception, the program has been striving for a meaningful and reasonably objective comparative evaluation of various processes. Several attempts at the development of such a method have been made, but have so far not led to a fully satisfactory result. The basic technical feasibility of a process can, in many cases, be assessed from fundamental physical principals (e.g. the Dow Corning thermodynamic assessment of potential silica reduction processes) or from direct experimental investigation (e.g. the U. of P. studies of hot rolling and the SiF_4/SiF_2 transport process). The larger questions, of, what it will cost in time and dollars to bring a basically feasible process to the point of commercial readiness, and how to estimate the relative desireability of various alternative process sequences if they should reach the commercial readiness stage, are somewhat more difficult to address in a simple and direct fashion. The Dow Corning group has had some success in using the raw materials costs as a basis for determining the relative desireability of differing process sequences for the production of raw and purified silicon. This factor alone, however, may not be a sufficient basis for decision in other areas. The problem is further complicated by the fact that a potential process must go through four phases (Figure 36), each requiring an investment of time and money, before reaching commercial readiness; with some possible processes being already in the later phases while others have not entered the first phase.

Clearly, a thorough economic analysis, which in fact includes all the technical considerations, would be the ultimate basis for decision. But such an analysis, the methodology of

which is outlined further on in this section, requires many inputs which can be obtained only from considerable experience with and understanding of the given process. For the Czochralski crystal pulling process, such a detailed analysis was recently carried out (see V-C), and it was very useful for making projections for potential future cost developments, and for pinpointing the areas which need primary attention for technology development.

For the processes we are dealing with, practically none of the required information is available. Even such key data as throughput rates, yield, required capital, and indirect material usage, are mostly not known. We have been obtaining data for three processes during the course of this research program which would permit us to make estimates of the most important economic inputs. For each process, an effort is being made to identify the dominating cost contributions and to estimate probable values for them from the process attributes being determined. When complete, this would permit comparison with other processes for which either similar estimates can be made, or for which better data already exists.

One troublesome aspect of this approach is that experience has shown that early estimates, based on an inadequate data base, are usually optimistic. This makes every novel idea, with hardly any data base, better looking than those with some known attributes, which in turn appear more favorable than well-understood processes. What is needed is the application of weighting factors based on the amount of available knowledge about the process. A good methodology for this has yet to be developed. In contrast to some earlier attempts at developing a "figure of merit", which included process speed, capital investment required, and the available knowledge, we now favor an approach more closely resembling a real cost analysis. This gives, in the early stages of data availability, a very coarse

and greatly simplified form, but has the advantage of successively increasing refinement as more data becomes available. What is still required is the development of a good weighting method to account for lack of knowledge in the early stages.

B. Methodology

The following is an outline of the basic considerations in an economic analysis. There are two basic quantities which play a role in the determination of the economic feasibility of a particular process step: its value, and its cost. The value of a product, VPT, is based on market forces. VPT is composed of the value of the original material used and the sum of the values added, VAPS, in each of a sequence of N individual process steps:

$$VPT = \sum_{K=0}^{N} VAPS(K); \qquad (1)$$

where K=0 refers to the value of the original material. Each VAPS is also determined through market forces, primarily by competing processes, by part suppliers, or job-shoppers.

In contrast to the value of the product is the cost to manufacture it, CPT. Again, CPT consists of a sum of the costs of the individual process steps:

$$CPT = \sum_{K=1}^{N} CPS(K) \qquad (2)$$

For profitability, the following condition should be fulfilled:

$$VPT \geq CPT \qquad (3)$$

While condition (3) should be fulfilled under all circumstances, one may, for good business practice, also impose the detailed conditions:

$$VAPS(K) \geq CPS(K); \quad K = 1,...N \tag{4}$$

or, if individual process steps may not be comparable in value added, replace this by the values VAGPS, and costs CGPS respectively, of comparable groups of process steps:

$$VAGPS(H) = \sum_{K=L}^{M} VAPS(K); \tag{5a}$$

and

$$CGPS(H) = \sum_{K=L}^{M} CPS)K); \tag{5b}$$

where

$$1 \leq L < N \text{ and } 1 < M \leq N,$$

so that

$$VGPS(H) \geq CGPS(H); \quad H = 1,...J \tag{6}$$

The annual costs CPY of operating the process step K are: (Fig. 37 for all processes following the basic material reduction)

$$CPY(K) = CCAP(K) + CDM(K) + CIM(K) - VSAL(K) + CEN(K) + CDL(K) + CIL(K) + CGA(K) \tag{7}$$

where

$$CCAP(K) = CP(K) \cdot FC$$

is the full annual cost of the capital CAP invested for the process step K, including machinery and allocatable parts of buildings, applicable inventory of supplies, spare parts, work in process, and finished goods. FC is the multiplier which relates the annual costs of capital, including interest on debts, return to stockholder, depreciation, property taxes, insurance, etc. to the amount of capital invested;

CDM(K) is the cost of direct material or semifinished parts entering the process step, part of which may be

$\sum_{I=0}^{K-1} VAPS(I)$, the values added to the material in the preceeding

process steps.

CIM(K) is the cost of the indirect materials used in the process step, including use of spare parts on equipment;

CEN(K) is the cost of energy consumed in the process step, including that for lighting and environmentally controlling the allocatable part of buildings;

CDL(K) is the cost of direct labor used in the process step;

CIL(K) is the cost of all applicable indirect labor, including equipment and building maintenance, material handling, process control, etc.

CGA includes all applicable general and administrative costs, including those of marketing.

There will normally be some credits, VSAL, available to the process step, for the salvage value of reject material and of used indirect materials:

$$VSAL = (1-Y(K))\cdot TP(K)\cdot VR(K) + CIM(K)\cdot FSAL(K) \qquad (8)$$

where

Y(K) is the yield in process step K;
TP(K) the annual throughput rate of the process step;
VR(K) the average unit value of the reject material resulting from the process stepl
FSAL(K) the fraction of the costs of the indirect materials used in the process step which is, in the average, recoverable in salvage.

The relationships for output, OUTP(K), and rejects, REJ(K) produced in the process step, are as follows:

$$OUTP(K) = TP(K)\cdot Y(K); \qquad (9)$$

$$REJ(K) = TP(K)\cdot (1-Y)(K)); \qquad (9a)$$

The required quantity of output in an individual process step is determined by the amount of finished product to be produced, PROD, and the yields of all N-K process steps following step K:

$$OUTP(K) = \frac{PROD}{\prod_{I=K+1}^{N} Y(I)} \qquad (10)$$

Similarly the throughput:

$$TP(K) = \prod_{I=K}^{\frac{PROD}{N}} Y(I) \qquad (10a)$$

Thus, finally, the unit cost can be determined, which is then to be compared to the value added:

$$CPS(K) = \frac{CPY(K)}{OUTP(K)}; \qquad (11)$$

The use of this approach is illustrated in the following example.

Example: Estimation of minimum rolling speed required for economical operation.

1. Step. Determination of upper limit of value added in process step.

a. Cost of direct material: Upgraded arc furnace output: \$2.-kg (currently, MGSI \$1.-/kg; \$2.-/kg is Dow Corning estimate).
Cost of gradient freezing should be less than cost of reduction.
Assume: \$1.-/kg.
Total direct material cost: $\gtrsim$ \$3.-/kg.

How much material required per unit area?
$1m^2$, 0.1 cm thick contains 100 cm^3.
Si density: 2.33g/cm^3
Si content of finished product: 233 g/m^2. Assume, as upper limit, 93% overall yield of total process to finished product, including rolling:
throughput $\geq$ 250 g/m^2
Value of direct material: $\geq$\$-.75/m^2

b. Value of output from process step:
Assume value of finished product: \$20.-/m^2

Assume value added in fabricating complete array in sheet is only 50% of finished product cost: $10.-/m^2$

Value of sheet: $\lesssim$ $10.-/m^2$

c. Additional processes to sheet output: annealing.
Although required several times, cost assumed to be low (relatively low technology, no labor, simple equipment, energy consumption low through good insulation) $\gtrsim$ $2.-/m^2$

d. Maximum value added in rolling step: VAPS b)-c)-a): $\lesssim$ $7.25/m^2$

2. Step. Determination of major cost component:
Rolling is a capital intensive operation, practically no indirect material (primarily replacement parts), little labor. Assume cost of capital to be 50% of cost of process step, as upper limit.

3. Step. Estimation of capital requirement.

a) How many mills are required?
Assume: 30% thickness reduction in each pass.
How many passes are needed?

A = thickness of output sheet = 0.1 cm
B = thickness of original ingot = 30 cm
R = Thickness reduction per pass = 0.3
N = number of passes = ?

It is:

$$A = B \cdot (I-R)^N;$$

$$N = \frac{\log \frac{A}{B}}{\log (1-R)};$$

For the given example: N = 22.

b) Estimation of cost of mill, including building, and accessories:

$500,000.-/each

(only preliminary, rough estimate)

c) Total capital: $5,000,000.-

for 10 mills. In first 2 mills, ingot is rolled back and forth, in last 8, sheet is thinned by passing through successive mills.

d) Assume 25% annual rate for cost of capital: CCAP = $1,250,000.-/y

4. Step. Combining results of steps 2 and 3.
Annual costs of process step:
CPY $\geq$ $2,5000,000. -/y

5. Step. Determine minimum annual throughput for breakeven:

$$TP \geq \frac{CPY}{VAPS} \geq \frac{2,500,000\$/y}{7.25\$/m^2}$$

$$\geq 340,000\ m^2/y$$

A 7500h/y effective utilization time of the rolling mills, the minimum required rolling speed is:

$$\underline{\underline{v = 46\ m^2/h.}}$$

C. COST ANALYSIS OF THE CZOCHRALSKI PROCESS

A tabular analysis of the economics of cylindrical crystal production by the Czochralski method has been made. This analysis is intended to develop a basis for comparision of other potential processes, and was prompted, in part, by the recent emphasis on high efficiency single crystal silicon devices and continued interest in the potential for further technical development of the Czochralski crystal pulling approach (91). During this reporting period, additional information has been acquired and the analysis has been updated and further refined. The effort in this area has been greatly aided by the availability of a productivity analysis prepared for one of the current large capacity crystal growers (92).

It was found that the most important cost elements in future crystal pulling result from the equipment, including replacement parts, the crucibles, and the silicon. The silicon cost was kept separate and entered as a parameter at the end of the current research efforts. To facilitate estimation of future large capacity crystal pulling equipment cost, the historical prices of crystal pullers of various capacities were plotted and extrapolated (Fig. 38). Similarly, the prices of crucibles of various sizes were obtained and analyzed. It was found that the cost per unit capacity of very small and very large crucibles increases significantly above that applicable to a large range of intermediate size crucibles (Fig. 39). The assumption was made that, as the large crucibles become more of a standard product, their price will come down to the level of the intermediate size crucibles. Several assumptions were made in the projections:

1. Melt-down and cooling times as well as loading and crystal removal times will increase with increasing crystal mass, the latter two because of the need for mechanical handling; 2. energy consumption will increase less than proportionately to ingot diameter, based on better control of heat losses; 3. cooling water costs can be made negligibly small; 4. argon costs can be eliminated by pulling in vacuum; 5. crucible costs per kg of good cylindrical crystal can be held in correspondence to the current intermediate size crucible prices; and 6. replacement part costs will be proportional to the equipment costs.

The results of the analysis show (Tables 30 to 35) that the crucible costs will dominate the future crystal pulling costs by a large margin, particularly as the silicon prices will decrease. Under the assumption that the kerf losses also will be considerably decreased (91), it is seen that the basic silicon wafer price will remain higher than acceptable for large scale silicon solar array fabrication within the cost goals. Changing this situation will require either repeated use of the crucibles, or the fabrication of crucibles at greatly reduced cost. This need has long been recognized, but efforts to satisfy it have so far not been successful. The use of opaque, in lieu of clear, fused quartz crucibles seems to be normal practice in several organizations, with a concomitant saving of approximately 25% in crucible costs.

D. REFERENCES - SECTION V

91. Kran, A.; Proc. Symposium on the Material Science Aspects of Thin Film Systems for Solar Energy Conversion, pp. 422-430, May 20-22, 1974, Tucson, Arizona (NSF/RANN Grant GI-43795).

92. Leybold-Heraeus Inc., "Productivity of the Leybold-Heraeus Crystal Grower EKZ 1200/3500 and EKZ 1600/6000", Ca. June 1974.
Also: "Productivity of EKZ 1600/6000 Crystal Growing Machine for Silicon" (superceded) in "Technical Specification # 0773-14 for Crystal Growing Machine Type EKZ 1600/6000, July 20, 1973, Monroeville, Pennsylvania.

Table 30

Crystal Geometry

Subject Group	Line No.	Attribute	Leybold-Heraeus Data for EKZ 1600/6000 July 1973	Leybold-Heraeus Data for EKZ 1600/6000 June 1974	Projected Data		
	1a	Crystal Diameter inch	2	3	4	6	8
	1b	Crystal Diameter mm	52.5	78	102	152	203
	2	Cylindrical Crystal Length mm	1450	1350	1400	1400	1400
	3	Cylindrican Crystal Mass kg	7.4	15.1	26.6	60	106
	4	Mass in Tapers (45^{o}) g	90	700	650	2200	5200
	5	Silicon Left in Crucible g	210	400	550	800	1300
4 + 5	6	Total Silicon not used g	300	1100	1200	3000	6500
3 + 6	7	Silicon Charge kg	7.7	16.2	27.8	63	112.5
	8	Theoretical Cylindrical Crystal Yield %	95.8	93	95.5	95.5	94

Table 31

Operation Times

Subject Group	Line No.	Attribute	Leybold-Heraeus Data for EKZ 1600/6000 July 1973	Leybold-Heraeus Data for EKZ 1600/6000 June 1974	Projected Data		
	9a	Pull Rate, linear mm/min	1.9	1.6	2.0	2.9	2.5
	9b	" " as % of Maximum	32	56	60	75	75
	9c	Pull Rate, mass g/min	9.7	18	38	124	425
	10	Pull Time min	765	974	700	483	560
	11	Melt Time min	60	90	100	120	150
	12	Cooling Time min	90	120	150	180	210
	13	Loading " min	10	10	20	30	30
	14	Balance Temp. min	5	5	5	5	5
	15	Crystal Removal Time min	15	10	30	45	45
	16	Cleaning after 5 Charges (100 Min total) min	20	15	20	30	30
	17	Service and Repair min	40	50	40	40	40
Σ(10 to 17)	18	Total Cycle Time min	1005	1274	1065	933	1070
		h	17.5	21.2	17.8	15.6	17.8

Table 32

Energy Use Per Pull

Subject Group	Line No.	Attribute		Leybold-Heraeus Data for EKZ 1600/6000 July 1973	June 1974	Projected Data		
	19	Melt Energy	kWh	6	13	22	50	90
	20	Energy Loss during Meltdown	kWh	44	90	110	200	270
19 + 20	21	Total Meltdown Energy	kWh	50	103	132	250	360
	22	Energy Loss During Pull	kWh	435	1000	920	1000	1440
21 + 22	23	Total Energy Consumption	kWh	485	1100	1050	1250	1800

Table 33

Operating Data

Subject Group	Line No.	Attribute	Leybold-Heraeus Data for EKZ 1600/6000 July 1973	June 1974	Projected Data		
	24	Maximum Number of Charges/Year (8100h)	500	395	460	525	460
	25	Successful Number of Pulls/Year	425	355	360	420	360
	26	Practical Yield of Cylindrical Crystal (80%) kg/y	2,500	4,600	7,600	20,000	30,500
(24-25) x 7	27	Silicon in Abandonded Pulls kg/y	810	650	2,780	6,600	11,250
from 4	28	Silicon in Tapers and Crucible kg/y	130	390	430	1,260	1,340
from 26	29	Silicon in Non cylindrical Parts of Crystals kg/y	630	1,150	1,900	5,000	7,625
Σ(27 to 29)	30	Total Non-output Silicon kg/y	1,570	2,190	5,110	12,860	21,215
	31	Portion of Non-output Silicon Non-recyclable kg/y	315	1,150	1,025	2,570	4,240
26 + 31	32	Total Silicon Input kg/y	2,815	5,750	8,630	22,600	34,700
	33	Furnaces Handled/ Operator	5	5	4	3	3
Σ(13 to 16)	34	Fixed Operator Times/Cycle h	1.5	1.5	2.0	2.5	2.5
	35	Total Manhours/ Cycle h	3.1	4.7	4.5	5.2	5.9
	36	Labor Cost/ Furnace @ $9.00/h $/y	14,760	15,120	18,900	25,200	25,200
	37	Annual Argon Cost $/y	4,945	3,860	--	--	--

Table 34

Single Crystal Cost Analysis

Subject Group	Line No.	Attribute		Leybold-Heraeus Data for EKZ 1600/6000 July 1973	June 1974	Projected Data		
from 36	38	Labor Cost/kg Cyl. Crystal	$/kg	6.55	3.29	2.48	1.26	0.83
from 23	39	Energy Cost/kg Cyl. Crystal at 3¢/kWh	$/kg	3.10	2.55	1.30	0.70	0.60
from 37	40	Argon Cost/kg Cyl. Crystal	$/kg	1.98	0.84	-	-	-
	41	Quartz Crucibles/ kg Cyl. Si	$/kg	10.-	19.29	1.20	1.20	1.20
	42	Replacement Parts/ kg Cyl. Si	$/kg	8.-	11.96	5.60	3.60	3.45
	43	Capital Costs/kg Cyl. Si at 25%/y	$/kg	19.20	9.81	4.68	3.00	2.87
Σ(38 to 43)	44	Total Direct Production Costs	$/kg	48.83	47.74	15.26	9.76	8.95
	45	G&A costs at 20%	$/kg	9.76	9.55	3.05	1.95	1.79
44 + 45	46	Total Cost w/o Silicon	$/kg	58.60	57.29	18.31	11.71	10.74
	47a	Silicon at $10./kg +20% G&A	$/kg	13.60	13.60	13.70	13.60	13.70
46 + 47a	48a	Cost of Cylindrical Silicon	$/kg	72.20	70.29	32.01	25.31	24.44
	47b	Silicon at $4./kg +20% G&A	$/kg	5.50	5.50	5.50	5.50	5.50
46 + 47b	48b	Cost of Cylindrical Silicon	$/kg	64.10	62.79	23.81	17.21	16.24

Table 35

Sheet Costs

Subject Group	Line No.	Attribute	Leybold-Heraeus Data for EKZ 1600/6000 July 1973	Leybold-Heraeus Data for EKZ 1600/6000 June 1974	Projected Data		
	49	Wafer Thickness mm	0.4	0.4	0.24	0.20	0.20
	40	Kerf mm	0.28	0.28	0.16	0.12	0.12
	51	Silicon Used per Unit Area kg/m^2	1.80	1.81	1.02	0.85	0.85
	52a	Silicon Wafer Cost w/o Cutting Costs $\$/m^2$	129.-	127.22	32.64	21.51	20.77
	52b	dto $\$/m^2$	115.-	113.65	24.29	14.63	13.80

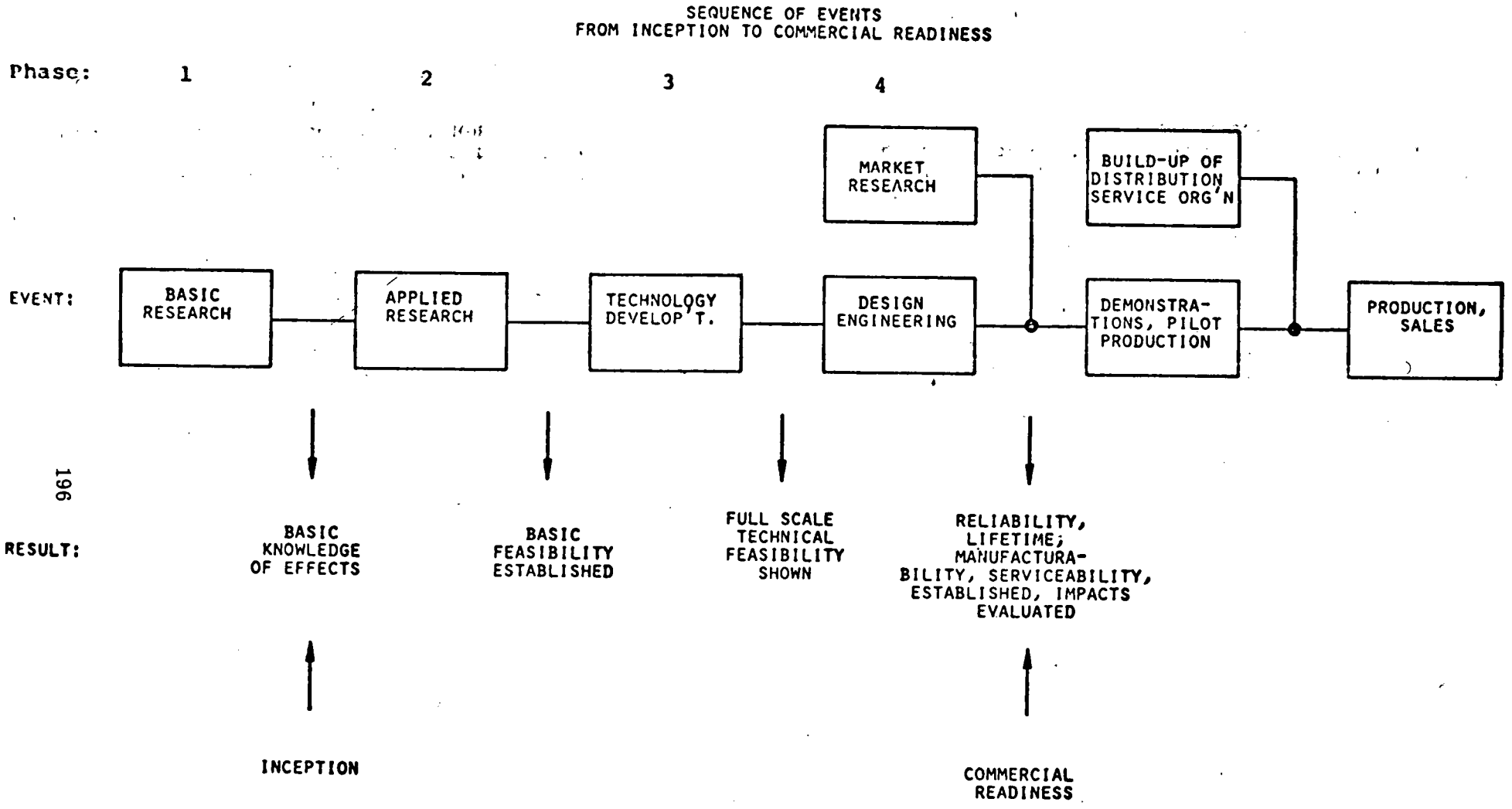
SEQUENCE OF EVENTS
FROM INCEPTION TO COMMERCIAL READINESS
Phase:
1
2
3
4
EVENT:
BASIC RESEARCH
APPLIED RESEARCH
TECHNOLOGY DEVELOP'T.
DESIGN ENGINEERING
MARKET RESEARCH
BUILD-UP OF DISTRIBUTION SERVICE ORG'N
DEMONSTRA-TIONS, PILOT PRODUCTION
PRODUCTION, SALES
RESULT:
BASIC KNOWLEDGE OF EFFECTS
BASIC FEASIBILITY ESTABLISHED
FULL SCALE TECHNICAL FEASIBILITY SHOWN
RELIABILITY, LIFETIME; MANUFACTURA-BILITY, SERVICEABILITY, ESTABLISHED, IMPACTS EVALUATED
INCEPTION
COMMERCIAL READINESS

FIGURE 36.

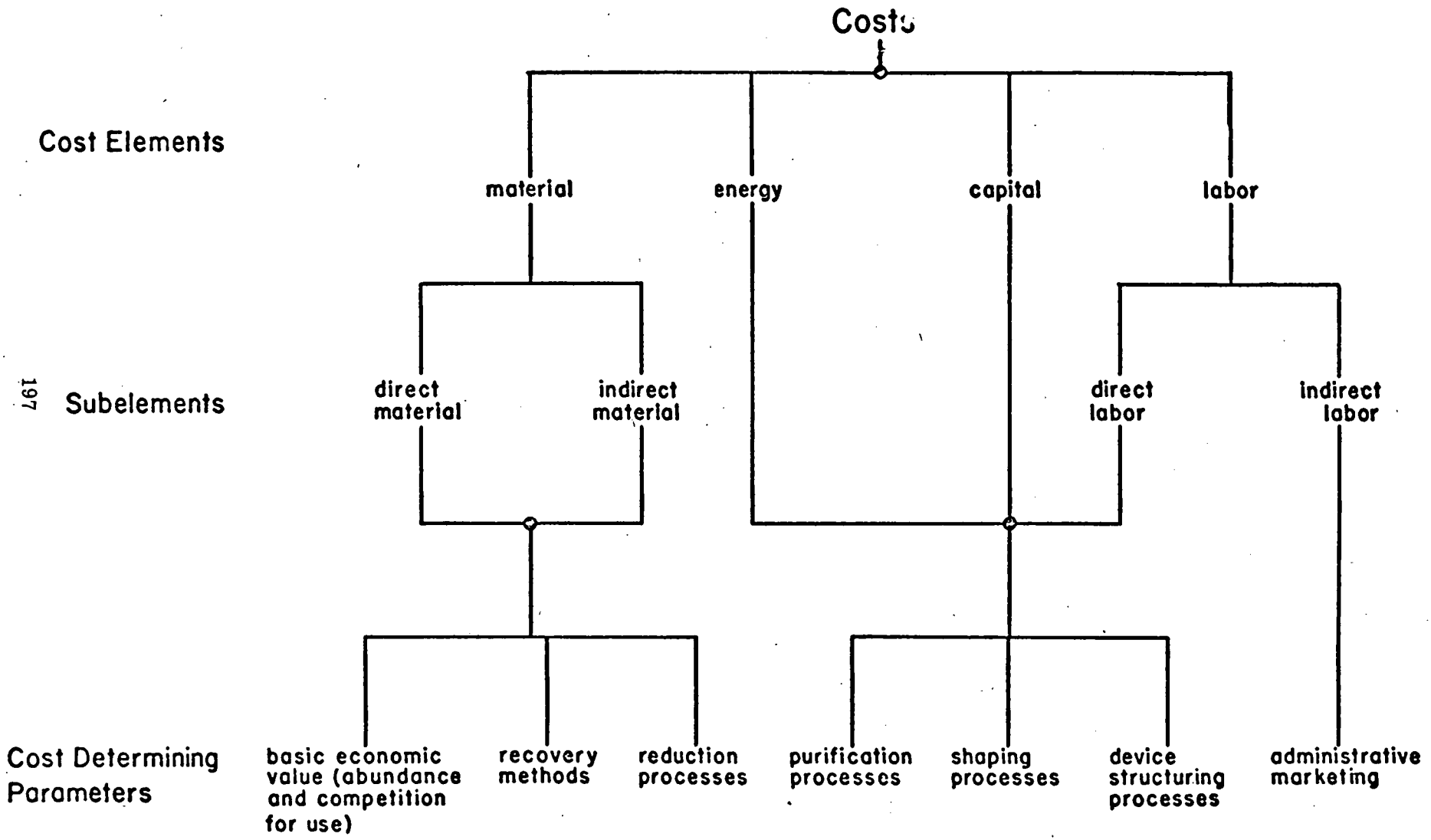

FIGURE 37 PROCESS COST ELEMENTS, SUBELEMENTS, AND COST DETERMINANT PARAMETERS

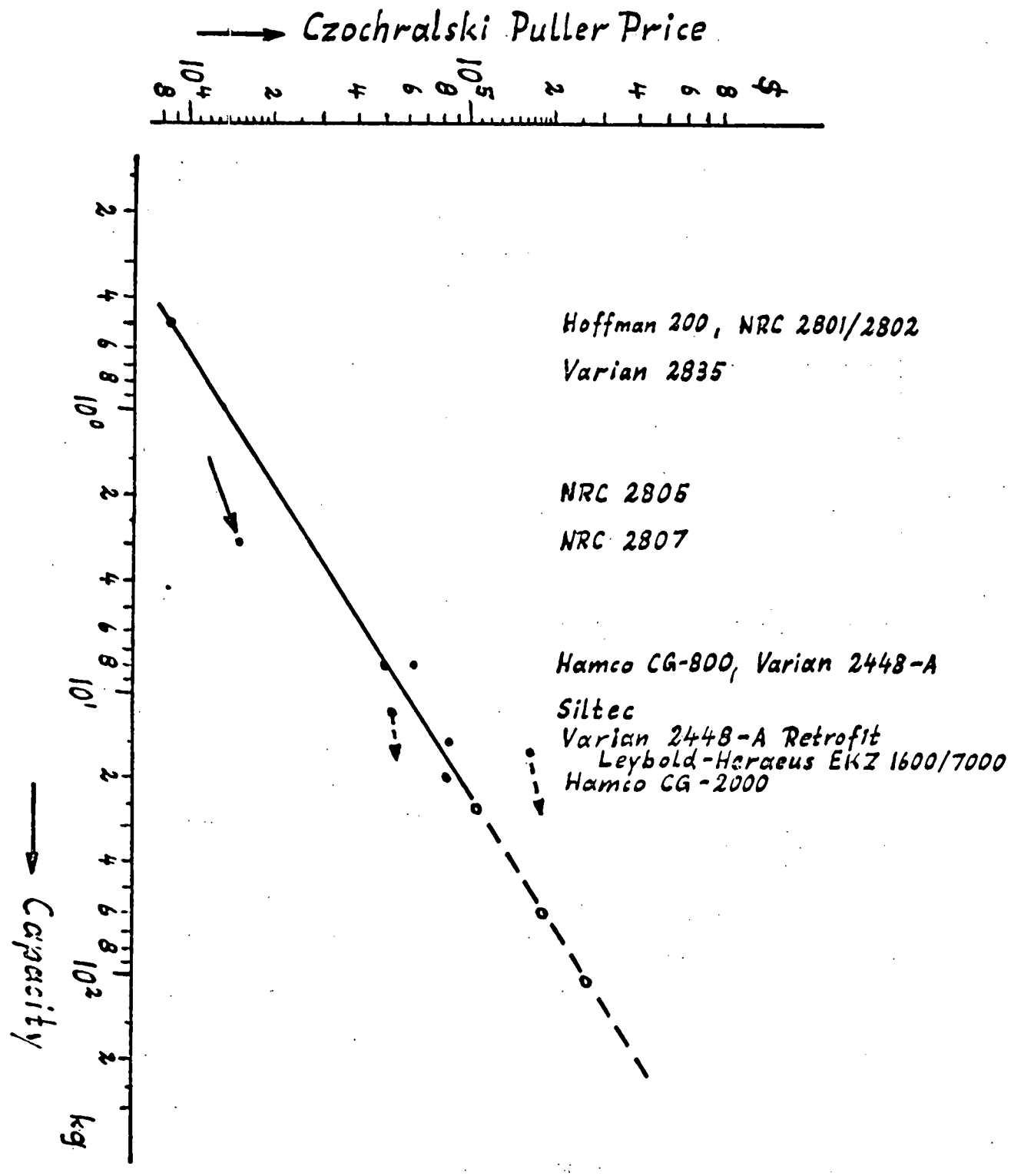
Czochralski Puller Price
$
Capacity
kg
Hoffman 200, NRC 2801/2802
Varian 2835
NRC 2805
NRC 2807
Hamco CG-800, Varian 2448-A
Siltec
Varian 2448-A Retrofit
Leybold-Heraeus EKZ 1600/7000
Hamco CG-2000

Figure 38

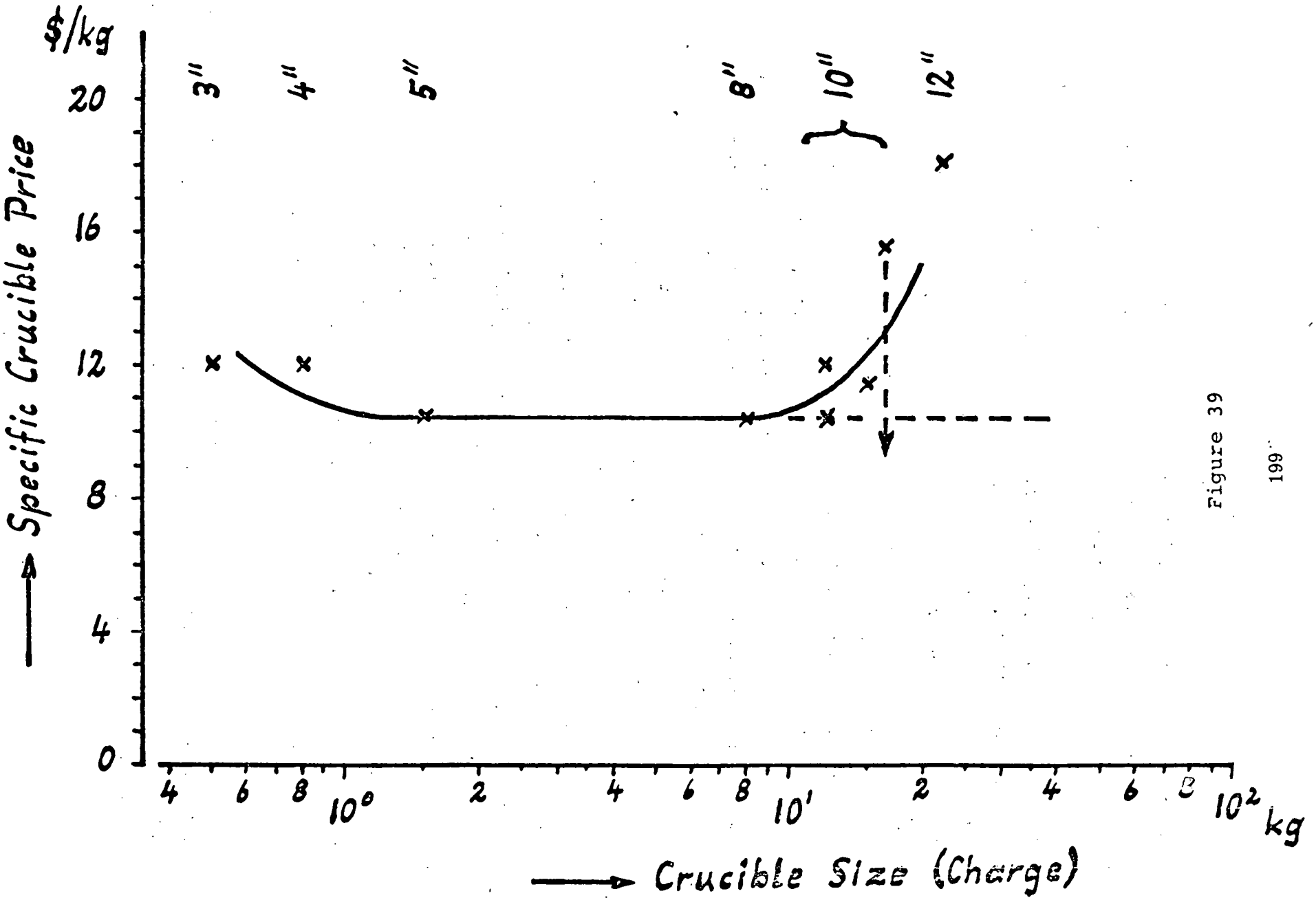
$/kg
20
16
12
8
4
0
3"
4"
5"
8"
10"
12"
Specific Crucible Price
4
6
8
10⁰
2
4
6
8
10¹
2
4
6
8
10²
kg
Crucible Size (Charge)

Figure 39

VI. CONCLUSIONS AND RECOMMENDATIONS

The following paragraphs provide brief summaries of the conclusions of the work reported in the preceeding sections of this report and, based on our assessment of these results, provide recommendations for future work in each of the areas covered.

A. Preparation of Solar Grade Silicon (Dow Corning)

Although many chemical reactions are thermodynamically feasible for preparing elemental silicon, very few lend themselves to a process capable of meeting the ERDA requirements of quality, quantity and cost. If one further considers the ERDA time goals of having a process at pilot plant scale by 1980 and at large plant scale by 1985, it is felt that only one process has a good probability of meeting all the above requirements: this is upgrading of the MG-Si process to yield a product of solar-grade quality.

Metallurgical silicon, today, is commercially produced in quantities far in excess of the 1985 large-scale goal of 2000 Mt/y and at a selling cost one order-of-magnitude lower than the 1985 goal of $10/kg Si. In order to meet overall ERDA goals, then, requires development of a process train that is capable of purifying MG-Si to solar-grade quality for less than $9/kg Si. It is only this process train, then, that must be developed in order to be in pilot plant stage by 1980 and in large plant scale by 1985. The final process train may consist of some combination of upgraded raw materials feeding the arc furnace, improved materials of construction for handling molten silicon, or upgrading of the arc furnace silicon by reactive gas refining, slagging, acid leaching, SiF_4 transport or unidirectional freezing.

Dow Corning has already demonstrated on a laboratory scale that MG-Si can be purified, through various combinations of upgrading processes to the recently proposed level for solar-

grade silicon, except with respect to boron and phosphorus. Analyses of raw materials entering the arc furnace indicates that boron and phosphorus can be significantly reduced by using higher purity raw materials. Analyses of higher-grade materials point out that boron and phosphorous should be able to be reduced to a low enough level to allow fabrication of greater than 10% efficient solar cells. The postulated concept of using purer raw materials to reduce the level of boron and phosphorus yet remains to be experimentally verified. This purification method should significantly reduce other arc furnace silicon impurities, thereby, allowing easier upgrading of the silicon by the other techniques discussed above. A favorable margin exists in terms of the cost of raw materials since they represent less than 10% of the $1/kg selling price of MG-Si.

It is recommended that the upgrading of MG-Si be continued since it has a high probability of meeting all the ERDA goals for SoG-Si. It is also recommended that special attention be given to producing higher-than-normal purity MG-Si by experimentally proving the postulated concept of using purer raw materials in the submerged-electrode arc furnace.

B. Si/SiF_4 Transport

The basic feasibility of the SiF_4 silicon transport and purification process has been established as a result of the work on this program. Cyclic operation of the process has been demonstrated and significant separation of the major impurities present in metallurgical grade silicon has been shown to occur as a result of the basic process. The stability of the transport species at room temperature and at atmospheric pressure has also been established and should enable the introduction of more sophisticated impurity removal techniques to further increase the purification capability. Deposition rates comparable to other CVD

processes have been measured and our kinetic studies indicate that transport rates compatible with the program goals should be achievable at higher temperatures and flow rates.

It is recommended that work on the next stage of development of this process be concentrated in the following areas:

1. Operation of the process with molten silicon, with the ultimate aim of direct coupling to the arc-furnace metallurgical grade silicon production process.
2. Investigation of the effect of higher flow rates in conjunction with 1.
3. Investigation of techniques to enhance impurity removal including freeze out, distillation, physical separation by multiple pass transport, and filtering.
4. Direct deposition of the silicon in sheet form on suitable substrates (e.g. low cost, conducting or removeable, etc.) and characterization of electrical properties and morphology.

C. Hot Rolling of Silicon

The results obtained to date have show that polycrystalline silicon is ductile at high temperatures. It can be stated with reasonable confidence that polycrystalline silicon can be successfully rolled into sheets at a sufficiently high temperature and further that this temperature will be of the order of 1300^{o}C or higher. It is clear that the rolling behavior will depend on the crystallographic texture of the starting ingot and that an effort to characterize the textural dependence of rolling properties is necessary. Observed recrystallization of compressed and annealed silicon samples indicates that strain-annealing of silicon can result in significant grain growth with

ultimate grain sizes of the order of millimeters.

It is recommended that work be continued in the following areas:

1. Determination of the maximum obtainable strain rates and total strains as function of temperature and crystallographic texture with the intent of specifying rolling speed limitations.
2. Developing suitable roll and bearing materials for operation at temperatures near 1300°C.
3. Further characterization of the recrystallization behavior of deformed silicon.
4. At a later stage, the construction and operation of a small laboratory sized rolling mill.

D. Traveling Zone Recrystallization

Theoretical analysis predicts a maximum zone travel speed of 9 meters per hour for silicon sheets 1 meter wide and 0.01 cm thick. A power level of the order of 2000 Watts will be required to maintain a molten zone in sheet of these dimensions. Cooling the clamps holding the silicon sheet or other components of the immediate environment will not grossly affect the zone travel speed.

The Pierce Gun is a simple and effective electron beam line source capable of producing fine lines (less than 0.5 mm using 0.3 diameter filament in the present set up) over extended areas. Proper focusing of the gun requires extremely accurate positioning of the gun components (focusing plates and filament). Modification of the present guns is necessary to provide finer control and permit reproducible operation. Molten zones have been produced in rectangular silicon bars (thicknesses 0.6-5.0 mm) with the Pierce Guns, however, it has not been possible to produce and move a molten zone while maintaining the rectangular geometry to date. Special beam shapes (e.g. arched) may be

needed to counteract the "pull in" tendency. Such beam shapes are within the capability of the Pierce Gun configuration assuming adequate control of component positioning can be achieved.

The following items should be included in future work in this area:

1. Development of a more refined version of the Pierce Gun incorporating an accurate and reproducible means of positioning the filament in the slot of the plate and of varying the plate spacing. Provision for adjustment during actual operation would be desirable.
2. Continued investigation of zone stability with linear electron beam heating using the gun developed in 1. above.
3. Investigation of the merits of alternative beam shapes.
4. Determine optimum conditions (speed, etc.) for single crystal growth.
5. Explore the possibility of increasing the recrystallization velocity by special heat removal techniques.

E. Technical and Economic Evaluation of Processes

The "detailed economic analysis" approach to process evaluation is clearly the technique best suited for a nonpartial (i.e. as free as possible of subjective judgements) comparative evaluation of competing processes, despite a present lack of necessary data in some process areas. The major needs at this time are the acquisition of a broad base of data for the candidate processes and the development of a means for factoring the state of available knowledge of a given process into the analysis.

VII APPENDICES

A. Preprint of Paper on Upgrading MG-Si

PURIFICATION OF METALLURGICAL-GRADE SILICON TO SOLAR-GRADE QUALITY*

L. P. Hunt, V. D. Dosaj, J. R. McCormick and L. D. Crossman

Dow Corning Corporation
Solid-State Research and Development
Hemlock, Michigan 48626

Various methods are discussed for upgrading metallurgical-grade silicon to the level required to produce solar cells. This requires impurities ranging from 50-2000 ppma to be reduced to about 0.3 ppma in the case of boron and to about 30 ppma for the transition elements. Analyses of raw materials used to produce metallurgical-grade silicon indicate that selection and purification of materials should result in lower levels of most impurities. Removal of impurities from molten silicon by their reaction with various gases shows up to 97% aluminum reduction and as much as a 60% lowering of boron and copper. Preliminary acid leaching experiments indicate that the level of transition element impurities can be reduced by more than an order-of-magnitude. Metallurgical silicon was also purified, with the exception of boron and phosphorus, by segregation of impurities during unidirectional solidification using the Czochralski process. Economic analysis indicates that this crystal growth process, coupled with chemical processes for upgrading metallurgical silicon, should be capable of meeting the ERDA cost goal for solar-grade silicon of less than $10/kg.

INTRODUCTION

Previous work (1) used thermodynamics and raw material prices to identify 20-some feasible processes for the manufacture of solar-grade silicon (SoG-Si) from over 200 proposed chemical reactions. It was assumed that individual raw material prices might comprise as high as 25% of the $10/kg selling price of polycrystalline silicon in a high-volume process. Of these 20-some processes, the submerged-electrode, arc-furnace production of silicon had a raw materials cost much lower than any other considered process.

Since the arc furnace process is commercially used today to produce metallurgical-grade silicon (MG-Si) at $1.00/kg, i.e., at only one-tenth of the $10/kg goal for SoG-Si, methods of upgrading MG-Si to SoG-Si should logically be under strong consideration. The methods reported below involve upgrading raw materials, the arc furnace process itself, as well as the MG-Si produced.

---

* Partially supported by Grants from the National Science Foundation GI-29729 and the Energy Research and Development Administration, EC(11-1)-2721.

An unequivocal definition of solar-grade silicon does not exist as of this writing. Some guide lines do exist, however, under which we are directing our investigations. Boron is the doping element that normally determines the doping type and level in SoG-Si. Recent papers (2,3) demonstrate that the efficiency of solar cells peak as a function of resistivity in the range of 0.3 ohm-cm. This suggests that SoG-Si should have an original resistivity of about 1 ohm-cm (0.3 ppma or 2×10^{16} atoms/cm^3) before processing. Very efficient cells can be prepared, in fact, as shown later in this paper, from silicon doped with boron even to the 0.04 ohm-cm level. As regards the transition group elements, Wakefield (4) has suggested that individual metal concentrations must be kept below the 5-50 ppma level.

PURIFICATION METHODS

The overall approach for purifying MG-Si to SoG-Si is clarified by referring to Fig. 1. A five-pronged approach is indicated since the many impurities existing in MG-Si (see Table 1) are not all effectively removed in any one step. The final combination of processes required to upgrade MG-Si will not necessarily involve all the steps discussed.

The last Purification step indicated in Fig. 1, namely unidirectional solidification, is very effective for removing aluminum and transition metals due to their favorable segregation coefficients. However, the initial high levels of iron (0.4%) and aluminum (0.2%) in MG-Si can result in poor Czochralski single-crystal yields due to excessive buildup of impurities in the melt (5). The unfavorable segregation coefficient of boron (0.8) results in its ineffective removal during unidirectional solidification. Therefore, special attention must be given to B, Al, and Fe removal in the other purification methods.

Acid leaching of MG-Si is an attractive procedure for reducing the level of elements with favorable segregation coefficients such as aluminum and iron, since these impurities concentrate at the grain boundaries of the polycrystalline material when it solidifies. The effectiveness of acid leaching, therefore, should be enhanced by crushing the MG-Si lumps to a particle size equivalent to the size of the polycrystalline grains.

Blowing a reactive gas through molten MG-Si can be an effective process for removing impurities. The level of aluminum, for example, can be easily reduced by more than an order-of-magnitude by blowing with chlorine due to the volatility of $AlCl_3$ at high temperatures. Lowering of the aluminum level prior to unidirectional freezing allows attainment of increased single-crystal yields.

The use of slagging, alone or in conjunction with gas blowing, has been suggested (6) as another method for removing impurities. The success of this liquid-liquid extraction technique is based on finding a slag that is stable in the presence of molten silicon and that has a density which is different enough from silicon to allow effective separation. It is also necessary that the solubility of individual

impurities be higher in the slag than the silicon and that the slag must not dissolve a significant amount of silicon.

Removal of impurities at the arc furnace is also being examined as a potential method of upgrading MG-Si. Impurity levels might be lowered through more appropriate materials-of-construction and/or through modification of furnace operating parameters.

A further method of purifying MG-Si is by upgrading the raw materials used as reactants in the arc furnace. Normally quartzite gravel is used as the source of SiO_2 while petroleum coke, coal, and wood chips are used as the carbonaceous reductants. Improved quartzite purity should be possible through selection of purer gravel while purification of selected reductants might be done by high temperature halogenation.

Raw Materials

Reference to Table 1 suggests that most of the impurities that occur in MG-Si should logically be associated with the raw materials used in the arc furnace process. This is a reasonable assumption since negligible errosion of the graphite liner occurs in the arc furnace even after many years of operation.

The consumption of raw materials in the arc furnace process is represented by the overall reaction

$$SiO_2 + 2C \rightarrow Si + 2CO.$$

Silica enters the furnace in the form of quartz or quartzite which is mined either in a crystalline form and crushed to size or is mined as gravel and sized accordingly. These silica materials are usually in the range of 98.5-99.5% pure (7-10) and have the impurity analyses indicated in Table 1. These analyses are expressed in parts per million atoms of silicon using the stoichiometry of the above reaction. The quartzite gravels from North Carolina and Alabama and the quartz crystals from Norway and Brazil indicate that these silica materials are not the major source of the impurities found in MG-Si. However, special efforts are directed at finding lower boron-level materials since quartzite would be the predominate boron contributor if the carbon materials could be sufficiently purified. Therefore, current work in this area is aimed at analyzing various quartz and quartzite samples in order to find a purer starting material than is currently used.

The carbonaceous reductants entering the arc furnace are obviously the major contributors of impurities to MG-Si as seen in Table 1. Petroleum coke and coal are the main reducing agents. Wood chips not only supply carbon but also provide mix porosity in the furnace to aid the escape of the large volume of emitted CO and SiO vent gases. The consumable graphite electrode supplies some carbon to the reaction but serves the major function of carrying current for the electric arc. Except for vanadium and nickel, petroleum coke is the purest of the carbon materials.

The present concept is to experimentally study the replacement of as much of the reductants as possible by charcoal since it can be purchased on a commercial scale with most impurities below the 1 ppma level (see Table 2). Charcoal had been used predominately as the major reductant in arc furnaces in the past but was gradually replaced due to its rising price. Its current price, however, represents only a very small fraction of the $10/kg goal for SoG-Si. The analysis of various charcoals before and after purification by high-temperature halogen treatment is being actively pursued since this process is particularly successful in the nuclear industry for removing boron from the graphite moderator used in certain reactors. An example of petroleum coke purification by this technique is shown in Table 3. The coke was purified at 2500 °C for three hours by purging with chlorine and fluorine using a halogenated hydrocarbon as carrier.

Arc Furnace Process Improvement

Upgrading the arc furnace process can be pursued from two different approaches: the effect on silicon purity from materials-of-construction and from operating conditions. Although the graphite lining within the arc furnace apparently does not contribute impurities to the MG-Si, we plan to analyze currently-used lining materials to determine their effect on the purity of MG-Si. We also plan to analyze other materials that contact molten silicon during processing; e.g., the tap-hole plug, ladel lining, and chill lining.

Some indication of what furnace operating conditions might have on purity is indicated by the impurity analysis of fumed silica as seen in Table 1. Fumed silica is produced by air oxidation of silicon monoxide exiting the arc furnace. The impurities in the fumed silica arise from the volatilization of the impurities within the high temperature (up to 3000 °C) zones of the arc furnace and their consequent entrainment in the CO/SiO vent gases. Of particular interest are boron and phosphorus. It is planned to study the effect of varying the furnace operating conditions upon the purity of the MG-Si and to determine if some trade-off exists between purity, energy consumption, and total cost.

Reactive Gas Blowing

Experiments for the removal of impurities from molten MG-Si by reaction of the impurities with gases were continued using the same apparatus described earlier (11). The gases listed below were used singularly or in up to three-component mixtures by passing them through a quartz tube into the molten silicon at flow rates of 400-1200 ml/min for times of 20-120 min and at mole ratios of gas to silicon between 5-530: Cl_2, O_2, HCl, H_2O, H_2, SF_6, and Ar. The latter was used both as a diluent and as a means to increase turbulence in the silicon.

Preliminary experiments (11) showed very favorable impurity removal when Cl_2 and O_2 were used as reactive gases. However, duplicate experiments have shown the removal of certain impurities to vary by as much as 0-97% depending upon the degree of impurity segregation in the particular

solidified sample chosen for analysis. A new sampling technique, developed to circumvent the segregation problem, is being employed in a matrix of experiments to precisely define the degree of impurity removal by blowing with various gases.

Although impurity segregation has been a problem, certain results directly attributable to gas blowing are still very apparent. The levels of boron and copper are reduced no matter which of the gases are used. However, maximum removal has been found to be only 60%. The level of aluminum is also reduced with all gases used; in this case 90-97% removal is common.

Acid Leaching

Purification of MG-Si by acid leaching has been reported in the literature over the last half century (12-14). A commercial process has been on stream in Norway since 1964 to purify 90% FeSi by leaching with hot $FeCl_3$/HCl solution (15). This Silgrain process is able to convert a material containing only 90% silicon to a product approximately equivalent to that of standard MG-Si. One of the interesting differences is the lower level of transition element impurities in the Silgrain silicon due to the leaching mechanism. The leach solution attacks the crystalline structure of 90% FeSi dissolving the intermetallic phases at the grain boundaries where the impurities are contained. The bulk of the material, namely the relatively pure silicon dendrites, are unattacked.

Acid leaching experiments were initiated with the primary aim of determining whether the major impurity iron could be reduced by acid attack at the MG-Si grain boundaries. Early results indicate that most transition element concentrations, including iron, can be easily reduced by over an order-of-magnitude.

Proof-of-concept experiments were carried out using standard MG-Si. Greater than ½-inch material was ground and then screened into different size classifications between 10-100 mesh. These materials were then separately leached with one or more of the following acids: HCl, HNO_3, HF, or H_2SO_4. Results are shown in Table 4 for a typical experiment in which 20 mesh MG-Si was acid leached with an HF/H_2SO_4 acid mixture for about 20 h at 80 °C. After leaching the silicon was washed, filtered, dried, and analyzed by emission spectroscopy. With the exception of copper, the concentration of all first row transition elements were reduced by more than an order-of-magnitude and, in most cases, to less than the limit of detection. The doping elements boron and phosphorus were not greatly affected, however.

The above results are especially encouraging since no optimization of leaching conditions was performed. It is planned to study the effect of the following parameters upon the degree of MG-Si purification: acid type and concentration, sequence of leaching, acid mixtures, leaching temperature and duration, and starting silicon particle size.

Unidirectional Solidification

Unidirectional freezing has been extensively employed in the purification of a variety of materials. The majority of impurity elements found in MG-Si have extremely small segregation coefficients as shown in Table 5. With the exception of boron and phosphorous which do not have favorable segregation coefficients and iron and aluminum which are present in extremely high concentrations, segregation during normal freezing should reduce the impurity concentration in the solid into the low ppba range. These impurity concentrations should be acceptable based on the results of Wakefield (4) regarding raw material requirements for solar-grade silicon.

The effectiveness of unidirectional freezing in upgrading MG-Si was investigated using the Czochralski crystal growth method. First-generation ingots were pulled directly from a MG-Si melt. No single-crystal growth has been observed, however, due to the high impurity concentration in the melt. While only preliminary data are available relating to segregation coefficient determination, the results warrant some discussion. In general, pull rates of less than 5 cm/h resulted in extremely low transition element impurity concentrations. Impurity concentrations found in ingots pulled at various speeds are shown in Table 6. Very little impurity removal occurs for boron or phosphorous, as expected, due to their unfavorable segregation coefficients. However, for those elements with small segregation coefficients, changes in growth rate have a dramatic effect on the degree of purification obtained. For example, the concentration of iron and aluminum changes by more than four orders-of-magnitude as growth rate is varied by a factor of four. It is significant that at slow growth rates all transition element concentrations are reduced to below 50 ppba. This is well below the level established in a preliminary specification for solar grade silicon raw material requirements (4). It is evident that the wide range of "effective segregation coefficients" is not the result of normal segregation. The fact that smaller grain sizes are observed in material prepared by fast growth suggests that impurity trapping at grain boundaries plays a major role in determining the impurity distribution and, thus, yield. These growth imperfections may be ascribed to the constitutional supercooling of the heavily doped melt. Impurity distribution typical of crystals pulled at slow rates (less than 5 cm/h) is shown in Table 7. The transition element concentration is sufficiently low to provide a yield of at least 50% (4).

Further evaluation of first-generation material was accomplished by either float-zone refining of the first-generation ingots or using these ingots to charge a crystal puller for second-generation, Czochralski crystal growth. In general, single-crystal growth was readily achieved for second-generation ingots using either growth method. Yield of second-generation, single-crystal silicon (defined as the ratio of weights of second-generation single crystal to first-generation charge) ranged between 18 and 25%. This low yield is typical of the small growth system in which these experiments were conducted.

Multiple-pass, float-zone refining was carried out to insure unambiguous boron determination by resistivity measurements. The resistivity of the ingots varied from 0.036 - 0.045 ohmcm. Boron concentration based on these resistivity values agrees reasonably well with values obtained by emission spectrographic analysis of the charge material.

Solar cells were fabricated from several six-pass, float-zoned ingots using standard processing methods developed for high-efficiency, solar-cell production. Performance of AR-coated cells are summarized in Table 8. A current-voltage plot in the power quadrant of a typical cell under AM0 illumination is shown in Figure 2. The overall performance of these cells is quite encouraging, particularly since no efforts were made to optimize cell processing for this low resistivity silicon material. Substantial improvement in future cell performance is expected since material upgrading prior to normal freezing reduces boron concentration.

Based on the relative importance of normal freezing to the entire upgrading process and the availability of data on the economics of the Czochralski process for large-scale production of single-crystal silicon (16,17), a preliminary analysis of the economics was undertaken. The following basic assumptions were used to evaluate upgrading through crystal growth:

- Equipment for eight-inch diameter crystal growth will be available within the time frame of interest.
- Energy consumption per kilogram of silicon will decrease as ingot diameter increases.
- Cooling water costs can be reduced to an insignificant level.
- Argon costs can be eliminated by growth under vacuum.
- Crucible costs per kilogram of produced silicon will remain constant.
- Replacement parts cost will be proportional to equipment cost.
- Crystal pulling equipment is depreciated over a four-year period.
- Upgraded MG-Si will be available with a total impurity content of 10^{19} atoms/cm^3, or less.
- A method exists to "dump" the melt after 80% has been completed. The crucible may then be recharged with raw material for at least four crystal-growth cycles.

The results of this analysis (17) for an 80% ingot yield are summarized in Table 9. A pull rate of 11.5 cm/h was chosen as the 75% point of the maximum allowable rate established for material doped with 10^{19} impurity atoms/cm^3.

The resulting cost estimate of $6.63/kg of silicon for the Czochralski upgrading process is extremely encouraging when compared to $10/kg as suggested by ERDA and the present price of $1.00/kg for MG-Si. The two dominant cost items are replacement parts cost, accounting for nearly 30% of the total cost, and the cost of capital equipment (approximately 25% of total cost). It may be noted that energy cost is relatively small (ca. 7%).

CONCLUSIONS

It appears possible to be within the ERDA cost goal of $10/kg for SoG-Si by pulling single-crystal ingot from chemically upgraded MG-Si using advanced Czochralski growth technology. Purification of MG-Si is necessary in order that effective segregation of impurities will result in good single-crystal yield at fast pull rates. This purification is attainable by several methods. An analysis of currently used raw materials entering the MG-Si arc furnace indicates that the use of purer raw materials should by itself be capable of supplying silicon at near the solar-grade level. This purification method is particularly significant for boron and phosphorus since it is the only means, now being considered, that is effective for significantly reducing their concentrations. Results from using purified raw materials in an arc furnace will be reported later.

The high-concentration impurities iron and aluminum can both be reduced by an order-of-magnitude by the acid leaching of metallurgical-grade silicon. Leaching also reduces the level of other transition elements by an equivalent amount. Aluminum concentration can also be lowered ten-fold by gas refining the molten silicon with chlorine after it leaves the arc furnace.

Final purification to SoG-Si occurs very effectively during crystal growth due to the small segregation coefficients of aluminum and the transistion elements. Chemical purification combined with Czochralski crystal growth has produced up to 11% efficient cells to date.

ACKNOWLEDGEMENT

The authors wish to thank A. Rauchholz for experimental assistance in many phases of this work. Appreciation is also extended to E. Ralph of Spectrolab for fabrication and evaluation of solar cells produced from Dow Corning silicon.

REFERENCES

1. L. P. Hunt, Proc. IEEE Photovoltaic Specialists Conf., 11, 259 (1975).

2. P. A. Iles and S. I. Soclof, Ibid., p.19.

3. H. Fischer and W. Pschunder, Ibid., p.25.

4. G. F. Wakefield, et al., "Solar Silicon Definition", Final Report (10/15/74-9/15/75), NSF/RANN/SE/AER75-03972/FR/75/1.

5. J. R. McCormick, L. D. Crossman, and A. Rauchholz, Proc. IEEE Photovoltaic Specialists Conf., 11, 270 (1975).

6. L. P. Hunt, et al., "Research and Development of Low Cost Processes for Integrated Solar Arrays", First Semi-Annual Progress Report (4/15/74-6/30/74), NSF/RANN/SE/GI-29729X/PR/74/2.

7. K. A. Feldmann and K. D. Frank, Ferrosilicium. In Durrer/Volkert, eds. Die Metallurgie der Ferrolegierungen, 2nd ed., p. 542, 1972.

8. F. Y. Dubrous and L. G. Septier, Trans. Met. Soc. AIME-Paper Selection, Paper No. A71-46 (1971).

9. W. T. Fairchild, Ibid., Paper No. A70-36 (1970).

0. W. H. Wise, Proc. Elect. Furnace Conf., 18, 465 (1963).

11. V. D. Dosaj, L. P. Hunt, and L. D. Crossman, IEEE Photovoltaic Specialists Conf., 11, 275 (1975).

12. N. P. Tucker, J. Iron and Steel Inst., 15, 412 (1927).

13. H. C. Theuerer, Bell Lab. Res. Bull., 34, 327 (1955).

14. W. Voos, U. S. Patent 2,972,521 (1961).

15. N. Aas, Trans. Met. Soc. AIME, Paper No. A70-36 (1970).

16. C. D. Graham, et al., "Research and Development of Low Cost Processes for Integrated Solar Arrays", Third Semi-Annual Progress Report (1/1/75-6/30/75), NSF/RANN/SE/GI-29829X/PR/75/2.

Table 1. Impurity Levels (ppma in silicon†) in Input and Output Material of the Arc Furnace as Determined by Emission Spectroscopy

	Input								Output	
	SiO_2				Carbon					
	Quartzite		Quartz		Pet.		Wood	Grap.		Fumed
Impurity	N.C.	Ala.	Norw.	Braz.	Coke*	Coal**	Chips***	Elect.	MG-Si	Silica
B	14	11	14	14	<10	40	<60	2	40	250
P	10	45	<10	<10	5	25	100	4	30	690
Al	620	1000	160	90	50	4600	70	440	1570	2400
Fe	75	90	20	20	30	1700	220	90	2070	650
Ti	10	40	<10	<10	8	270	<10	45	160	<10
Cr	20	50	20	30	2	260	370	3	140	280
V	<10	<10	<10	<10	100	20	<10	<4	100	<10
Mn	<10	20	<10	<10	<1	3	100	1	70	100
Ni	<10	<10	10	10	90	3	<10	<1	<50	<10
Cu	<5	<5	<5	<5	<1	10	<10	1	<50	20

* 88% free carbon; ** 68%; *** 15%

† Assumes all impurities end up in MG-Si according to

$$SiO_2 + \begin{matrix} 0.72C\ (coke) \\ 1.06C\ (coal) \\ 0.77C\ (wood) \\ 0.18C\ (elect.) \end{matrix} \rightarrow Si$$

Table 2. Analysis of Charcoal Supplied by Burger Brothers (Chicago)

Impurity	Concentration (ppma in Si)*
B	<1
P	<75
Al	<0.3
Fe	<0.1
Ti	<0.3
Cr	<0.1
V	<0.1
Mn	<0.4
Ni	<0.1
Cu	<0.1

Table 3. Petroleum Coke Analysis Before and After Halogen Purification

Impurity	Concentration (ppma in Si)*	
	Before	After
B	<1	<1
P	<75	<75
Al	>9	4
Fe	>4	0.06
Ti	3	0.6
Cr	>5	<0.1
V	>5	<0.1
Mn	>8	<0.1
Ni	>4	<0.1
Cu	>2	0.1

* Assumes all impurities are transferred to silicon.

Table 4. The Effect of Acid Leaching Upon MG-Si

Impurity	Concentration in Silicon (ppma)		Percent Removal
	MG-Si	Leached	
B	37	28	24
P	27	17	37
Al	1200	220	82
Fe	1600	100	94
Ti	200	<5	>98
Cr	110	<5	>95
V	120	<5	>96
Mn	80	<5	>94
Ni	70	<5	>93
Cu	24	17	29

Table 5. Segregation Coefficients for Impurities in Silicon

Impurity	Segregation Coefficient
B	0.8
P	0.35
Al	2×10^{-3}
Fe	8×10^{-6}
Ti	10^{-5}
Cr	10^{-5}
V	10^{-5}
Mn	10^{-5}
Ni	10^{-6}

Table 6. Effect of Growth Rate On Impurity Segregation Measured at the Seed End of the Crystal

Impurities (ppma) \ Growth Conditions	Slow	Intermediate	Fast	Melt
B	26	26	26	34
P	14	13	14	27
Al	<0.05	31.2	187	1040
Fe	<0.05	4.5	400	1156
Ti	<0.05	12	41	334
Cr	<0.05	10.8	39	50
V	<0.05	5.5	27.5	72
Mn	<0.05	0.5	2.0	102
Ni	<0.05	0.4	1.6	57
Cu	<0.05	4.0	8.8	39

Table 7. Impurity Distribution In Ingot Pulled From MG-Si*

Impurity (ppma) \ Sample Location	Melt	Seed (2% Wt)	20% Wt	35% Wt	50% Wt
B	40	40	40	42.5	42.5
P	31	25	26	23	23
Al	1000	ND**	ND	ND	60
Fe	1081	ND	ND	ND	0.170
Ti	315	ND	0.03	0.03	22
Cu	33	0.03	0.03	0.04	0.120

* Ni, Mg, V, Mn, and Cr not detected in crystal.
** ND implies <0.05.

Table 8. Performance Characteristics of Cells Fabricated from Metallurgical-Grade Silicon

Sample	I_{sc} (ave.) (mA/cm^2)	V_{oc} (ave.) (V)	Efficiency* (%)	Max.* Efficiency (%)
37	26	0.590	7.4	9.0
49	26	0.590	7.4	9.1
58	28	0.603	9.5	11.1

* Efficiency based on total cell area - 17% contact coverage.

Table 9. Cost Summary for Upgrading MG-Si by Czochralski Crystal Growth Assuming 80% Ingot Yield

Item	Cost ($/kg Si)
Labor	0.71
Energy (0.03/kWh)	0.63
Crucible	0.31
Replacement Parts	2.72
Capital	2.26
Total Direct Production Cost Less Raw Materials	6.63

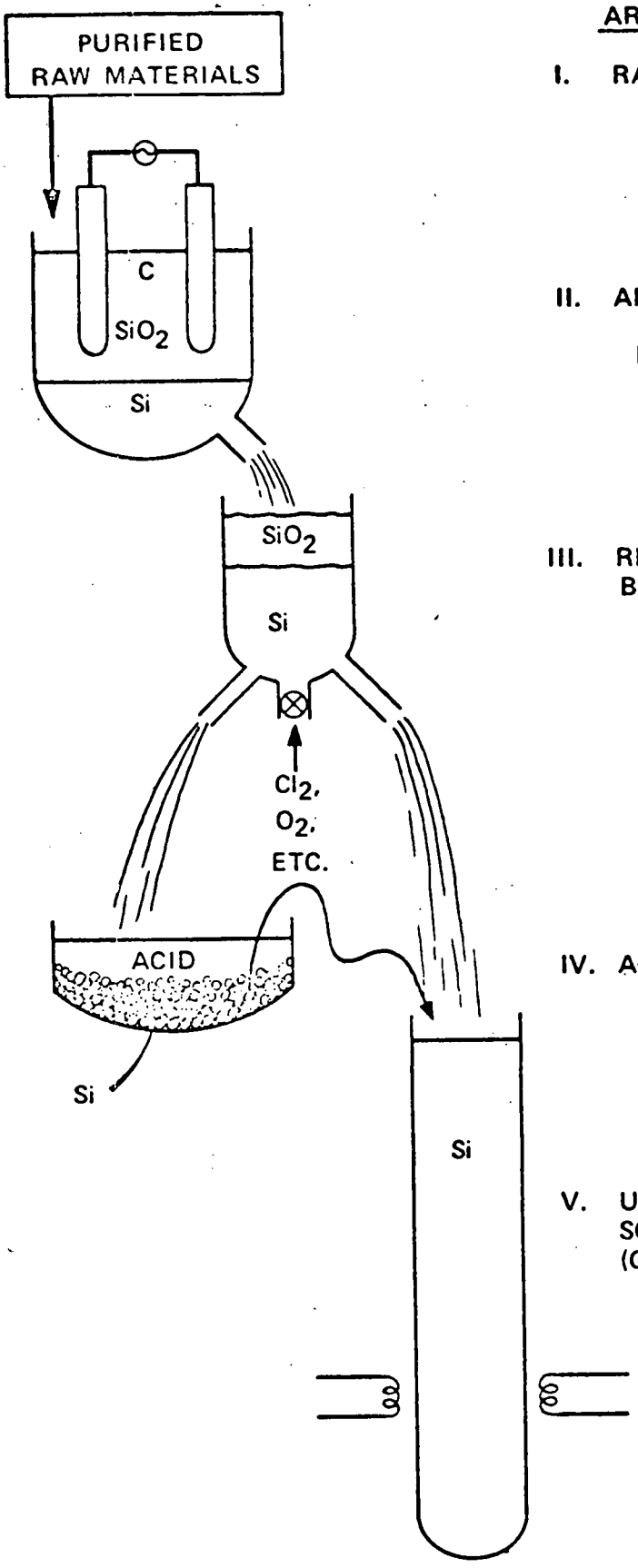

AREAS OF WORK	IMPURITIES AFFECTED
I. RAW MATERIALS	ALL
II. ARC FURNACE AND EQUIPMENT	UNKNOWN
III. REACTIVE GAS BLOWING AND SLAGGING	B, Al, CA, MG, & SOME TRANSITION METALS
IV. ACID LEACHING	FE & TRANSITION METALS
V. UNIDIRECTIONAL SOLIDIFICATION (CZOCHRALSKI AND BRIDGEMAN)	AL & TRANSITION METALS

Fig. 1. METHODS FOR PURIFYING METALLURGICAL-GRADE SILICON

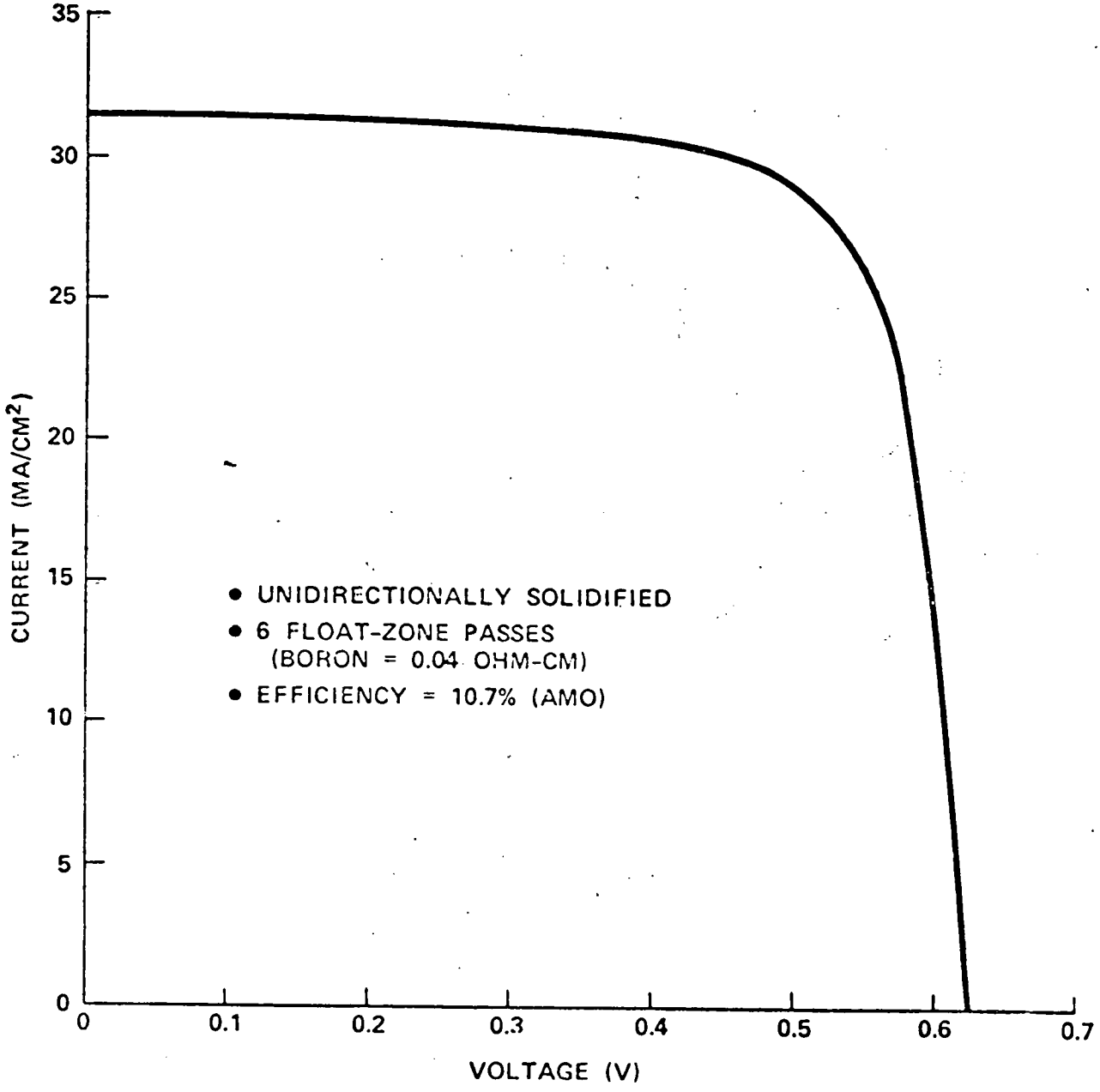

Fig. 2. CURRENT-VOLTAGE CHARACTERISTICS OF ILLUMINATED CELL FABRICATED FROM UNIDIRECTIONALLY SOLIDIFIED METALLURGICAL-GRADE SILICON

B. Research Contributors

The following members of the faculty and professional staff of the University of Pennsylvania contributed to the research reported herein.

Thomas J. Carroll, Research Specialist
Charles D. Graham, Professor
Subash Kulkarni, Post Doctoral Researcher
Edwin Louis, Post Doctoral Researcher
Alan G. MacDiarmid, Professor
Gerald T. Noel, Research Specialist and Project Manager
David P. Pope, Associate Professor
Baruch Pratt, Visiting Professor (On sabatical from Technion)
Kusuma Thallum, Post Doctoral Researcher
Martin Wolf, Professor and Principal Investigator
John H. Wohlgemuth, Post Doctoral Researcher
Jay N. Zemel, Professor

The following members of the professional staff of the Dow Corning Corporation contributed to the research reported herein.

Ronald H. Baney, Associate Scientist
Leon D. Crossman, Manager-Solid State Research and Development
Vishu D. Dosaj, Project Specialist
Ronald L. Halm, Senior Project Engineer
Lee P. Hunt, Senior Project Chemist
James R. McCormick, Project Physicist
Lee E. Nelson, Group Leader
Alvin W. Rauchholz, Senior Technical Assistant
John L. Speier, Scientist
Earl L. Warrick, Consultant

C. Meetings, Presentations, and Publications

During the course of this contract, work on this program has been discussed, presented, or published by key project personnel as indicated below:

1. 9th Intersociety Energy Conversion Engineering Conference, August 26-30, 1974, San Francisco, California, for which M. Wolf organized the Solar Power sessions.

2. International Conference on Photovoltaic Power Generation, September 25-27, 1974, Hamburg, West Germany, M. Wolf: "Historic Development of Photovoltaic Power Generation"; "Process Development for Low Cost Integrated Solar Arrays"; and participation in Round Table on "Present and Future Trends of Development and Use of Photovoltaic Power Generation".

   Paper published in proceedings to above, pp. 49-68 and 699-718, available from DGLR, Deutsche Gesellschaft fur Luft-und Raumfahrt, e.V., Koln, Germany.

3. Electrochemical Society Meeting, October 13-17, 1974, New York, New York, M. Wolf, Session Chairman in: "The electrochemical challenge of solar energy utilization", and presented paper: "Low Cost Integrated Silicon Solar Arrays: The Process Development Challenge".

4. ASME Winter Annual Meeting, November 17-22, 1974, New York, New York, M. Wolf: "Methods for Low Cost Manufacture of Silicon Solar Arrays".

   Paper published in proceedings to above: ASME Publication 74-WA/Ener.-4.

5. "Progress in New Low Cost Methods"; Presented by M. Wolf at the 11th IEEE Photovoltaic Specialists Conference, Phoenix, Arizona, May, 1975.

6. "Outlook for Silicon Photovoltaic Devices for Terrestrial Solar Energy Utilization"; Presented by M. Wolf at the AVS Symposium, IBM Research Center, May, 1975.

7. "Feasible Reactions for the Synthesis of Silicon as Determined by a Thermodynamic and Economic Screening Process"; Presented by L. Hunt at the Electrochemical Society Meeting, Toronto, Canada, May 1975. Also presented at 11th Photovoltaic Specialists Conference (see 5 above).

8. L. P. Hunt, L. D. Crossman, N. D. Dosaj, and J. R. McCormick, "Solar-grade Silicon from Purified Metallurgical-grade Silicon"; Presented at the American Ceramic Society Meeting, Indianapolis, Indiana, September, 1975.

9. M. Wolf, "Outlook for Si Photovoltaic Devices for Terrestrial Solar Energy Utilization", Jour. Vac. Sci. Technol. 12, (#5), 984 (October, 1975).

10. M. Wolf, "Materials for Solar Energy Conversion", presented at the 3rd American Crystal Growing Conference, July 13-17, 1975, Stanford University, Palo Alto, California.

11. M. Wolf, "Photovoltaic Power", published in Solar Energy for Earth - An AIAA Assessment, pp. 46-58, American Institute for Aeronautics and Astronautics, New York, New York, 1975.

D. Acknowledgements

The University research group would like to thank the following people for their able assistance in the work described in this report.

Bruce Bleiweiss, Student
Peter Fonash, Graduate Student
Richard Fruncillo, Student
James Gorman, Research Technician
William Hale, Graduate Student
Vijay Kapur, Graduate Student
Alan Kepple, Student
Michael Kotlikoff, Student
Steven Loughlin, Graduate Student
John Velimese, Student
Thomas Wolf, Student

E. Summary From Previous Semi-Annual Report

The Dow Corning efforts were concentrated on upgrading MG-Si which currently sells for about $1/Kg as compared to the $10/Kg cost SoG-Si. Discussions were carried out with suppliers of MG-Si, quartz, and submerged-electrode arc furnaces, resulting in requests for cost quotes to purchase a small 50KVA arc furnace to study upgrading of raw materials. Requests for cost quotes were also issued for carrying out experiments in appropriate facilities before delivery of the furnace.

The chemical upgrading of MG-Si by reactive gas blowing with oxygen and chlorine resulted in a reduction in the level of many impurities, except, notably, for boron which is also difficult to remove by segregation. Single crystal ingots were pulled from the blown MG-Si using the Czochralski technique. The ingots represented 30-45% of the original weight of the MG-Si and had resistivities from 0.06 to 0.20 ohm-cm.

The effect of physically purifying MG-Si through unidirectional freezing was studied. The base level of boron in second generation Czochralski crystals was found to be 0.03-0.06 ohm-cm (20-55 ppma), stressing the need to find a method for reducing the boron level in MG-Si. Most other impurity levels were significantly reduced during pulling, particularly as pull rates were decreased from 10 to 5 cm/mm.

A thorough survey was made of electrolytic processes for producing silicon. No known process exists which is capable of producing "solar grade" quality silicon at a rate suitable for high volume production.

Investigation of the SiF_4/SiF_2 silicon transport process has continued with a study of the process characteristics when run at atmospheric pressure. The SiF_2 gas has been successfully

transported over distances of 50 cm at room temperature and atmospheric pressure without significant decomposition. At constant temperatures above 1100°C it has been demonstrated that decomposition of the SiF_2 does not occur for a time period of 3 seconds or more. Both of these properties are encouraging from the stand point of impurity removal. Silicon deposition at atmospheric pressure can occur over a wide temperature range (500-1000°C and in some cases higher), and there is some evidence that the "amorphous" material which deposits at the higher temperatures tends to recrystallize.

Contamination of the SiF_4 with impurity gases was felt to have a significant influence on the experimental results. A multistage distillation technique was introduced as a means of purifying the gas prior to use.

With regard to the process screening tasks, a brief discussion is given of techniques being developed to further screen previously identified processes to produce SoG-Si. One such technique involves comparing the energy of the process as well as that required to produce the raw materials; another concerns comparing total raw materials prices of each process.

In the sheet formation area, the results of the silicon deformation studies have been highly encouraging. Polycrystalline samples have been successfully deformed by as much as seventy percent with deformation rates up to 1% per second. Strong evidence of recrystallization due to strain annealing has been observed. Apparent grain size changes of a factor of 10 (up to 1 mm dia.) have been observed.

Experimental work on the binary solution growth process has been terminated in order to concentrate efforts on areas which, at present, appear to hold more promise in terms of meeting the program goals.

Construction of "Pierce Gun" electron beam zone melting

apparatus has been completed. Analytical studies of the problems of electron beam zone melting have continued, with the calculation of beam power and filament temperature requirements for the maximum feasible zone dimensions and travel speeds. A refined analysis of the maximum zone travel speed has been performed with the aid of a computer, using numerical techniques for the solution of the differential equation describing heat flow and heat loss in a silicon sheet.

The analysis of the economics of cylindrical crystal production by the Czochralski method which was presented in an earlier report has been revised and updated as a result of new information acquired in the interim. It is concluded that future crystal pulling costs will be dominated by the crucible cost.

F. Distribution List

Dr. Wayne A. Anderson — 1
Department of Electrical Engineering
Rutgers University
New Brunswick, New Jersey 08903

Dr. Joseph Apfel — 1
Optical Coating Laboratories, Inc.
P.O. Box 1599
Santa Rosa, California 95403

Dr. Charles E. Backus — 1
Mechanical Engineering Department
Arizona State University
Tempe, Arizona 85281

Dr. Joan B. Berkowitz — 1
Arthur D. Little, Inc.
20 Acorn Park
Cambridge, Mass. 02140

Mr. Daniel Bernatowicz — 1
M/S 302-1
NASA Lewis Research Center
21000 Brookpark Road
Cleveland, Ohio 44135

Dr. H. Richard Blieden — 1
Energy Research and Development
Administration
1800 G Street, N.W.
Washington, D.C. 20550

Professor Karl W. Boer — 1
University of Delaware
Institute of Energy Conversion
Newark, Delaware 19711

Dr. Henry W. Brandhorst, Jr. — 1
M.S. 302-1
NASA-Lewis Research Center
21000 Brookpark Road
Cleveland, Ohio 44135

Dr. Rolf Buchdahl — 1
Monsanto Research
800 N. Lindberg Blvd.
St. Louis, Missouri 63166

F. Distribution List (con't)

Dr. Bruce Chalmers Division of Engineering and Applied Science Harvard University Cambridge, Mass. 02138	1
Mr. William R. Cherry Energy Research and Development Administration 1800 G Street, N.W. Washington, D.C. 20550	1
Dr. Ting L. Chu Electronic Sciences Center Southern Methodist University Dallas, Texas 75275	1
Dr. Ernest Cohn NASA Headquarters Code RPP Washington, D.C. 20546	1
Dr. J. W. Edwards Monsanto Company 800 N. Lindbergh Blvd. St. Louis, Mo. 63166	1
Dr. Paul Fang Physics Department Boston College Chestnut Hill, Mass.	1
Mr. John V. Goldsmith Jet Propulsion Laboratory 4800 Oak Grove Drive Pasadena, California 91103	1
Dr. Lloyd O. Herwig Energy Research and Development Administration 1800 G Street, N.W. Washington, D.C. 20550	2
Mr. Peter A. Iles OCLT 15251 E. Don Julian Road City of Industry, CA 91746	1
Dr. George S. James, Program Manager Information Resources Advanced Energy Research and Technology Division National Science Foundation - Room 1149-G 1800 G Street, N.W. Washington, D.C. 20550	5

F. Distribution List (con't)

Mr. B.K. Jindal 1
Honeywell Radiation Labs
2 Forbes Road
Lexington, Mass. 02173

Dr. K.M. Koliwad
MS 198-248
Jet Propulsion Lab.
4800 Oak Grove Drive
Pasadena, Calif. 91103

Dr. Joseph Lindmayer 1
The Solarex Corporation
1335 Piccard Drive
Rockville, Maryland 20850

Dr. Joseph H. Loferski 1
Dept. of Engineering
Brown University
Providence, Rhode Island 02910

Dr. Ralph Lutwack 1
198/220
Jet Propulsion Laboratory
4800 Oak Grove Drive
Pasadena, Calif. 91103

Dr. Leonard Magid 10
Energy Research and
Development Admin.
1800 G Street
Washington, D.C. 20050

Dr. A.I. Mlavsky 1
Tyco Laboratories, Inc.
16 Hickory Drive
Waltham, Massachusetts 02154

Dr. J. M. Morabito 1
Bell Telephone Laboratories
Allentown, Pa. 18103

Prof. Fred H. Morse 1
Dept. of Mechanical Engineering
University of Maryland
College Park, Maryland 20742

Dr. Tapan K. Mukherjee 1
Advanced Energy Research and Technology
Research Applications
National Science Foundation
1800 G Street, N.W.
Washington, D.C. 20550

F. Distribution List (con't)

Mr. William O'Mara
6701 East Palm Lane
Scottsdale, Arizona 85257 — 1

Dr. M.B. Prince
Energy Research and Development Administration
1800 G Street, N.W.
Washington, D.C. 20050 — 1

Mr. E.L. Ralph
Spectrolab
Subsidiary of Hughes Aircraft Corp.
12500 Gladstone Ave.
Sylmar, California 91342 — 1

Mr. Paul Rappaport
David Sarnoff Research Center
RCA Laboratories
Princeton, New Jersey 08540 — 1

Dr. Roy Rice
Mail Stop 6860
Naval Research Laboratories
Washington, D.C. 20375 — 1

Dr. G.H. Schwuttke
IBM Corporation
Systems Products Division
East Fishkill
Hopewell Junction, New York 12533 — 1

Dr. Bernard O. Seraphin
Optical Science Center
University of Arizona
Tucson, Arizona 85721 — 1

Dr. W.J. Siekhaus
Lawrence Berkeley Laboratory
Bldg. 62, Room 357
University of California-Berkeley
Berkeley, California 94720 — 1

Dr. Friedolph Smits
Bell Telephone Laboratories
Allentown, Pa. 18103 — 1

Dr. Gabor A. Somorjai
Dept. of Chemistry
University of California-Berkeley
Berkeley, California 94720 — 1

F. Distribution List (con't)

Dr. Franklin F.Y. Wang 1
Materials Science Dept.
State University of New York
Stony Brook, New York

Mr. Joseph Wise 1
AFAPL/POE-2
Wright Patterson AFB
Dayton, Ohio 45433

Dr. Carl L. Yaws 1
Assoc. Prof. of Chem. Eng.
Lamar University
P.O. Box 10053
Beaumont, Texas 77710

Dr. John Zoutendyk
MS 198-248
Jet Propulsion Laboratory
4800 Oak Grove Drive
Pasadena, Calif. 91103

Dr. John Teem
Deputy Assistant Administrator for
Solar, Geothermal, and Advanced Energy Systems
Energy Research and Development Administration
1800 G Street
Washington, D. C. 20550

Dr. Donald Beattie
Energy Research and Development Administration
1800 G Street
Washington, D. C. 20550

Dr. J. Thomas Ratchford
Committee on Science and Astronautics
United States House of Representatives
Washington, D. C. 20515

Mr. Sam Taylor
Federal Energy Administration
12th and Pennsylvania Avenue, N. W.
Washington, D. C. 20461